AD-A056 381 NAVAL POSTGRADUATE SCHOOL MONTEREY CALIF F/G 11/6
EFFECTS OF HYDRODYNAMIC VARIABLES ON CORROSION: STUDY OF 90/10 --ETC(U)
MAR 78 G H LEUMER

UNCLASSIFIED NL

1 OF 2
AD A056381

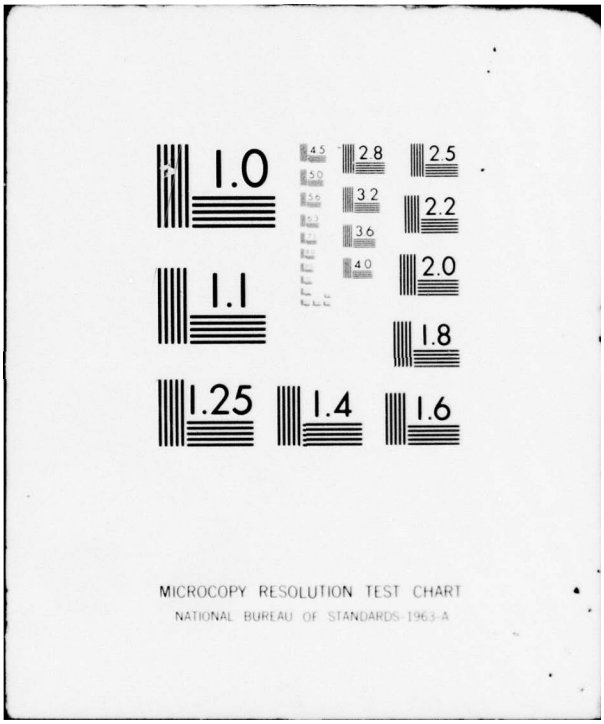
1.0
1.1
1.25
1.4
1.6
1.8
2.0
2.2
2.5
2.8
3.2
3.6
4.0
4.5
5.0
5.6
MICROCOPY RESOLUTION TEST CHART
NATIONAL BUREAU OF STANDARDS-1963-A

AD A056381

AD No. ____
DDC FILE COPY

(2) LEVEL II

NAVAL POSTGRADUATE SCHOOL
Monterey, California

DDC
RECEIVED
JUL 18 1978
B

(9) Master's

THESIS

(6) EFFECTS OF HYDRODYNAMIC VARIABLES ON CORROSION: STUDY OF 90/10 Cu-Ni IN A CIRCLING FOIL WITH SYNTHETIC SEAWATER.

by

(10) Gerhard Hannes Leumer

(11) March 1978

(12) 143 p.

Thesis Advisor: J. Perkins

Approved for public release; distribution unlimited.

251450

78 07 10 005

UNCLASSIFIED

SECURITY CLASSIFICATION OF THIS PAGE (When Data Entered)

REPORT DOCUMENTATION PAGE		READ INSTRUCTIONS BEFORE COMPLETING FORM
1. REPORT NUMBER	2. GOVT ACCESSION NO.	3. RECIPIENT'S CATALOG NUMBER
4. TITLE (and Subtitle) Effects of Hydrodynamic Variables on Corrosion: Study of 90/10 Cu-Ni in a Circling Foil with Synthetic Seawater		5. TYPE OF REPORT & PERIOD COVERED Master's Thesis; March 1978 6. PERFORMING ORG. REPORT NUMBER
7. AUTHOR(s) Gerhard Hannes Leumer		8. CONTRACT OR GRANT NUMBER(s)
9. PERFORMING ORGANIZATION NAME AND ADDRESS Naval Postgraduate School Monterey, California 93940		10. PROGRAM ELEMENT, PROJECT, TASK AREA & WORK UNIT NUMBERS
11. CONTROLLING OFFICE NAME AND ADDRESS Naval Postgraduate School Monterey, California 93940		12. REPORT DATE March 1978 13. NUMBER OF PAGES 143
14. MONITORING AGENCY NAME & ADDRESS(if different from Controlling Office)		15. SECURITY CLASS. (of this report) Unclassified 15a. DECLASSIFICATION/DOWNGRADING SCHEDULE

16. DISTRIBUTION STATEMENT (of this Report)

Approved for public release; distribution unlimited.

17. DISTRIBUTION STATEMENT (of the abstract entered in Block 20, if different from Report)

18. SUPPLEMENTARY NOTES

19. KEY WORDS (Continue on reverse side if necessary and identify by block number)

Cu-Ni
Corrosion

20. ABSTRACT (Continue on reverse side if necessary and identify by block number)

The effects of hydrodynamic variables and fluid properties on corrosion of 90/10 Cu-Ni (CDA 706) in single metal exposures and in galvanic couples with platinum were studied in synthetic seawater. An apparatus utilizing circling foil as the specimen holder was redesigned as an experimental apparatus for this study. Various methods were applied to develop corrosion rate data for different flow

DD FORM 1 JAN 73 1473 (Page 1)

EDITION OF 1 NOV 65 IS OBSOLETE
S/N 0102-014-6601

UNCLASSIFIED

SECURITY CLASSIFICATION OF THIS PAGE (When Data Entered)

78 07 10 005

(20. ABSTRACT Continued)

situations. Particular emphasis was placed on the determination of variable parameters of fluid dynamics, and on the correlation of nondimensional hydrodynamic and mass transfer parameters with experimentally determined corrosion rates. Also, the corrosion morphology was studied macroscopically and microscopically for different velocities. A consideration of theoretical and practical factors concerning mass transfer and corrosion in a flowing medium concluded this study.

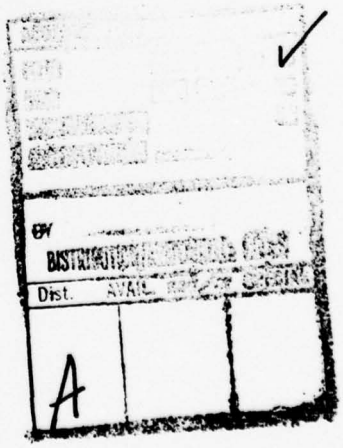

Approved for public release, distribution unlimited.

Effects of Hydrodynamic Variables on Corrosion: Study of 90/10 Cu-Ni in a Circling Foil with Synthetic Seawater

by

Gerhard Hannes Leumer
Lieutenant Commander, Federal German Navy

Submitted in partial fulfillment of the requirements for the degree of

MASTER OF SCIENCE IN MECHANICAL ENGINEERING

from the

NAVAL POSTGRADUATE SCHOOL

March 1978

Author _____

Approved by: Jeff Perkins
Thesis Advisor

Thomas Hamilton
Second Reader

D. Marto
Chairman, Department of Mechanical Engineering

George J. Haltiner
Dean of Science and Engineering

ABSTRACT

The effects of hydrodynamic variables and fluid properties on corrosion of 90/10 Cu-Ni (CDA 706) in single metal exposures and in galvanic couples with platinum were studied in synthetic seawater. An apparatus utilizing circling foil as the specimen holder was redesigned as an experimental apparatus for this study. Various methods were applied to develop corrosion rate data for different flow situations. Particular emphasis was placed on the determination of variable parameters of fluid dynamics, and the correlation of non-dimensional hydrodynamic and mass transfer parameters with experimentally determined corrosion rates. Also, the corrosion morphology was studied macroscopically and microscopically for different velocities. A consideration of theoretical and practical factors concerning mass transfer and corrosion in a flowing medium concluded this study.

TABLE OF CONTENTS

I. INTRODUCTION ---------- 14

II. DESIGN OF THE EXPERIMENTAL APPARATUS ---------- 18

A. TANK ---------- 18

B. DEPLOYMENT OF SPECIMENS IN THE FOIL -------- 19

C. ELECTRICAL AND DRIVE SYSTEM ---------- 29

III. EXPERIMENTAL PROCEDURE ---------- 33

A. GENERAL ---------- 33

B. LINEAR POLARIZATION METHOD (LPM) ---------- 39

C. POTENTIODYNAMIC POLARIZATION CURVES -------- 45

D. ZERO-RESISTANCE AMMETER (ZRA) ---------- 46

E. HOT-FILM ANEMOMETRY ---------- 47

IV. RESULTS ---------- 59

A. CORROSION RATES FROM DIFFERENT METHODS ----- 59

1. Weight Loss ---------- 59

2. LPM ---------- 59

3. Potentiodynamic Polarization Curves ---- 68

4. ZRA ---------- 72

B. EFFECT OF VELOCITY ON CORROSION RATES ------ 75

C. CORROSION PRODUCTS ---------- 77

1. Identification ---------- 77

2. Morphology ---------- 84

V. HYDRODYNAMIC CONSIDERATIONS IN CORROSION ------- 106

A. BOUNDARY LAYERS IN TURBULENT FLOW ---------- 106

B. MASS TRANSFER ---------- 117

C. POSSIBLE PARAMETERS FOR CORROSION RATE CORRELATIONS ---------- 128

VI. SUMMARY AND CONCLUSIONS ---------- 134

APPENDIX A: PREPARATION OF ARTIFICIAL SEAWATER ---- 137

LIST OF REFERENCES ---------- 139

INITIAL DISTRIBUTION LIST ---------- 143

LIST OF TABLES

1. Legend to Figure 2 ---------- 22

2. Specifications of 90-10 Cu-Ni Alloy (CDA 706) -- 34

3. List of Experiments Performed ---------- 38

4. Results of Hot-Film Anemometry ---------- 58

5. Formulas for Corrosion Rate Determination ------ 60

6. Results of Corrosion Test of 2 m/sec with 90-10 Cu-Ni in Synthetic Seawater ---------- 78

7. Results of Corrosion Test at 4 m/sec with 90-10 Cu-Ni in Synthetic Seawater ---------- 79

8. Results of Corrosion Test of 6 m/sec with 90-10 Cu-Ni in Synthetic Seawater ---------- 80

LIST OF FIGURES

1. (a) Side View and (b) top view from interior of the exposure tank ---------- 20

2. Cross-section of exposure tank (note: Legend, see Table 1 next page) ---------- 21

3. Exposure Tank and apparatus for LPM-determination -- 23

4. Detail of specimen-carrying foil (all dimensions in cm) ---------- 25

5. Schematic of the arrangement of the foil with respect to the supporting arm ---------- 26

6. Strut and foil carrying one specimen ---------- 27

7. Electrical arrangement and drive system ---------- 32

8. LPM-measurement curve ---------- 40

9. Equipment needed for LPM determinations: potentiostat, programmer and x-y recorder ---------- 44

10. ZRA equipment ---------- 48

11. Schematic of ZRA ---------- 49

12. DC-power controller for drive system; counter, and equipment for hot-film anemometry ---------- 52

13. Probes used im hot-film anemometry (note: Model 1218 is equivalent to Model 1261 used in these tests) ---------- 53

14. Strut-foil arrangement carrying hot film probe ----- 54

15. Plot for the determination of $V_o(x)$ for test I, II and III ---------- 56

16. Actual LPM-results at different velocities (velocity = m/sec, E = 10 mV/unit, I = 100 μA/unit - 63

17. Corrosion rates versus time as determined by using LPM at 2 m/sec (number on curves refers to sequence number of test-run) ---------- 64

18. Corrosion rates versus time as determined by using LPM at 4 m/sec (number on curves refers to sequence number of test-run) ---------- 65

19. Corrosion rates versus time as determined by using LPM at 6 m/sec (number on curves refers to sequence number of test-run) ---------- 66

20. Comparison of averaged corrosion rates plotted versus time at given velocities determined by weight loss and LPM method ---------- 67

21. Actual polarization plot at 2 m/sec (surface area = 2.85 cm^2) ---------- 69

22. Actual polarization plot at 4 m/sec (surface area = 2.85 cm^2) ---------- 70

23. Actual polarization plot at 6 m/sec (surface area = 2.85 cm^2) ---------- 71

24. Corrosion rate of a galvanic couple Cu-Ni/Pt plotted versus time at given velocities ---------- 73

25. Schematic of possible corrosion products over a pit ---------- 85

26. Cu-Ni surface, coupled with Pt, exposed at 6 m/sec for 24 hours, 10x ---------- 86

27. (a) Cu-Ni surface, coupled with Pt, exposed at 4 m/sec for 24 hours, 100x, (b) Cu-Ni surface, coupled with Pt, exposed at 4 m/sec for 24 hours, 400 x ---------- 88

28. Cu-Ni surface, coupled with Pt, exposed at 6 m/sec for 24 hours, 500x(SEM) ---------- 89

29. Cu-Ni surface, etched, 400x ---------- 90

30. Cu-Ni surface, coupled with Pt, exposed at 6 m/sec for 24 hours, 2000x(SEM) ---------- 91

31. Cleaned Cu-Ni surface, coupled with Pt, exposed at 6 m/sec for 24 hours (a) 500x(SEM), (b) 2000x(SEM) ---------- 93

32. Cleaned Cu-Ni surface, coupled with Pt, exposed at 4 m/sec for 24 hours, (a) 200x, (b) 400x, (light microscope) ---------- 94

33. (a) Clean Cu-Ni surface after preparation for exposure, 100x, (b) Cleaned Cu-Ni surface, single corrosion, exposed at 6 m/sec for 48 hours, 100x ---------- 96

34. Cleaned Cu-Ni surface, single corrosion, exposed at 2 m/sec for 48 hours, 400x ---------- 97

35. Cleaned Cu-Ni surface, single corrosion, exposed for 48 hours, 2000x, (a) at 2 m/sec), (b) at 6 m/sec ---------- 98

36. Cleaned Cu-Ni surface, single corrosion, exposed for 48 hours, 500x(SEM), (a) at 2 m/sec), (b) at 6 m/sec ---------- 100

37. Uncleaned Cu-Ni surface, single corrosion, exposed statically for 3 days, 500x(SEM) ---------- 101

38. Pourbaix-diagram of Cu in an electrolyte containing a high percentage of Cl^-, as given by Pourbaix [41] himself ---------- 103

39. Pourbaix-diagram for Cu in seawater (source: Bianchi and Longhi [11]) ---------- 104

40. Schematic of boundary layers important for mass transfer (b.z. = buffer zone, d_h = hydrodynamic boundary layer, d_{sl} = viscous sublayer, d_d = diffusion boundary layer, U_o = free stream velocity ---------- 107

41. Boundary layers over a flat plate calculated by formulas given in the text using actual data ------ 113

42. Boundary layers over a flat plate calculated by formulas given in the text using actual data (smaller scale than in Fig. 41) ---------- 114

LIST OF ABBREVIATIONS AND UNITS

A	=	atomic weight
b	=	width of plate
b.z.	=	buffer zone
CuS	=	copper sulfide
Cu	=	copper
Cu^{++}	=	cuprous copper ions
Cl	=	Chlor
c	=	concentration
c_b	=	concentration of bulk electrolyte
c_e	=	concentration of electrolyte in contact with the surface
C	=	grad Celsius
CE	=	counter electrode
cm	=	centimeter
COA	=	Copper Development Agency
d	=	thickness
d_{sl}	=	thickness of laminar sublayer
d_h	=	thickness of hydrodynamic boundary layer
d_d	=	thickness of diffusion boundary layer
d_T	=	thickness of thermal diffusion boundary layer
D	=	diffusion coefficient
E_o	=	potential wrt to reference electrode
e,e'	=	voltages read during anemometry measurements
F	=	Faraday's constant
h	=	heat transfer coefficient

h_d = mass transfer coefficient

i = current density

i_c = corrosion current density

i_l = limiting current density

I = current

in = inch

j = mass transfer rate

j_d = dimensionless "colburn" factor

k = constant in LPM

k_f = local friction factor

K_f = total friction factor

L = length

LPM = linear polarization method

IR = voltage drop in electrolyte

Na_2SO_4 = sodium sulfate

m = meter

mA = milliampere

mV = millivolt

Mpy = milli-inch per year

μmpy = micrometer per year

mg = milligram

Ni = nickel

Nu = Nusselt number

n = number of electrons

O = Oxygen

Pr = Prandtl number

Pt = platinum

Re = Reynolds number

Re_x = Reynolds number dependent on x

RE = reference electrode

RPM = revolutions per minute

RPS = revolutions per second

RMS = root mean square

sec = second

Sc = Schmidt number

Sh = Sherwood number

SEM = scanning electron microscope

SCE = Standard Calomel Electrode

TSI = Thermo System Incorporated

U = velocity

U' = fluctuation in velocity

$\overline{U}$ = average velocity

V = volt

V = voltage

V_o = voltage at zero velocity

WE = working electrode

WL = weight loss

x = characteristic length

x_o = initial length

x_{Cu}, X_{ni} = mole fraction of copper and nickel

ZRA = zero resistance amperemeter

z = valence

α = thermal diffusivity

ε = turbulent diffusivity

Rho = specific weight

ν = kinetic viscosity

β_a, β_c = Tafel slope of anodic and cathodic curve

I. INTRODUCTION

When the corrosion rate of a metal is higher in a flowing corrodent than in a stagnant system, the process is called erosion-corrosion. Erosion-corrosion must be distinguished from simple erosion. Whereas erosion is a purely mechanical effect, erosion-corrosion is a process partly involving both a mechanical and electrochemical process. In fact, even if the mechanical part of the process decreases to zero, as at lower velocities, the enhanced corrosion due to flow is still called erosion-corrosion. (Syrett [45]) Erosion by liquids is described by Preece and Macmillan [36] as the effect a jet or drop impact has on the surface including cavitation; these features are not normally found in flow over a plate or through a channel. The word erosion is also used in the literature simply in connection with corrosion when a metal is exposed to a flowing electrolyte, in which case the term erosion is being related generally to any influence the velocity may have on the electrochemical process of corrosion.

One effect of relative electrolyte motion is that the ions causing corrosion, such as oxygen or chlorine, are transported faster and more intensively to the metal surface resulting in a higher corrosion rate. Depending on the nature of the surface film (whether it is coarse or dense), the corrosion rate might accelerate because of local

galvanic action or decelerate because of improved film protection. Different materials exhibit different sensitivity to a flowing corrodent depending upon the kind of corrosion products and upon their specific sensitivity to erosion which becomes more important at high velocities.

Syrett [45] mentions three basic groups of materials (mostly alloys) which in general show good resistance to a flowing electrolyte. First there are alloys like those of titanium which obtain high resistance to velocity by building up a tenacious and adhesive surface film. The second group exhibits resistance to intermediate and high velocities, but is very sensitive to pitting and crevice corrosion at low velocities; this is the case for stainless steels and nickel alloys. The third group shows excellent corrosion resistance at lower velocities, but suffers at higher velocities from degradation through accelerated erosion-corrosion caused by the film being stripped from the surface. Copper alloys for example belong to this group.

Cu-Ni alloys are widely used in cooling systems containing corrosive liquids like seawater. The flow velocity in these systems has to be limited, because it is recognized that the corrosion rate increases slowly at lower velocities with increasing velocity, but increases more drastically when a certain velocity is reached, the so-called breakaway or critical velocity. For Cu-Ni alloys the breakaway velocity is in the range of 2 to 4 m/sec, a value which is seldom

reached in normal pipe flow. The actual critical velocity for a system is dependent on the local intensity of the turbulence: the higher the turbulence intensity is, the lower is the critical value of the average velocity.

This points out that the average velocity is not a sufficiently descriptive factor to account for all the influences on corrosion rate in a flowing electrolyte. There are variables of the electrolyte, such as temperature, oxygen content, pH-value, and the content of chlorine and other constituents of seawater such as sulfides. More descriptive hydrodynamic parameters than the average velocity can be better used to describe the effect of flow on corrosion rates. For example surface roughness increases the local shear stress, which would be expected to result in a higher corrosion rate; intermittent flow also may have a positive effect on corrosion, because in a period of low velocity or stagnant exposure the surface film formation may recover resulting in a lower corrosion rate for that period. The diameter of a tube or channel may influence the corrosion resistance, because the boundary layer thickness and turbulence may vary with the diameter even at the same velocity. Turbulent flow and laminar flow have very different effects on corrosion, and within a turbulent flow the intensity of the turbulence is important. Considering this variety of influencing factors (only some have been mentioned here), differences in the results of corrosion experiments involving velocity as described by the literature

seems not to be astonishing. Only if a model can be developed which includes the most important parameters, can one be sure to achieve consistancy in the experimental results, and be able to predict corrosion rates for a certain material under given conditions.

The purpose of the present research was to apply this philosophy to the study of velocity-affected corrosion. Experimentally, it was of interest to alter and redefine the experimental "circling foil" apparatus developed by Storm [1] and to study various methods by which one can characterize the effect of velocity on corrosion rate of metals. It was of particular interest to determine the variable parameters of fluid dynamics in order to try to correlate non-dimensional parameters concerning hydrodynamics and diffusion with the different corrosion rate results gained in this study. Also, it was of interest to study the corrosion morphology macroscopically and microscopically for different velocities.

II. DESIGN OF THE EXPERIMENTAL APPARATUS

Various problems inherent in the original circling foil apparatus design by Storm [1] were solved by changes in equipment and design.

One problem Storm encountered was a stirring effect at velocities higher than 3 m/sec, which caused difficulty in determining the real velocity of the foil through the water, i.e. the true relative velocity. Furthermore, the vertical strut holding the foil had to be streamlined to minimize drag. However, being constructed of PVC only, at higher velocities the strut was too slender and weak to hold the foil horizontally down and finally, at the maximum speed of 6 m/sec the centrifugal forces became so strong that the foil hit the outside baffles of the tank and was destroyed; thus this strut must also be stiffened.

Another reason for limitation to modest velocities was the power of the motor and the driving gear arrangement; also "wobbling" of the main shaft that held the slip-rings produced a noise problem. In order to eliminate or at least diminish those problems the apparatus was redesigned as described below.

A. TANK

The original tank built by Storm [1] was also used for the experiments in this study. The existing baffle strips at the wall were retained, but extra baffles ranging from

those strips about 10 cm above the bottom of the tank into the middle portion where they were held by an open cylinder helped to significantly decrease the stirring effect (see Fig. 1(a),(b)). The stirring velocity, even at highest velocity, was negligibly small with respect to the foil velocity. However, the baffles produced a considerable turbulence in the free-stream, which will be discussed later (see Ch. III.E).

Due to the velocity twice as high as before, the splashing increased enormously, so that a new, much tighter cover had to be put on top of the tank. This served to prevent water losses by splashing and evaporation and to prevent the synthetic seawater from being contaminated by the surroundings.

The air-sparging holes which were originally intended to provide continuous aeration of the system were no longer necessary, because at velocities higher than 2 m/sec, aeration caused by the turbulence was sufficient. At velocities higher than 5 m/sec the aeration was so extreme that the water became milky because of many little bubbles whirling through the water. This problem will be mentioned again later (see Ch. III.E, IV.B).

B. DEPLOYMENT OF SPECIMENS IN THE FOIL

The radius of the circle the foil was moving in was increased by an extension of the horizontal arm by 5 cm, so that the foil would run at a higher velocity for a given RPM.

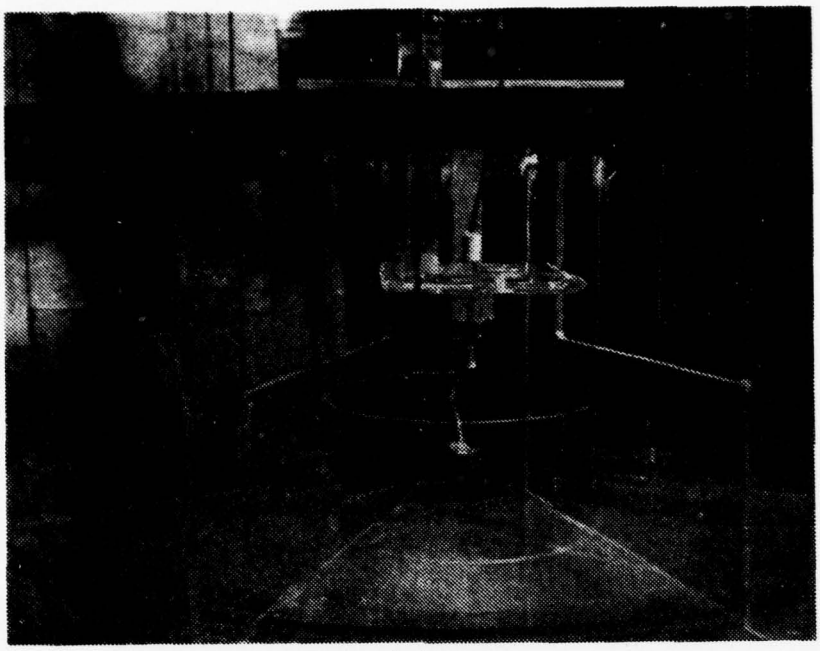

(a)

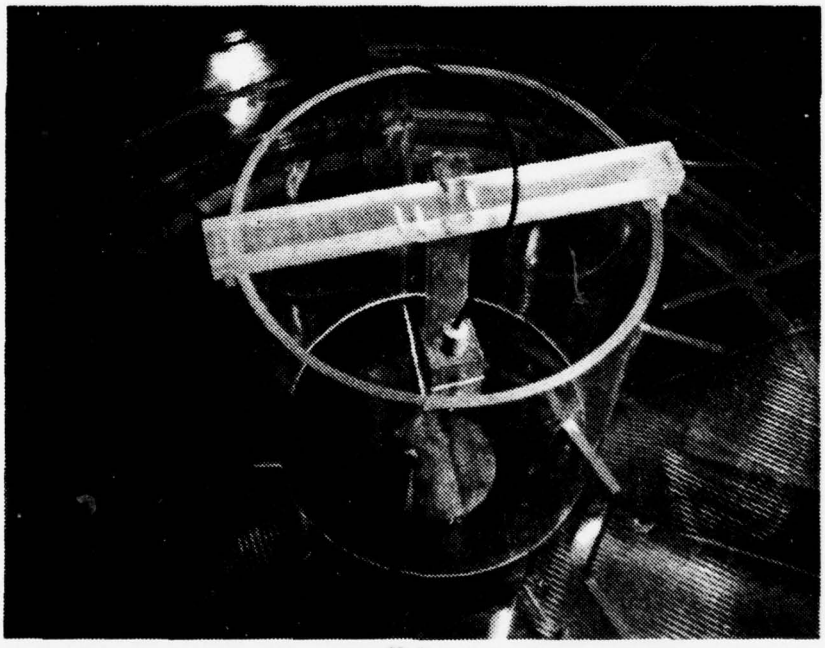

(b)

Figure 1. (a) Side view and (b) top view from interior of the exposure tank.

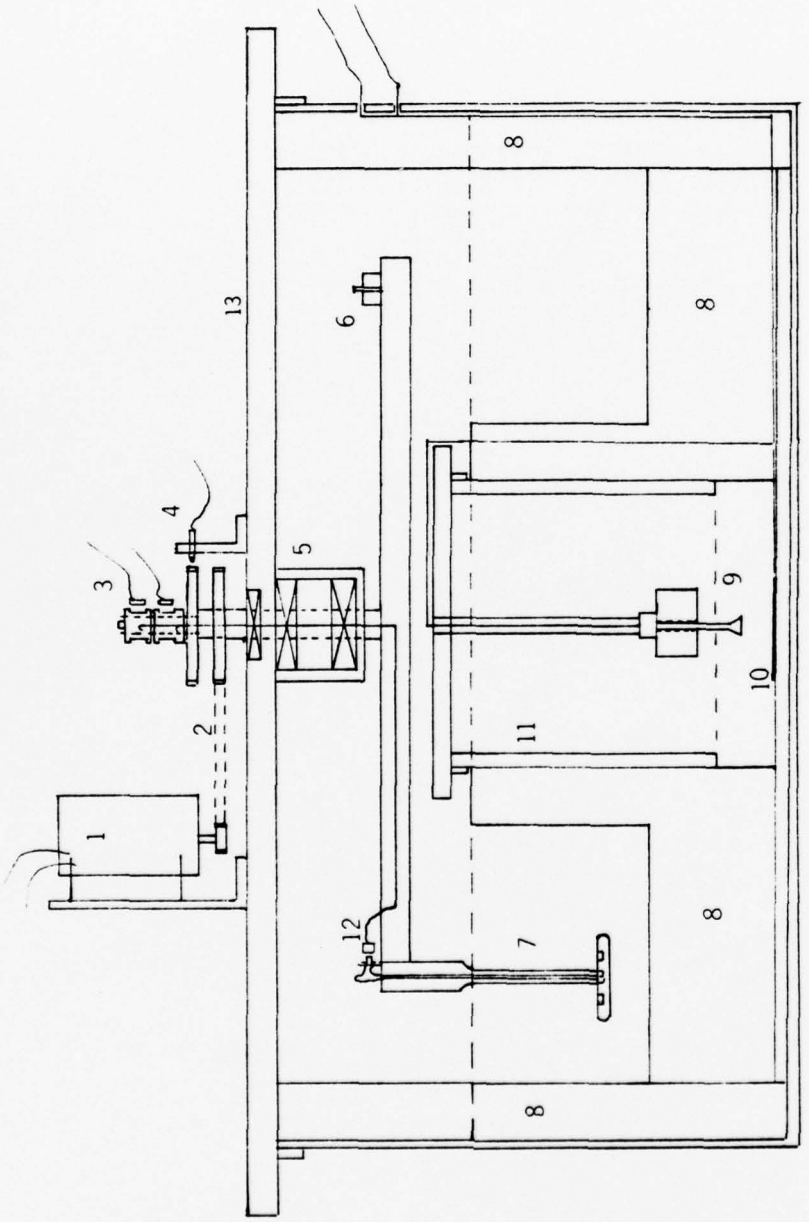

Figure 2. Cross-section of exposure tank
(note: legend see Table 1 next page)

Table 1

Legend To Figure 2

1	=	1/4 Hp controllable DC-motor
2	=	driving belt arrangement including two pulleys in the ratio 1:4 and timing belt
3	=	slip rings and brushes
4	=	toothed wheel and magnetic sensor
5	=	set of three bearings for main shaft
6	=	counter weight for balance
7	=	vertical strut and foil
8	=	baffle system
9	=	reference electrode (Ag-AgCl)
10	=	counter electrode (Pt)
11	=	hollow cylinder to hold baffles and RE
12	=	electrical wiring system
13	=	tank cover

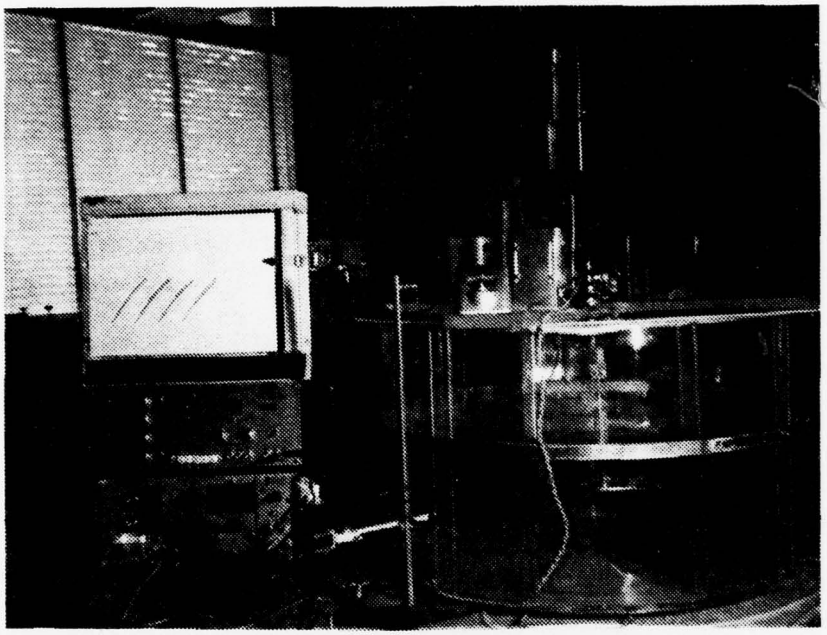

Figure 3. Exposure tank and apparatus for LPM-measurements

The vertical strut which holds the foil about 10 cm below the water surface, was not only streamlined to reduce drag, but also reinforced over the whole length of 21.6 cm by a stainless steel tube with an outside diameter of 0.476 cm. The inside diameter of 0.34 cm was just big enough to provide space for the wires from the two electrodes on the foil. This design eliminated a strut bending problem and increased the strength of the strut to an extent which would allow much higher velocities.

In the new design the foil was connected to the strut at an angle of ~9 degrees (see Figs. 5,6), in order to ensure a straighter flow over the foil coming over the front of the foil (not diagonal as it was in the case of Storm's design [1]). However, diagonal flow could never be overcome completely because of the limits in size of the foil and because of the circling motion itself.

The foil itself was also redesigned. As it was not the intention in this study to test proximate galvanic couples, the central recess provided in the foil of Storm was eliminated, so that the foil could be smaller, with less drag. In order to increase the exactness of the weight-loss determination the total weight of the sample was kept low with regard to the size of the exposed surface area. This was especially critical, because a rather low corrosion rate was expected (≈ 6 Mpy). Therefore the dimensions of the specimens were chosen to be 1.91 cm in diamter and .318 cm in height. The

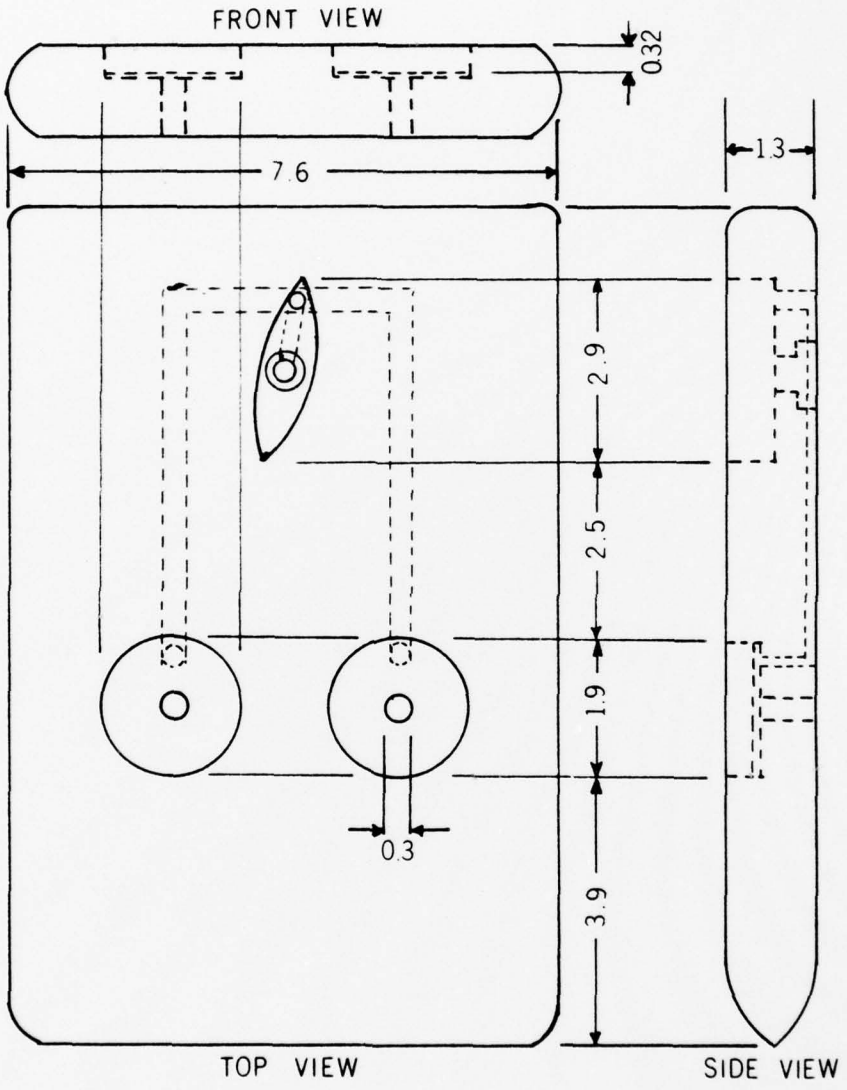

Figure 4. Detail of specimen-carrying foil (all dimensions in cm)

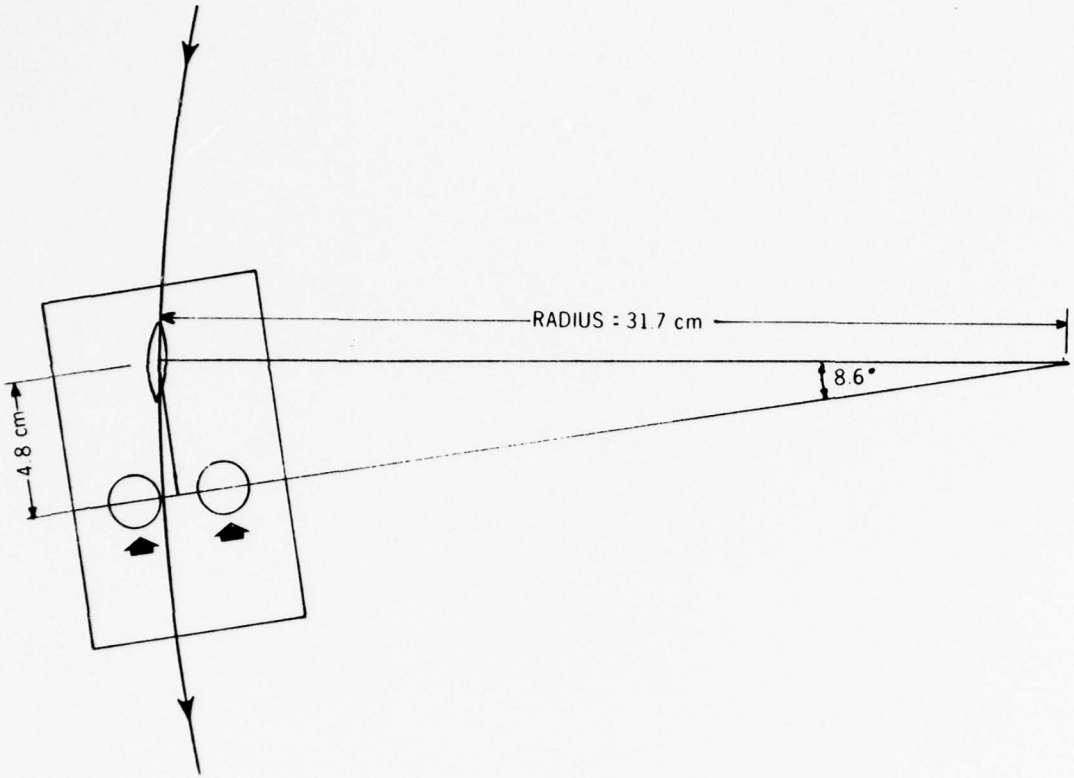

Figure 5. Schematic of the arrangement of the foil with respect to the supporting arm

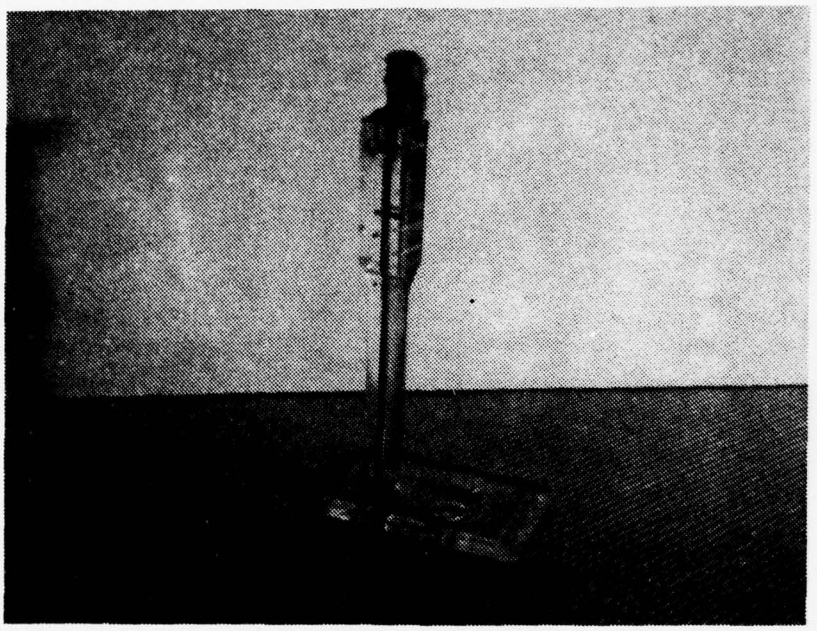

Figure 6. Strut and foil carrying one specimen

surface area (of the specimen) could hardly be increased because of two problems: first, making the specimen wider without increasing the foil width would result in difficulties in determining the fluid dynamic parameters across the specimen, because the closer the specimen is to the edge of the foil, the less comparable is the flow over the foil with the well known flow over a flat plate (as the foil surface could be approximated). Also, making the foil bigger increases the drag, causing additional problems with the propulsion system and with the stirring and splashing effect. The actual design therefore had to be a compromise (Figs. 4,6).

Another problem that had to be solved was the question of how to put the specimen into the foil, how to mount flush with the surface of the foil and how to keep the back surface of the specimen dry and uncorroded so as not to influence the weight-loss determinations. The holes in the foil were machined with small tolerances for a rather tight fit, but to ensure a good watertight mount the two methods were tested. Hot paraffin was filled into the holes where it instantly solidified and a pre-warmed specimen was pressed into the hole and the paraffin thereby again melted and was squeezed around the specimen filling up any space between hole and specimen; after solidification the mount was watertight and the surplus paraffin could easily be wiped off with alcohol. The other method used Silaster 732

Rtv General Purpose basically in the same fashion, only that the specimen did not have to be warmed up.

Both methods had the advantage that the specimen could be pushed out of the seat through a hole in the foil after the exposure and be cleaned very easily. But both were sometimes tedious and laborious, because one had to ensure that there was an electrical connection between the specimen and the platinum foil on the bottom of the hole in spite of the paraffin or the Silaster. This was accomplished by applying a fairly high pressure on the specimen by using a clamp and a clean plastic plate to protect the exposure surface. The advantageous and necessary side-effect of this method was that the specimen was as flush as possible with the foil-surface. Unfortunately, these methods could not prevent a tiny dip at the interconnection-line of the specimen and the wall of the hole, which could affect the general disturbance of the flow over the specimen. After each mounting a test with an ohmmeter showed whether there was an electrical contact between the specimen and the platinum-plate.

C. ELECTRICAL AND DRIVE SYSTEMS

A vertical strut containing two thin copper wires coming from the contacts in the foil was detachable from the horizontal support-arm via a BNC-connector. One general problem concerning the electrical system was to transport the signal from the electrodes moving on the foil to the

meter-equipment. As in the original design by Storm [1], the top of the main shaft held the brass slipring-brush arrangement which consisted of two sliprings, each with one brush. The brushes made out of phosphor bronze were rather stiff to exert enough pressure for good electrical contact, but at higher velocities a certain noise level could not be avoided completely because of the "wobbling" of the main shaft.

Another possible solution of this problem was a design which involved the same sliprings, but instead of the spring brushes, spring-loaded carbon brushes, normally used in electro-motors, should provide the contact to the sliprings. But probably due to poor choice of material the contact resistance was much higher than in the original design, and the noise was not remarkably reduced, so that the first design involving copper brushes was used for all experiments performed in this study.

The top of the vertical main shaft was fitted with the pulley wheel and a gear with 60 teeth. The latter was needed to determine the speed of the foil via a magnetic sensor close to the gear which sent a signal at every tooth to a digital counter. Using the displayed Hz-number the speed could easily be determined. A reading of 60 Hz for example represented a speed of 60 RPM or 1 RPS. As the circumference of the circle the foil described happened to be exactly 2 meters, 1 RPS equalled 2 m/sec. Because the radii to the specimens from the tank center were only a

little smaller or little larger than the radius to the center of the foil, the velocities of the specimens were assumed to be equal to the velocity of the center of the foil.

The shaft was driven by a pulley wheel which was actually a member of a timing-belt drive system, which also consisted of a 1/4 Hp DC-motor with a small gear pulley on its axis and a timing belt which transferred the speed of the motor to the greater pulley on the shaft in a 1:4 ratio. The original design had to be changed because of a problem of slipping at higher velocities when a V-belt system was used. Tightening the V-belt tended to enhance "wobbling" and increased the wear of the bearings and other moving parts. In order to improve stability of the system, an extra bearing was installed below the original two (see Figs. 2,7).

The demand for a higher velocity made also a stronger motor necessary. A DC-motor was chosen because of its advantage of being controlled easily by a DC-power unit up to its highest speed of 1800 RPM with a tolerance of about 1%. The unit used in the experiments was a Minarik Speed control Model sh-63 AH (Fig. 12) with a maximum output of 3.5 amperes. Unfortunately, even this stronger motor was not able to increase the velocity up to more than 7 m/sec for long time periods. (Note that the drag of the foil and strut increases with the second power of the velocity).

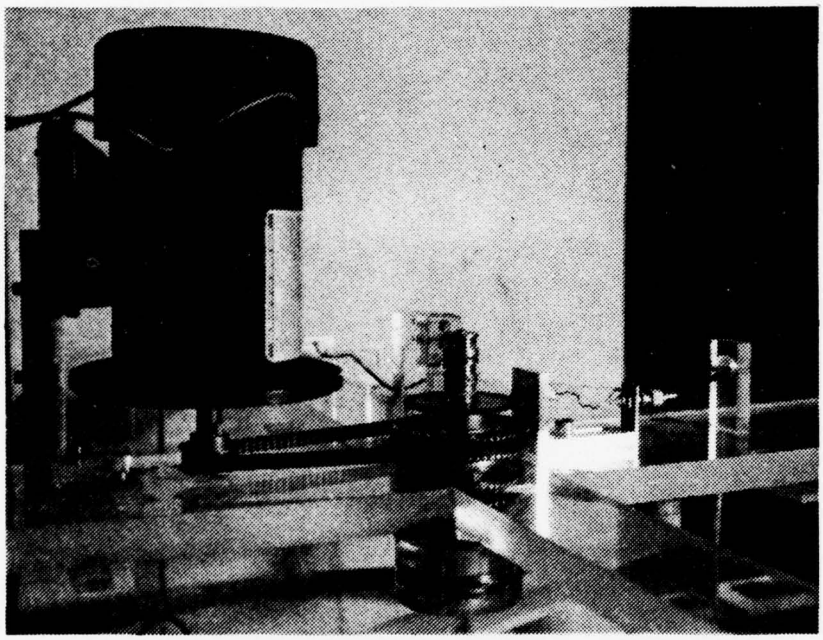

Figure 7. Electrical arrangement and drive system

III. EXPERIMENTAL PROCEDURE

A. GENERAL

In this study, several different methods were applied to determine corrosion rates, including (1) polarization resistance measurement, also called the linear polarization method (LPM); (2) potentiodynamic polarization curves; (3) weight loss determination; and (4) galvanic current measurements (for galvanic couples). The material studied was 90/10 copper-nickel (CDA Alloy 706). Specimens were tested as single metal coupons and as members of galvanic couples with platinum. The electrolyte in all cases was synthetic seawater prepared by standard methods (Appendix A).

Samples were cut and machined from a 30.5cm x 20 cm x 1.9cm (12in x 8in x 3/4in) plate delivered by Anaconda Company Brass Division, Detroit. For specification see Table 2. The size of the specimen corresponded to the dimensions of the hole in the foil (Fig. 4) such that there was a fairly tight fit: they were small, flat cylinders with a diameter of 1.9 cm and a height of .318 cm.

Before the test each specimen was ground with fine grinding paper with grits in the sequence of 0,00,000. After that they were thoroughly rinsed with alcohol and dried. Figure 33(b) shows a typical surface ready to be exposed. The weight was determined to the first decimal

Table 2

Specification of 90-10 Cu-Ni Alloy (CDA 706)

Mil-C-15726 E Amend=2
Constituents:

	%
Copper	87.4
Nickel	10.4
Iron	1.5
Manganese	0.49
Zinc	0.13
Silicon	0.02
Tin	0.02
Phosphor	0.013
Lead	0.01
Sulphur	0.001

no Mercury contamination

no Ferrum

Properties:

Yield Strength	=	24 KPSI
Max. Tensile Strength	=	53 KPSI
Elongation (at 2 in)	=	40%

Producer:

Anaconda Company Brass Division, Detroit

of a milligram, as accurate as it was possible with the Sartori balance. Then the specimen were mounted as described before and cleaned carefully in situ with alcohol to get rid of the excess Silaster. Tests showed that it was no problem to achieve the same clean surface as before mounting. Conductivity tests with an ohmmeter checked whether good electrical contact existed between the specimen and platinum plate. Then the holes through the foil were filled with Silaster or liquid paraffin to ensure watertight enclosure.

The foil, including the vertical arm, was connected mechanically to the horizontal support arm and the BNC-plug provided the necessary electrical connection. As soon as possible the motor was started to avoid an unwanted length of time of static exposure before the velocity exposure. This delay time was chosen to be a constant 1 min for every run to achieve equality, although the actual time needed for hook up was often shorter.

Depending on the kind of run the appropriate method to determine the corrosion rate was chosen as described earlier and it was tried to start the measurements as early as possible. But due to the method itself, a short delay time could never be avoided when applying the LPM method, so that it was impossible to determine the corrosion rate at time zero as it was possible with the ZRA for galvanic couples. The number of measurements taken in the first hours of each run was considerably higher than later, because

after an exposure of time of about 4-6 hours a very low rate of change of corrosion rate was noticed (see Results and Figs. 17,18,19). Some of the single metal corrosion tests were run for 48 hours, because after 24 hours little corrosive action was noticed. Even 48 hours were too short for good weight loss determination with the desired accuracy, but individual runs could not be extended further due to lack of time. Runs of coupled specimens were made for 24 hours because the corrosion rate was considerably higher.

After the runs the specimen was cleaned with a mixture of HCL, H_2SO_4 and water in the ratio of 5:1:4, as recommended by ASTM Standard [15]. Because the oxidation layer sometimes was difficult to remove just by putting the specimen into the solution, a soft brush helped to clean the surface completely. After rinsing it with alcohol and distilled water and drying it, the weight after exposure was measured and the weight-loss could be determined. The specimens were kept in a vacuum container to prevent the corroded surface from corroding further until the microscopic observations were finished.

During the tests the temperature was measured and after each run the conductivity and the pH-value of the electrolyte were determined by using a test set from Markson Science Corporation called Electromarks Analyzer. The oxygen content was measured by a Hach Model OX-2P Dissolved Oxygen Test Kit.

The surface of the specimen was later researched by using different microscopes. For low magnification from 10 to 70 X a Bausch and Lomb stereomicroscope was used, whereas for higher magnifications up to 400X a Balplan conference microscope was used. In order to increase the magnification further and to achieve much better depth of field the Scanning Electron Microscope (SEM) from Cambridge, Model S4-10 was used, with which it was able to get clear micrographs at least up to 2000X. All pictures were taken by a Polaroid camera using a high speed film.

In the course of the tests some runs were conducted without the LMP-method, partly because the equipment was not always available and also because it was of interest to check whether the intermittant application of the LPM-method influenced the overall corrosion rate as determined by weight loss. Some others were needed to obtain standard polarization plots at different velocities. Also a few static exposures were done by using the same arrangement as in all the other tests, but with the foil not moving. Three test velocities were used: 2 m/sec, 4 m/sec and 6 m/sec as well as some measurements at zero velocity. Although higher velocities were attempted, the velocity of 6 m/sec turned out to be just below the maximum which could be reached with the chosen equipment (see Table 3 for a list of experiments).

Some parameters like pH-value, conductivity and temperature which could affect the corrosion behavior of the test

Table 3

List of Experiments Performed

Run	Time (hr)	Velocity (m/sec)	Measurements	Remarks
1	24	2	WL, LPM, ZRA	galvanic couple
2	24	2	WL, LPM, ZRA	galvanic couple
3	24	4	WL, LPM, ZRA	galvanic couple
4	4	4	LPM, ZRA	small galvanic couple
5	20	6	WL, LPM, ZRA	galvanic couple
6	24	2	WL, LPM	single, 2 specimens
7	48	4	WL, LPM	single, 2 specimens
8	45	6	WL, LPM	single, 2 specimens, LPM stopped after 3 hours
9	.5	2	LPM, ZRA	galvanic couple, test for transient behavior
10	.5	4	LPM, ZRA	see RUN 9
11	.5	6	LPM, ZRA	see RUN 9
12	.5	6	LPM, ZRA	see RUN 9
13	22	stagnant	WL, LPM	single, 1 specimen
14	45	2	WL	single, 1 specimen
15	24	4	WL, LPM	single, 1 specimen
16	24	6	WL, LPM	single, 1 specimen
17	24	2	WL, LPM	single, 1 specimen
18	24	6	WL, LPM	single, 1 specimen

Runs 19 to 24 were shorter runs using only LPM to determine transient behavior after initial phase.

Several more runs were performed to achieve polarization plots at 2 m/sec, 4 m/sec and at 6 m/sec.

material remained throughout the test runs fairly constant: the pH-value decreased after the first runs from 7.85 to about 8 where it stayed constant; the conductivity was a little lowered from about 4×10^4 μmhos down to 3.7×10^4 μmhos because of some salt crystallization on the walls of the tank. The temperature of the water was in general equal to the room temperature of 20°C, but during the higher velocity tests the electrolyte was heated up to 24°C due to high drag at those velocities (see discussion of results at 6 m/sec).

B. LINEAR POLARIZATION METHOD (LMP)

The word "linear" in this name is an exact description of the behavior of the applied current as a function of the electrode potential within a range of plus or minus 10 mV (i.e. 10 mV more noble or active) over the corrosion potential (see Fig. 8).

The relation:

$$\text{Resistance} = \Delta E/\Delta I \text{ (applied)} = \frac{\beta_a \beta_c}{2.3\, i_{corr} (\beta_a + \beta_c)}$$

opens a way to determine the corrosion current by solving for I_c:

$$I_c = \frac{\beta_a \beta_c}{2.3(\beta_a + \beta_c)} \frac{\Delta I_{appl.}}{\Delta E}$$

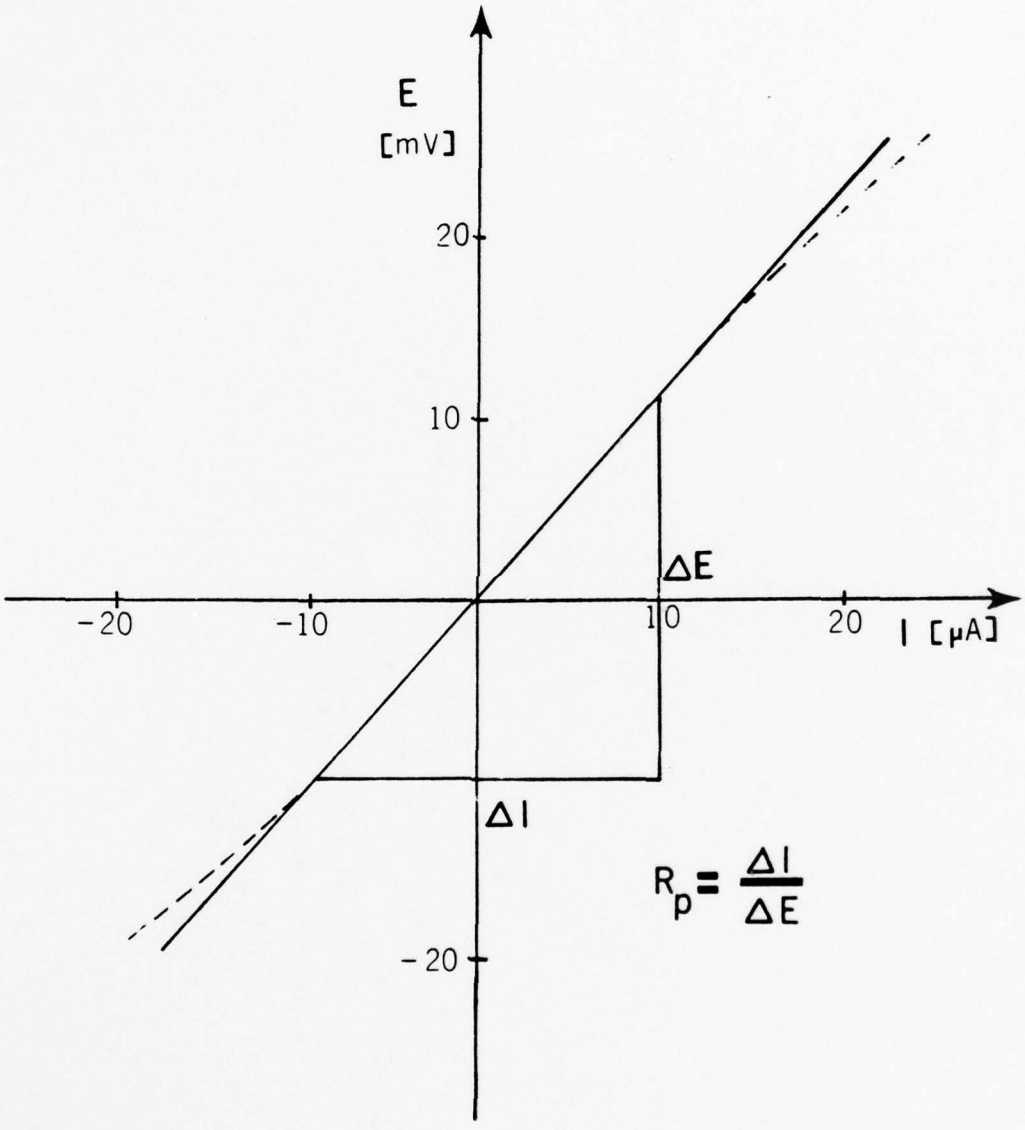

Figure 8. LPM-measurement curve

where β_a and β_c are the anodic and cathodic Tafel slopes of a polarization diagram and $(\beta_a \cdot \beta_c)/(\beta_a+\beta_c)$ is a constant k .

Stern and Geary determined the value of the constant by assuming a theoretical value of 0.12 volts for the Tafel slopes. Pye [2] also calculated k for various materials and came to the same result of k = 0.026, so that the final formula for the corrosion current density reads:

$$i_c = 0.026\ I_{appl.}/\Delta E \cdot Area$$

where

i_c = corrosion current density ($\mu A/cm^2$)

Area = area of the exposed surface (cm^2).

The value of k determined in this study using the data from the polarization curves achieved by the experiments amounted to 0.024, which was very close to the theoretical value for copper.

The LPM method provides a rapid measurement of relative corrosion rates or changes in corrosion rates, with much better reliability than for measuring the actual corrosion rate, because the accuracy of the LPM method is a concern of many electrochemists, for example of Pye [2] and Stern [3]. Generally the corrosion rate determined by the LPM

method is within a factor of two or three of the actual corrosion rate.

The advantages of LPM are that this method is not nearly as tedious, difficult and time-consuming as conventional weight loss determinations, and it can be applied to electrodes which are very difficult to reach, for example in pipes. Also because of the possibility of measuring small corrosion rates and the transient behavior of the corrosion, this method if preferable to others.

In a recent report by Macdonald and Syrett [10] the LPM-method and other polarization resistance methods, the AC impedance method and the potential step method, were used to study seawater corrosion in flowing electrolyte. The agreement of the three methods with weight loss determinations was very good. Thus, one can assume that the LPM-method is quite reliable if correctly applied. In this paper two problems concerning the LPM-method are mentioned. First, any electrochemical reaction whether it leads to corrosion or not will contribute to the current; for example, hydrogen oxidation can give rise to an anodic current which is not distinguishable or separable from the corrosion current when measured by the LPM-method. The other problem refers to the polarization resistance $R_p = dE/dI$, which,as experimentally determined, actually is the impedance of the interface, containing capacitive and inductive components in addition to the ohmic resistance when time dependent signals are involved. Only at low

frequencies are the capacitive and inductive parts negligibly small. Thus slow scan rates will help to avoid this problem. In these experiments a scan-rate of 1mV/sec, the lowest rate possible with the equipment available, was applied, in order to minimize the problem mentioned above.

In the LPM measurements of this study the IR drop in the electrolyte was neglected, because the resistivity of sea-water is fairly low ($\approx$ 25 Ohms per cm) so that this resistance is small compared to the Linear Polarization resistance R_p. This assumption is supported by the fact that the result with the silver-silverchloride reference electrode is not as much affected by the distance between the reference and the working electrode as with other reference electrodes like the Standard Calomel Electrode (SCE).

During these experiments LPM measurements were used to determine the corrosion rate of a single metal as a function of time and velocity. These data were then compared to those ones obtained from weight loss determination. The equipment for these measurements consisted of a PAR potentio-state/galvanostat Model 173 and Universal Programmer, Model 175, both from Princeton Applied Research, and an X-Y Recorder 7040a from Hewlett-Packard (see Fig. 9).

Independent LPM data were gathered using a standard laboratory corrosion cell and the circling foil tank. The standard laboratory cell procedure used a silver-silver chloride reference electrode, two carbon sticks as the counter electrode, and the specimen itself as the working

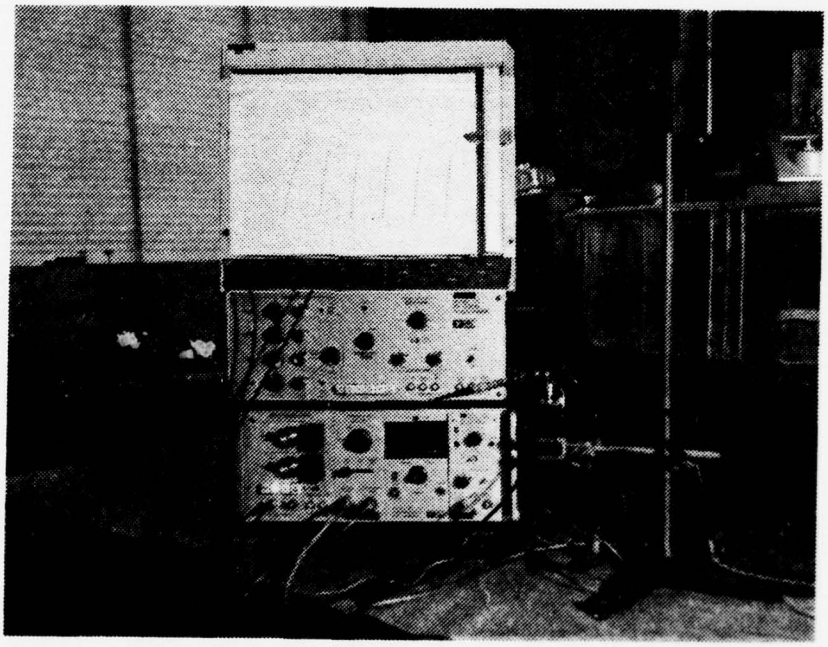

Figure 9. Equipment needed for LPM-determinations: potentiostat, programmer and x-y recorder

electrode, altogether in a beaker filled with synthetic seawater which was stirred by a magnetic device. For the tests in the circling foil tank, the counter electrode was a platinum plate, placed in the center of the bottom of the tank to maintain the same distance to the rotating foil at all times. (See Figs. 2 and 3.) In two special tests the platinum counter electrode was put together with the specimen on the foil, but no apparent difference was noticed, so that in the further tests the counter electrode centered on the bottom was used in order to be able to place two working electrode specimens on the foil at once. In this way one specimen could be used for weight loss determination and the other for macroscopic and microscopic examination of the corrosion of the exposed surface.

Some of the actual results of the LPM method are shown in Figs. 16 to 20. The experiments, including the calibration before the tests, were performed corresponding to the manuals of Princeton Applied Research [4] and Hewlett Packard [5].

C. POTENTIODYNAMIC POLARIZATION CURVES

The polarization method is essentially similar to the LPM method concerning the equipment used, and as the method itself is widely known, a detailed description will not be given here. The same manual used in the LPM method applied also in these tests. Although the polarization method is usually performed with the standard corrosion cell, the

author tried to support and compare the corrosion data gained by other methods in this research by obtaining polarization plots for specimens in the circling foil tank at different velocities, as well as with the standard laboratory cell. For a typical polarization plot see Figures 21-23. The results of these methods in relation to others will be discussed later in Chapter IV.A.3.

D. ZERO-RESISTANCE AMMETER (ZRA)

The design of the foil (see Fig. 4) allowed tests involving natural galvanic couples. Because the corrosion rates of the copper nickel alloy were expected to be very low and the time for extended tests was not given, the author intended to make use of the accelerated corrosion of a galvanic couple, in order to get more distinctive features of the corrosion behavior and especially of the corroded surface. Furthermore, galvanic coupling made it possible to examine the relative corrosion rate changes with respect to time at different velocities by using a Zero-Resistance Ammeter (ZRA). Because those were the only two reasons to use a ZRA, a detailed discussion of the corrosion of a galvanic couple will not be given.

The ZRA has been described by different authors. G. Lauer and F. Mansfeld [7] performed different tests with a ZRA and V. Fraunhofer and Banks [8] mentioned in their book (on applications of the potentiostat) the electrical view of a ZRA and the possiblity of using a potentiostat

as a ZRA as J. Devay et. al [9] first tried. Corresponding to the descriptions given by references 7 and 8, Mr. Tom Christian, electronics technician in the NPS Department of Mechanical Engineering, constructed a ZRA which operated well in this work. A schematic drawing of the ZRA is shown in Figure 11.

In the arrangement actually used in these tests electrode I (working electrode) was a copper nickel specimen, electrode 2 (counter electrode) was a platinum foil and the reference electrode was the silver-silver chloride electrode. The size and distance of the counter electrode were varied to achieve different corrosion rates. Because the basic interest lay in the determination of the transient behavior and therefore only in the relative change was important, the exact area ratio was not significant as long as it was kept constant. The two ZRA output voltages E_o and V_o (see Fig. 11) were measured by two digital voltmeters (Weston, Model 1240 and Model 4444) and recorded versus time by a stripchart recorder (Moseley Autograf Model 7100 Bx) (Fig. 10).

E. HOT FILM ANEMOMETRY

Since one purpose of this study was to find a correlation between corrosion rate and hydrodynamic variables, one has to determine those variables. One variable is simply the relative velocity of the sample with respect to the fluid, in this study the relative velocity of the moving

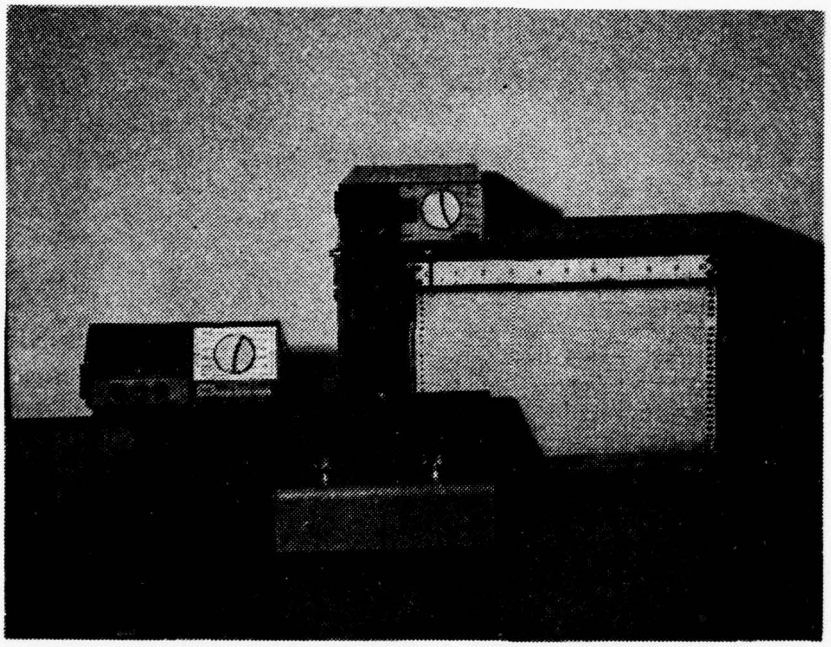

Figure 10. ZRA equipment

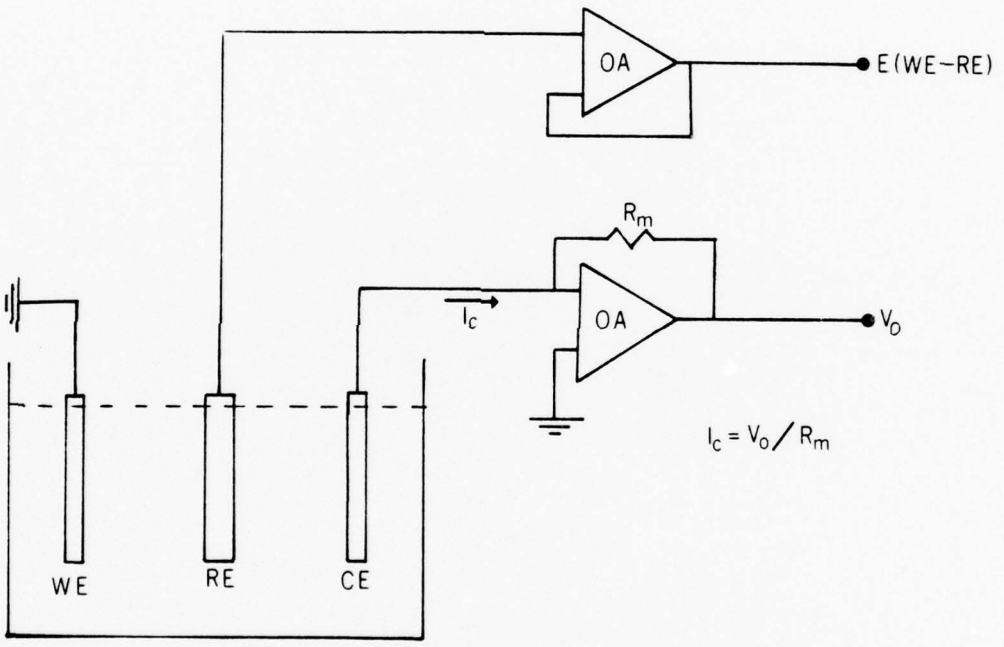

Figure 11. Schematic of ZRA

moving foil with respect to the static electrolyte. If one neglects any possible velocity of the electrolyte, the relative velocity can be determined most simply from the RPM of the main shaft converted into a linear velocity of the specimen. Another variable, the non-dimensional Reynolds number, is calculated by using flow and fluid properties as mentioned before. The Schmidt number is also determined without any experiments just by using viscosity and diffusion coefficient (see Chapter V). A variable which can be obtained only by direct measurements is the turbulence intensity, defined as the ratio of the fluctuation in velocity and the mean velocity ($U'/\overline{U}$). In the present work, only fluctuations in the direction of net flow (horizontal or x-direction) could be determined with the equipment available, so that the vertical component in the y-direction will be neglected.

For this study an equation was derived from relations given by Hinze [34] and by the manual for the TSI test equipment [35] in order to calculate the turbulence intensity:

$$\frac{U'}{\overline{U}} = \frac{4\ e'\ V}{V^2 - V_o^2}$$

where

e' = turbulence, read on the RMS-meter (Volt)

V = bridge voltage, read on Digital-meter (Volt)

V_o = Voltage at zero velocity (Volt) .

In order to measure the unknown quantities in this equation the following equipment was used: (Fig. 12)

- TSI Model 1050 constant temperature anemometer,
- TSI Model 1051-1D monitor and power supply, and
- TSI Model 1060 RMS voltmeter;

two types of hot film probes were used (Fig. 13):

- TSI Model 1231 conical probe, and
- TSI Model 1261 miniature boundary layer probe.

Probe 1231 is a widely-used, rugged sensor that inhibits contamination and resists breakage, but its sensitivity is limited due to its shape, the size of the cone and the position of the sensor tip which does not allow measurements closer than 1 mm to the surface. Also, it is difficult to determine the exact distance to the wall.

The 1261 probe is designed to measure velocity and turbulence as close as 0.1 mm to the surface, in order to determine the hydrodynamic boundary layer. However, this probe is very sensitive to contamination and mechanical load. Figure 14 shows the design to hold the probe above the surface of the foil. Thin plates of a known thickness put under the protecting pin could be used to determine the exact distance to the wall, which is 0.125 mm without any plate.

All unknowns in the turbulence intensity equation, shown above can be read directly from the instruments described. The voltage at zero velocity, V_o, has to be

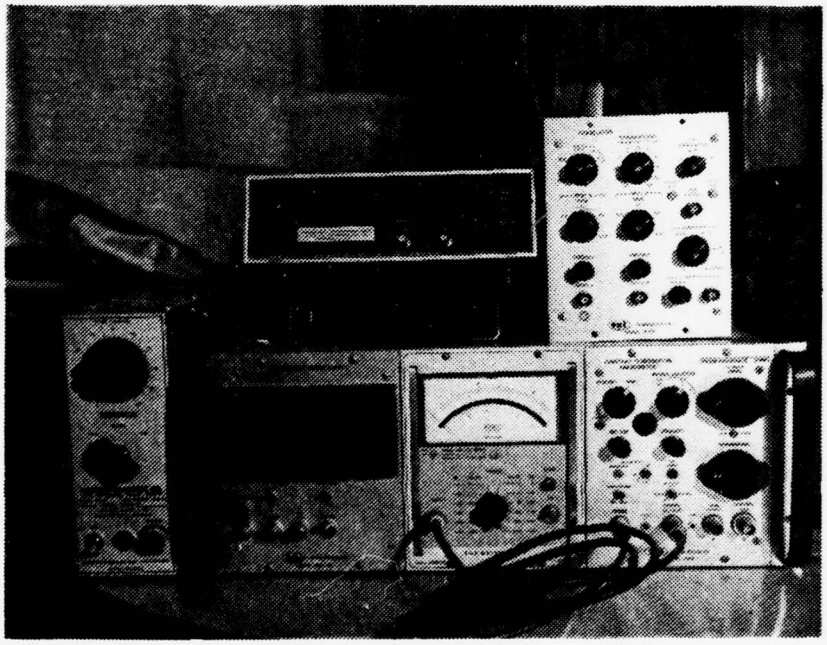

Figure 12. DC-power controller for drive system; counter, and equipment for hot-film anemometry

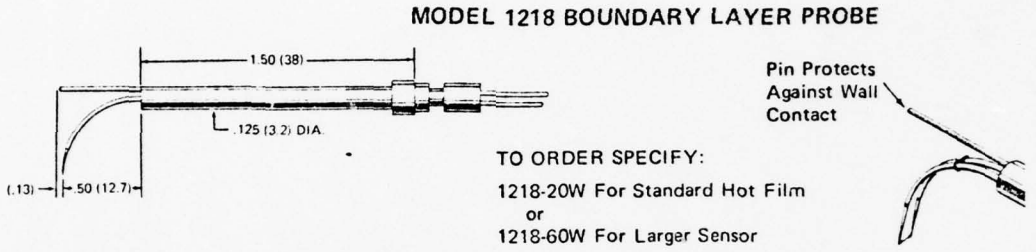

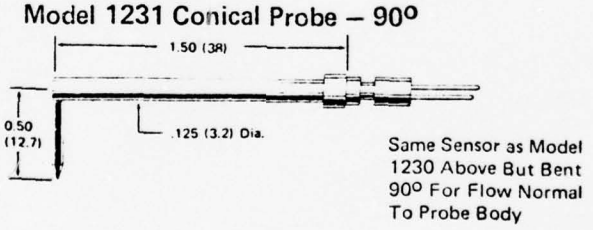

Figure 13. Probes used in hot-film anemometry (note: Model 1218 is equivalent to Model 1261 used in these tests)

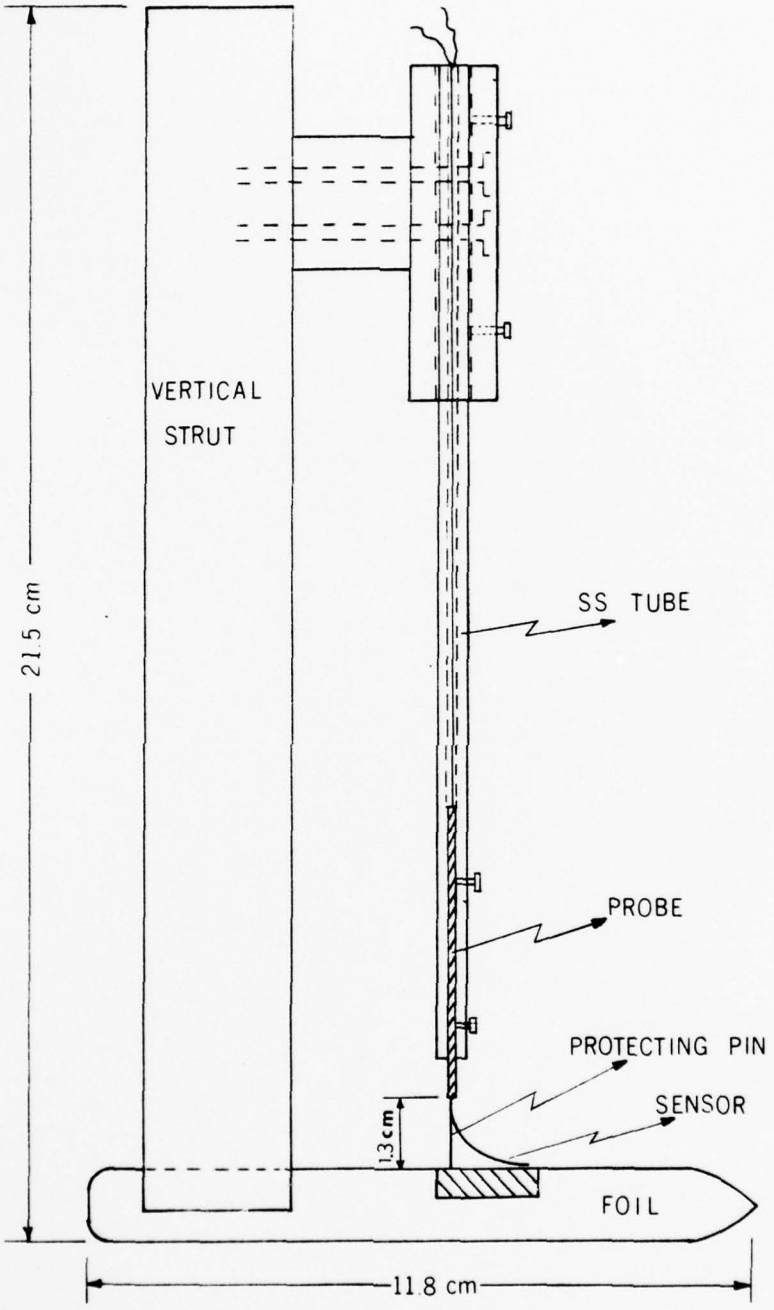

Figure 14. Strut-foil arrangement carrying hot-film probe

calculated from a plot of e^2 versus the square root of the apparent velocity (Fig. 15). The apparent velocity U is obtained from the RPM and e is the voltage given on the digital meter. V_o^2 is the intersection of the extrapolated line of e^2 versus the square root of U with the e^2 axis (not as described by Storm [1] as the intersection with the axis of square root of U). The value of V_o could be approximated by measuring e at zero velocity directly, but one has to be aware of the possible error due to the influence of free convection at a zero velocity whereas it is negligible at higher velocities. It would have been desirable to measure e at lower velocities than 2 m/sec, but at those velocities the counter which measures the RPM was not sufficiently accurate.

Unfortunately, the anemometric measurements were subject to some problems. First, due to the sensitivity of the boundary layer type probe to mechanical wear it failed before any reliable measurments were obtained and replacement was not possible due to lack of time. Thus the boundary layer thickness was not determined as intended. Using a less sensitive probe, turbulence intensity was measured at distances from the wall greater than 1mm, and with sensitivity probably not sufficient to completely detect the size of the eddies of the turbulence structure. Therefore the result must be regarded as insufficiently descriptive. Another difficulty in determining the turbulent intensity by using a hot film probe was the existence of

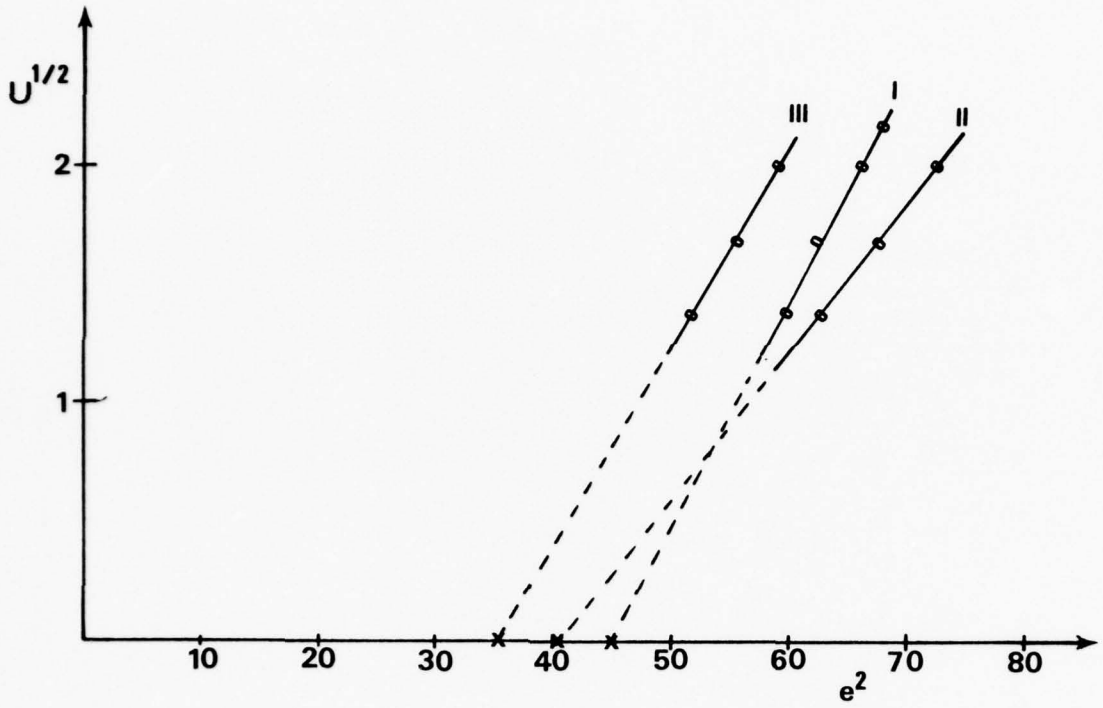

Figure 15. Plot for the determination of $V_o(x)$ for Test I, II and III

wake due to the motion of the foil through the water. Because of the relatively small size of the tank the foil continuously ran through its own wake, with the effect more pronounced at higher velocity. In this situation, the probe might only measure a kind of steady turbulence occurring in a special order depending on the velocity and the geometry of the tank and not the turbulence intensity directly caused by the motion of the plate through the water if the free stream were rather free of turbulence. A spectrum analysis would have helped to determine the size and energy of the eddies, but because of the problems mentioned above and the noise problem of the system which made the results even more unreliable this determination was renounced.

The actual results (Table 4) seem to be rather high, but having observed the amount of big scale turbulence in the tank at higher velocities, one could regard the results for a distance of h = 1.5 cm to be reasonable. This turbulence intensity was assumed to be equal to the free stream turbulence intensity. A result of 3% is rather high but appears not to be impossible. Considering this high free stream intensity the result of 30% for the intensity close to the foil seems not to be unreasonable. The velocity determinations by using the bridge voltage never dropped considerably, so that the probe must never have been brought inside the boundary layer, as expected.

Table 4

Results of Hot Film Anemometry

I. Distance from the wall : 1.5 cm

Velocity	$\frac{U'}{\overline{U}}$
2 m/sec	0.035
3 m/sec	0.045
4 m/sec	0.054
4.7 m/sec	0.063

II. Distance from the wall : 1.5 mm

2 m/sec	0.24
3 m/sec	0.197
4 m/sec	0.21
3 m/sec	0.203
2 m/sec	0.238

III. Distance from the wall : 1 mm

2 m/sec	0.326
3 m/sec	0.247
4 m/sec	0.26
3 m/sec	0.253
2 m/sec	0.302

IV. RESULTS

A. CORROSION RATES FROM DIFFERENT METHODS

1. Weight Loss Corrosion Rate Results

The weight difference before and after exposure determines the corrosion rate. For the calculation of the corrosion current density i_c ($\mu A/cm^2$), the equation number 1 in Table 5 was applied. By a relation (see same table) between i_c and the weight loss rate it was possible to determine the corrosion rate in Mpy or in μmpy.

The accuracy of the weight loss determination depends beside other factors on the accuracy of the scale which can be read to one tenth of a milligram exactly. Since the weight loss averaged about 1-3 mg, the uncertainty due to the scale alone was about 5-10%. The uncertainty whether some base metal has been brushed off or whether all the corrosion product could have been wiped off the surface by the cleaning action of the HCl-solution including the scrubbing is difficult to set equal to a number, but an uncertainty of about 10% appears to be reasonable.

2. LPM Corrosion Rate Results

The calculation of the corrosion rate by the LPM-method applied the equation 4 in Table 5. As already described the measurement was performed 2 minutes after the velocity started and the frequency of the measurements decreased with increasing time (Figs. 17, 18, 19 and Tables 6, 7, 8).

Table 5

Formulas For Corrosion Rate Determination

1. From weight loss to corrosion current density, i_c:

$$i_c = \frac{Wl \cdot F \cdot 10^3}{(A/Z) \cdot time \cdot area}$$

Wl = mg
F (Faraday's constant) = 96500
A/Z = 1 equivalent (see next page)
time = seconds
area = cm^2
i_c = $\mu A/cm^2$

2. From weight loss to Mpy:

$$Mpy = \frac{534 \cdot Wl}{Area \cdot time \cdot rho}$$

Area = in^2
time = hours
Wl = mg
rho = g/cm^3
Mpy = milli-inch per year

3. From i_c to Mpy:

$$Mpy = \frac{.13 \cdot i_c \cdot (A/Z)}{rho}$$

4. LPM-method to i_c:

$$i_c = \frac{k \cdot dI}{dE}$$

k = 0.026
dI = μA
dE = Volt

Table 5 (Cont'd)

5. From Mpy to μmpy:

$\mu mpy = 25.4\ Mpy$ μmpy = micrometer per year

6. Determination of (A/Z) of Cu-Ni (90/10):

- From Pourbaix diagrams valence for Cu = 1
  for Ni = 2

- $\bar{A} = A_{Cu}\, x_{Cu} + A_{Ni}\, x_{Ni}$ x = mole fraction

  $\bar{Z} = Z_{Cu}\, x_{Cu} + Z_{Ni}\, x_{Ni}$

- $$x_a = \frac{\text{weight \% of alloy}}{\text{mol. weight}_a \cdot \text{number of total moles}}$$

  $$\text{number of total moles} = \frac{\text{weight}_a}{\text{mol. weight}_a} + \frac{\text{weight}_b}{\text{mol. weight}_b} \text{ etc.}$$

- other components are neglected

- result: <u>A/Z = 56.6</u>

In order to increase the readibility of the slope on the plots, the sensitivity of the current axis was adjusted very high which resulted in a slope of about 45° instead of 80° at a lower sensitivity (Fig. 16). This change to a higher sensitivity, however resulted in a noise problem caused by the "wobbling" slip rings, especially at 6 m/sec. But even with small fluctuations of the line the readings were more accurate with the higher sensitivity and one could read the current correctly with ± 3%. Thus, the uncertainty became about 10%, because the absolute value of I ranged from 25 to 50 μA. Neglecting the IR-drop was another possible origin for an error. But as already mentioned, the IR-drop is small and if there were any influence at all, the IR drop would be greatest at a higher corrosion current.

One other concern was the fact that the readings of the specimen having double the surface (exposed) were not double as high as one could expect, but were only about 50% higher, which in the end resulted in a significant difference in the corrosion current densities. One possible reason for this phenomenon might be the IR-drop. Since the corrosion current increases proportional to the exposed surface, the IR-drop does the same and might become more significant. Furthermore, since the corrosion current increases with velocity, an IR drop effect increases with increasing velocity. These assumptions are considered to be hypothetical and will have to be proved by further experiments.

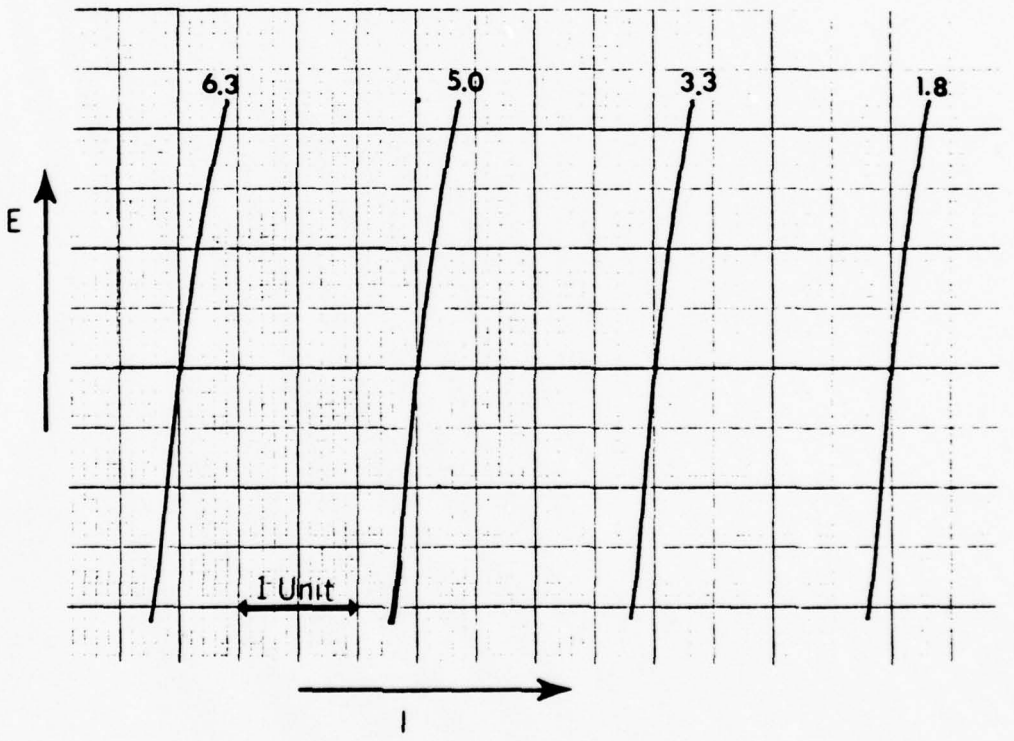

Figure 16. Actual LPM-results at different velocities (velocity = m/sec, E = 10 mV/unit, I = 100 μA/unit)

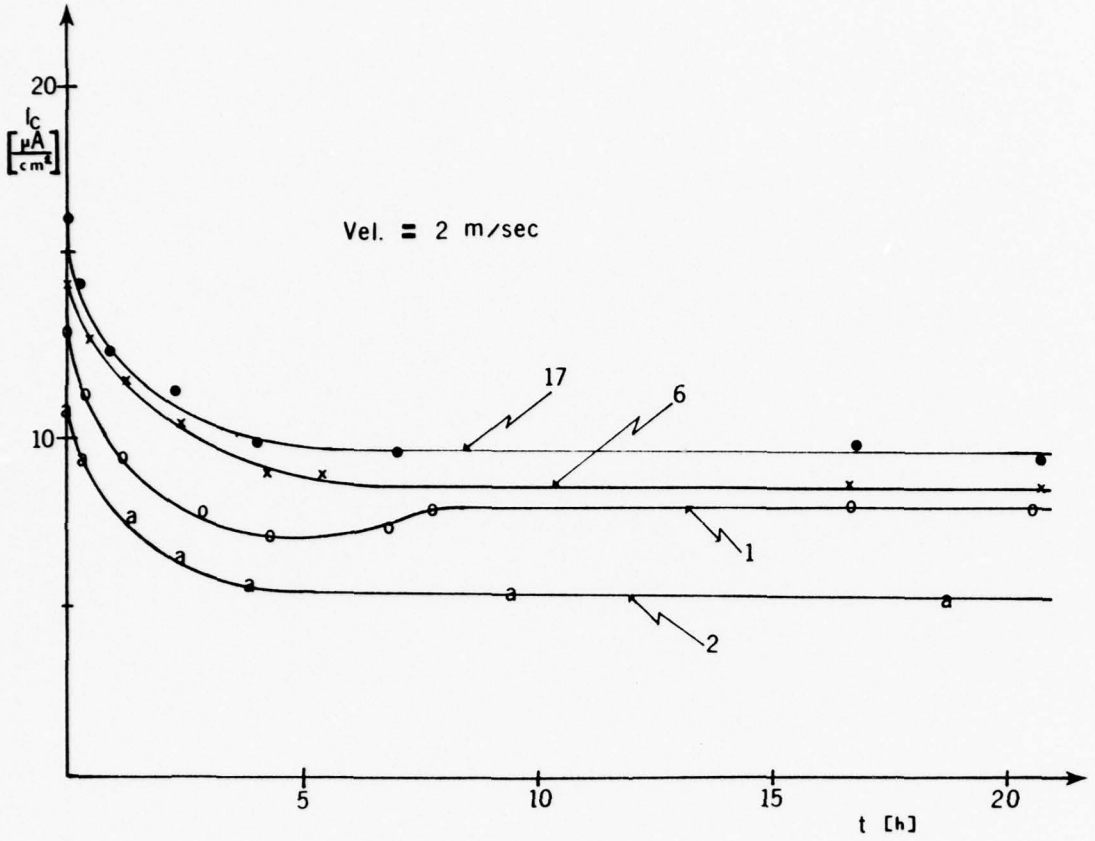

Figure 17. Corrosion rates versus time as determined by using LPM at 2 m/sec (number on curves refers to sequence number of test-run)

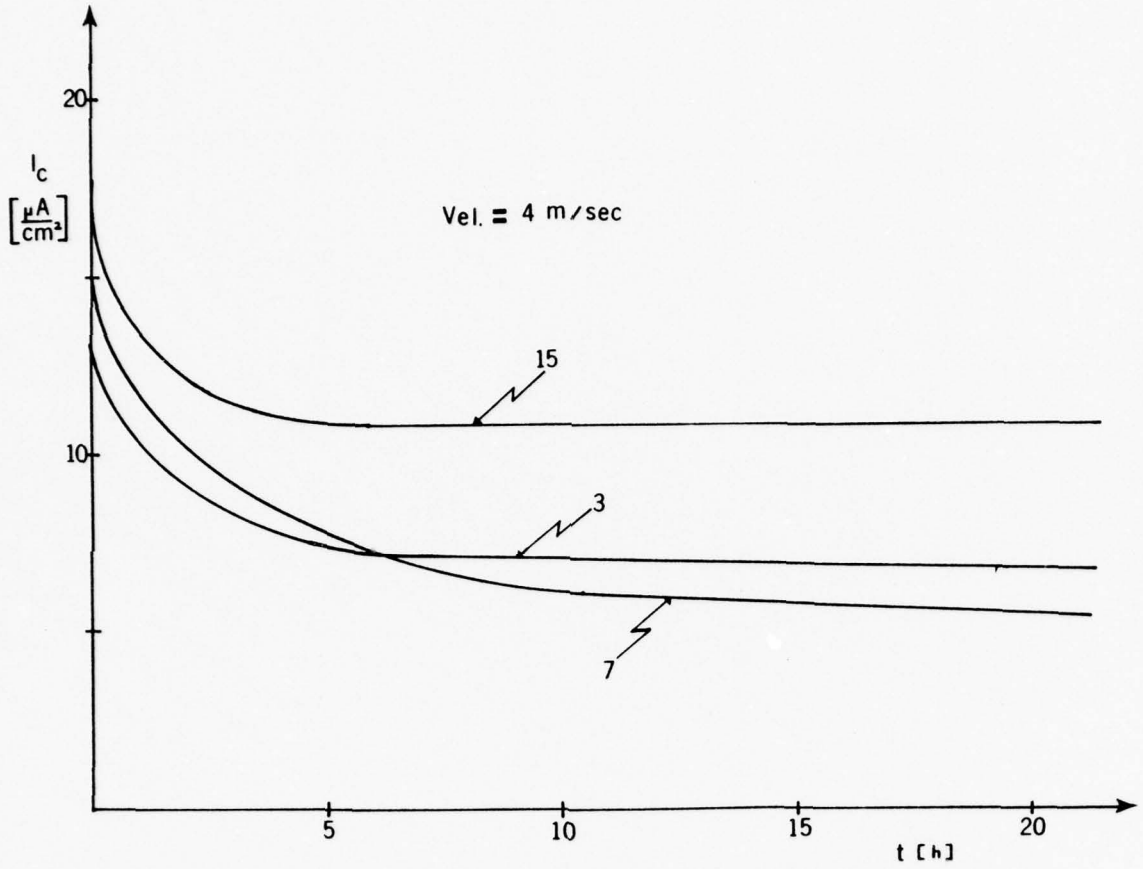

Figure 18. Corrosion rates versus time as determined by using LPM at 4 m/sec (number on curves refers to the sequence number of test-run)

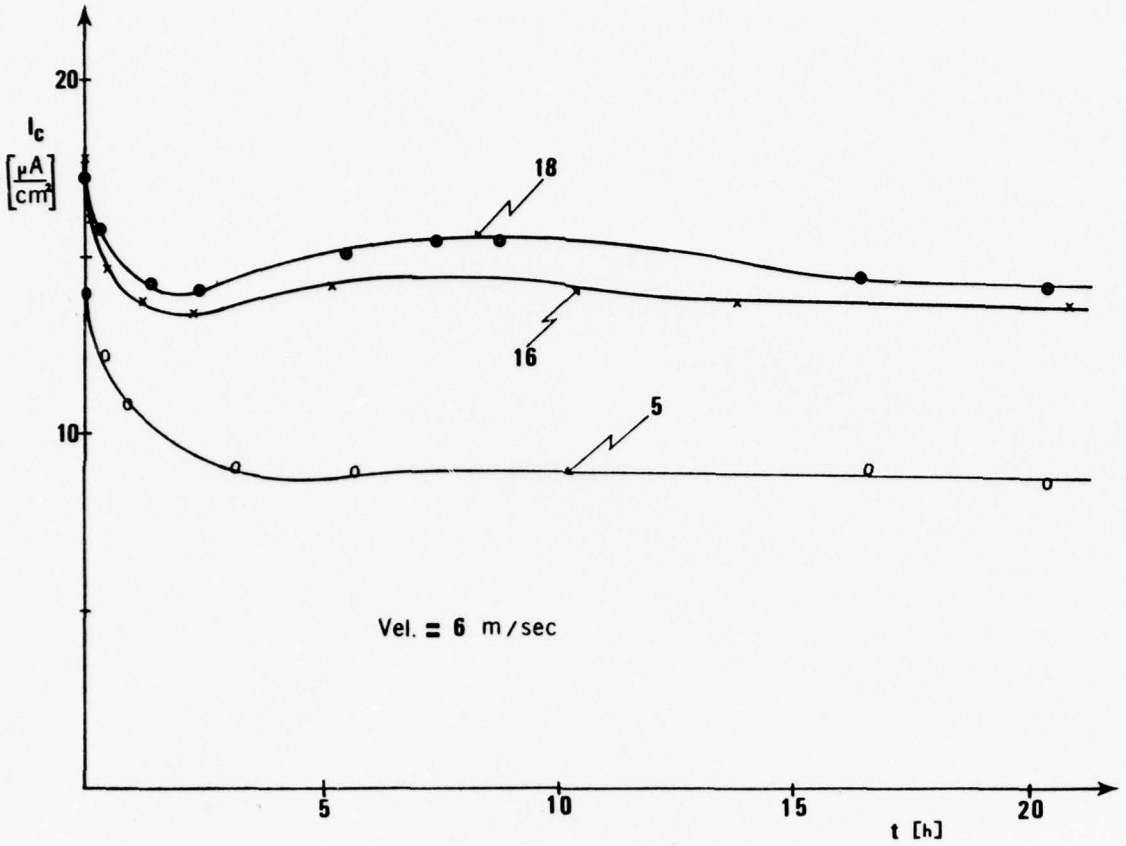

Figure 19. Corrosion rates versus time as determined by using LPM at 6 m/sec (numbers on curves refer to the sequence number of test-run)

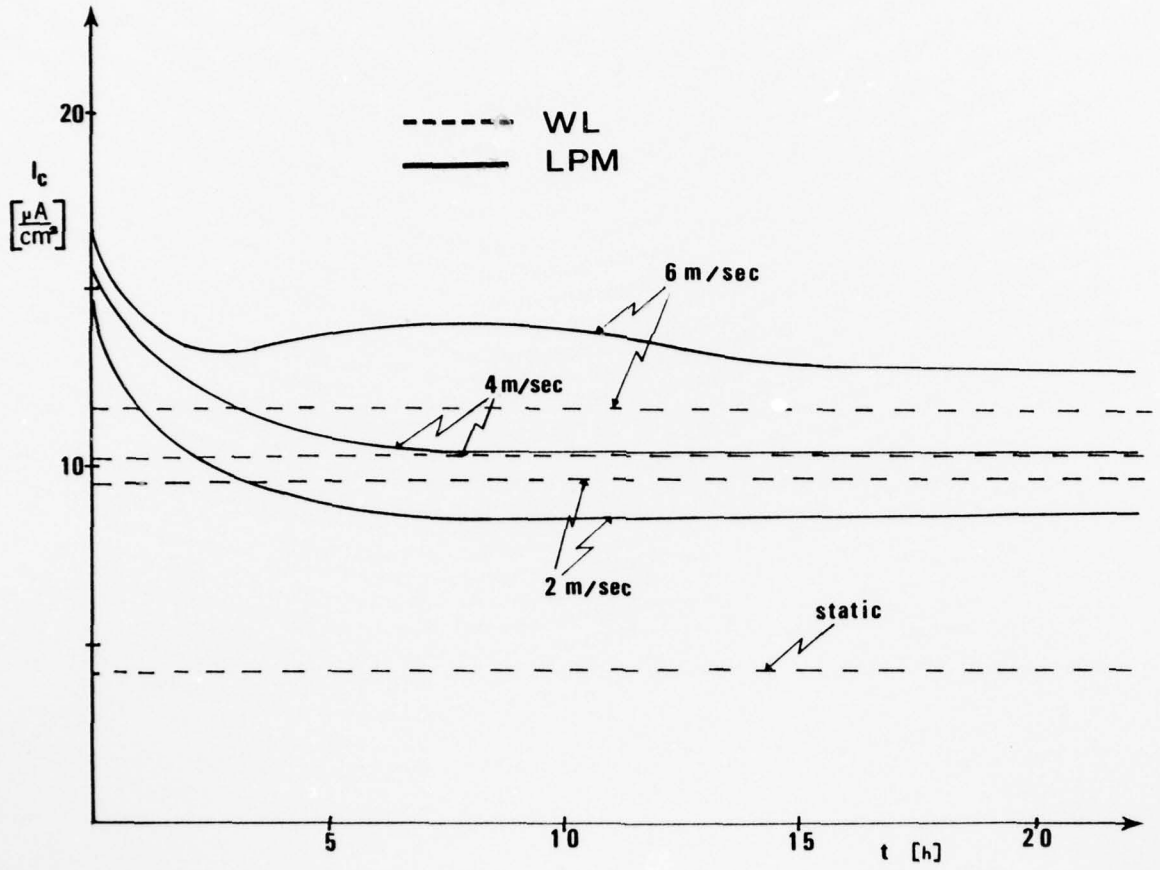

Figure 20. Comparison of averaged corrosion rates plotted versus time at given velocities determined by weight loss and LPM method

Since the corrosion rate changes with time, the individual points obtained by the LPM method were plotted versus time. In order to obtain data comparable to that gained by other methods an average value of i_c was determined. This was accomplished graphically on the plots: the horizontal line which divided the area between the curve and the I-axis into two equal parts determined the average corrosion current density $\bar{i}_c$. Including this procedure in the list of possible errors, one can assume the total uncertainty to be at about 20%. Not included are possible deficiencies in the equipment and in the method itself.

3. Potentiodynamic Polarization Curves

Potentiodynamic polarization curves were obtained at all possible velocities. Although in this test there are only small currents involved, the results were good considering the speed and the noise (Figs. 21-23). Since the polarization plots are basically developed in the same way as the LPM-plots one could expect similar noise problems. But the sensitivity to noise was much less, because the range of the current was much greater: 100 mA to 0 on these plots and -30 to +30 μA on the LPM plots. In general, the other problems described in the last section could be adopted for the polarization method also. In order to detect flaws in the set-up, several test runs were performed with a standard flask (see description of test runs). No significant difference could be observed, and a repetition of the test run on the same plot showed good reproducibility.

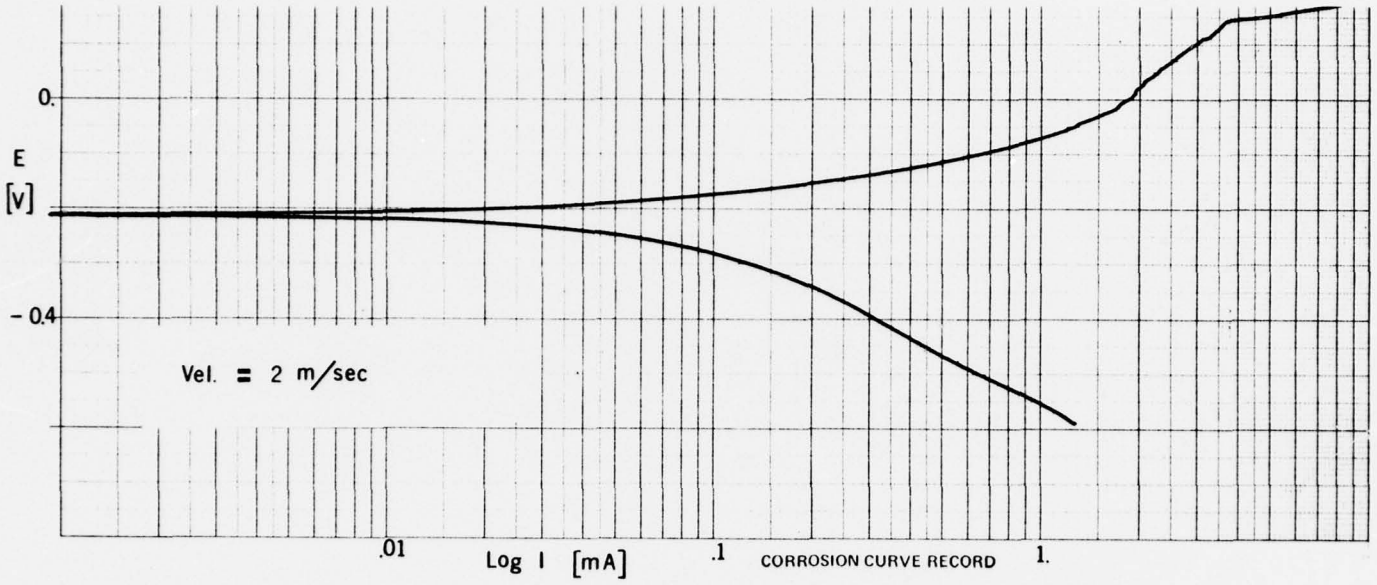

Figure 21. Actual polarization plot at 2 m/sec (surface area = 2.85 cm^2)

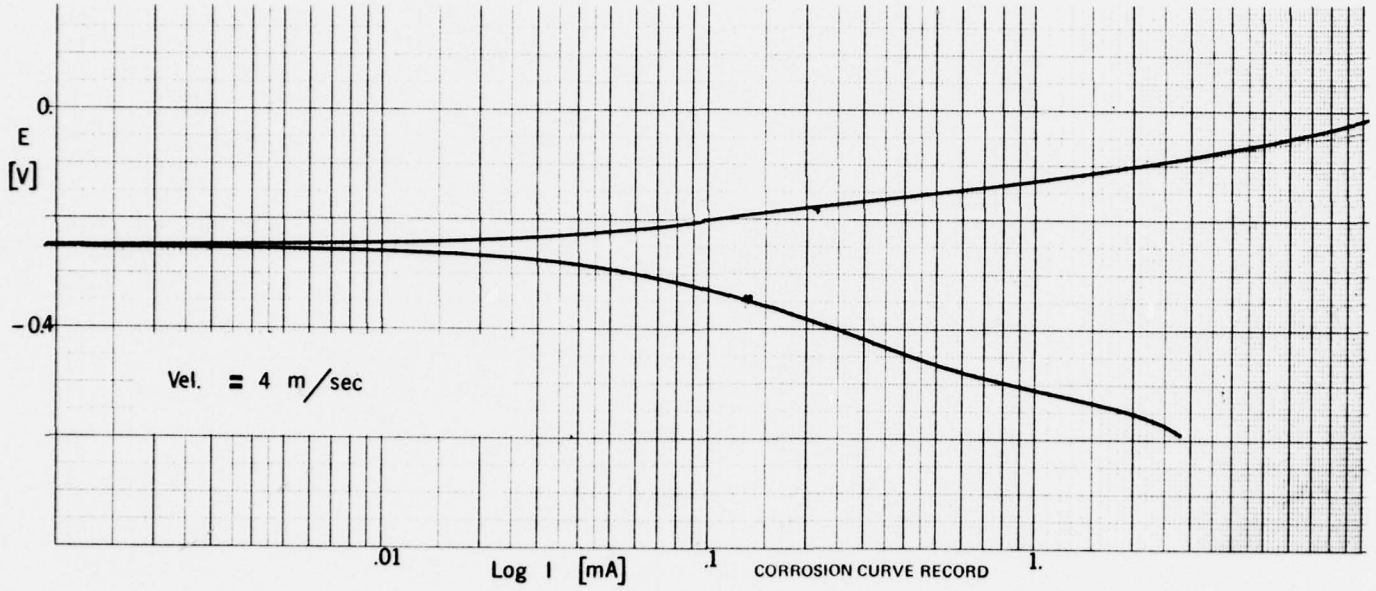

Figure 22. Actual polarization plot for 4 m/sec (surface area = 2.85 cm^2)

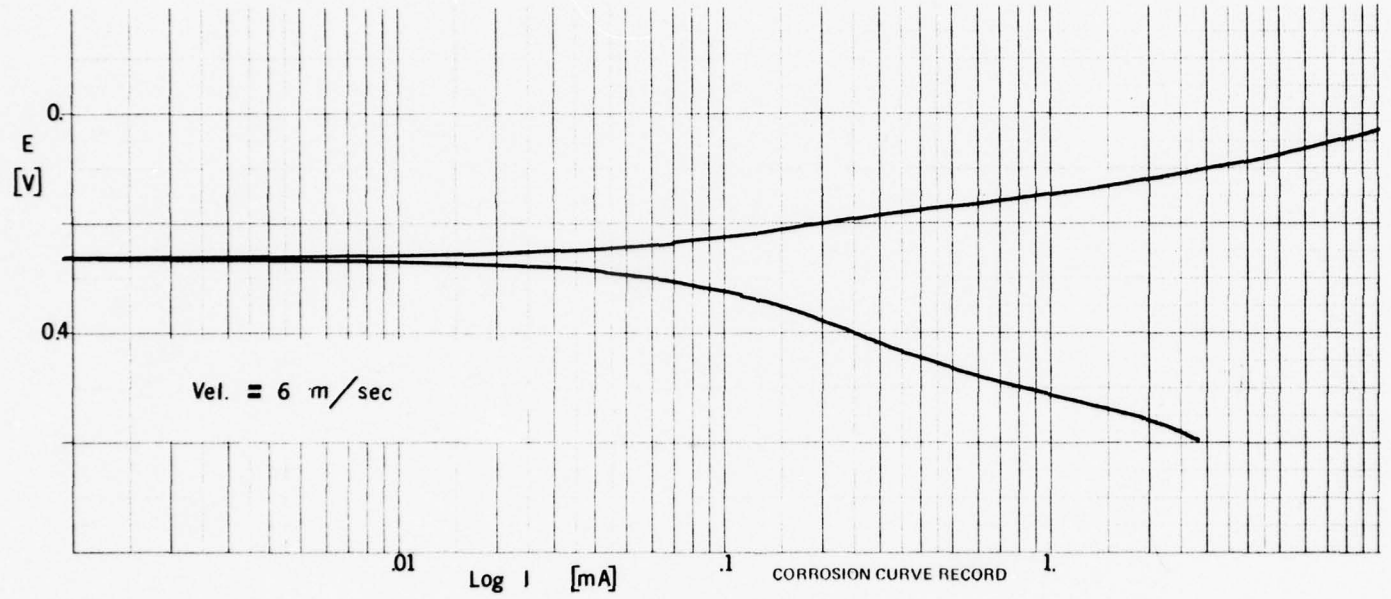

Figure 23. Actual polarization plot for 6 m/sec (surface area = 2.85 cm^2)

The corrosion current density can be approximated by the intersection of the Tafel slopes of the anodic and cathodic part of the polarization curve. However, the application of this method in this matter demands curves the slopes of which can easily be determined and drawn. The actual plots, however, did not show this nice feature (see Fig. 21). The determination of the corrosion rate by the Tafel slopes revealed fairly reasonable values for the higher velocities, whereas the result for 2 m/sec cannot be regarded to be reliable (the value of i_c = 21 $\mu A/cm^2$ is more than double that obtained by the weight loss and LPM methods) because the slopes of the polarization plot are difficult to measure exactly (Figs. 21-23). The results for 4 m/sec and 6 m/sec are 14 $\mu A/cm^2$ and 16 $\mu A/cm^2$ respectively. They are also above the other measurements, but only by about 25%, and they exhibit the same trend of an increase of corrosion rate with increasing electrolyte velocity. All three plots, however, show that the equilibrium corrosion potential becomes more negative with higher velocity. This behavior was also recognized by the other methods.

4. ZRA Corrosion Rate Results

The results of galvanic current tests using a ZRA are important relative to the time-dependent behavior of a couple. The results will be compared with the weight loss and other results. Some of the ZRA results are given in Figure 24. All results of tests involving couples were comparable to those determined by weight loss. The

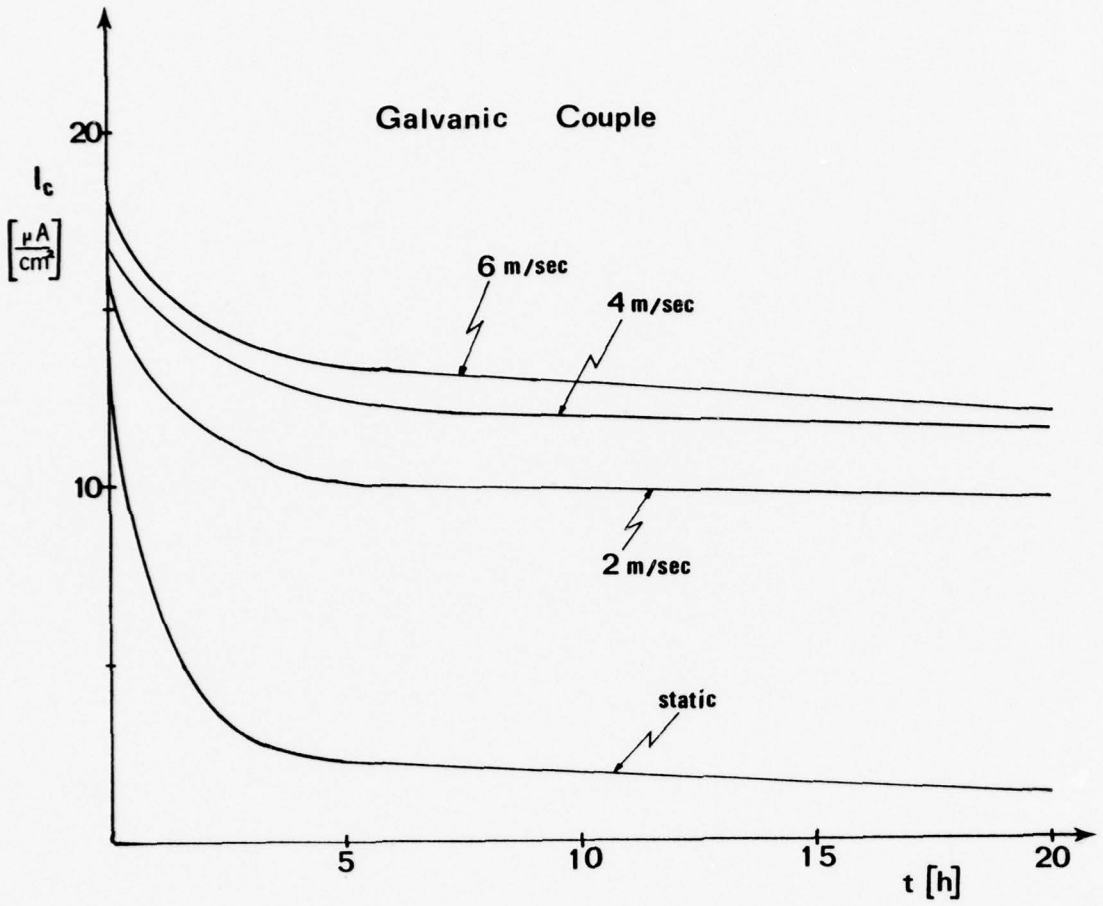

Figure 24. Corrosion rate of a galvanic couple Cu-Ni/Pt plotted versus time at given velocities

transient ZRA curves of the corrosion rate shown in Figure 24 showed in general the same trend the LPM measurements revealed as shown in Figures 17-19. Starting from a fairly high initial value the corrosion rates dropped until, after 5-6 hours, a plateau value is obtained, with a gradual decrease in corrosion rate beyond. The curves plotted by the x-y recorder clearly show that the corrosion rate has not stopped decreasing after 24 hours (Fig. 24). This is not so obvious in the plots shown in this paper, because of the compressed axis. Due to the limited amount of measurements with the LPM-method that curve of corrosion current vs. time shows a nearly straight line after some time of corrosion (Figs. 17-19), whereas Figure 24 shows a small decrease after the initial steep slope. Comparing the curves gained by the ZRA and by the LPM-method one may recognize a parabolic shape, which Popplewell [43] suggested is typical for a Cu-Ni alloy. Although the Cu-Ni alloy cannot be included in the group of the real "passive" metals, the drop in corrosion rate caused here by formation of an oxide film is similar to the behavior of passive metal. All the transient curves of corrosion rate show about the same time spent to reach the plateau condition (stable corrosion rate), but there is a marked difference in magnitude of the rate (after 24 hours) for different velocities.

B. EFFECT OF VELOCITY ON CORROSION RATES

In this section the corrosion rates determined by weight loss and by LPM will be compared for different velocities. Tables 6-8 show a survey of all important results for 2 m/sec, 4 m/sec and for 6 m/sec.

At a velocity of 2 m/sec the corrosion rate determined by both methods were approximately equal at about 9.5 $\mu A/cm^2$, which is about 40% higher than the rate given in the literature for 1.6 m/sec [10]. Comparable data could not be found in the literature. It is interesting to note the lower corrosion rate determined by the LPM method when taking measurements from a sample which is disconnected from a galvanic couple. Although the corrosion rate of a coupled specimen is higher when coupled than that of a single metal specimen, the coupling has the opposite effect on the LPM results for the coupled specimen when disconnected. During the time the LPM measurement is being performed, the couple is disconnected and only the single metal corrosion is determined. Since the surface is already heavier corroded due to the galvanic action, a thicker barrier has built up and the single metal corrosion rate is therefore less decreased. This effect is observed at any velocity, so that those data were not used for a direct comparison of the corrosion rates.

An increase in velocity to 4 m/sec did not bring a significant increase in corrosion rate with it. Using

the only valid LPM determination for this velocity (Run 15) an increase is observable, but weight loss (Runs 7, 15) showed no increase. Note again the lower rate when a galvanic couple is involved (Run 3). Run 7 should be disregarded for consideration of the LPM method, because of the problems when two specimen are involved. The strange decrease after several hours makes this run especially suspicious (Fig. 18). A possible reason might have been a problem with the electrical connection between the specimen and the meter because of which two other runs had to be stopped. This was also the problem with Run 8, but because it shows the trend, it was included in the table. Other runs at 6 m/sec, however, showed an increase of corrosion rate with velocity. Except for the result from a coupled specimen (Run 5) which was the same as at lower velocities when applying the LPM method, the rate increased noticeably from 12 to 14 (LPM) and from 10 to 12 (weight loss) relative to 4 m/sec.

Runs 16 and 18 exhibit a peculiar behavior not observed at other velocities: the rate in both runs declined from a high point at the beginning as expected, but did not stay nearly constant as it was the case before and increased again after 5 or 6 hours in order to decrease finally again after several hours. The answer to this deviation from the average might lie in the higher velocity itself. After a certain corrosion layer has built up, the rate may be due to the greater barrier, but under the continuing action of

a high shear stress over the plate, or by amplified action of energetic eddies (note the high turbulence intensity), perhaps in combination with the action of entrained bubbles, the layer may be effectively "worn" thin and so the corrosion rate may increase again.

Another possible effect could be due to temperature, which was increasing during the first hours of the run (from 20"C to 24"C), constant afterwards. This temperature increase was only recognized at 6 m/sec. As is generally known, an increase in temperature accelerates corrosion and at higher velocity the solubility of oxygen decreases which could also cause an increase in the corrosion of 90-10 Cu-N9 as Syrett showed [10].

Further tests to research this behavior in more detail could not be performed because of time limitations. But since two similar runs showed the same effect, the time dependent trends should be regarded as quite reliable. The plots gained by the ZRA did not exhibit an increase at this velocity; the corrosion current between a couple decreased slowly but steadily after 5 hours, showing no sign at all of a possible increase of i_c.

C. CORROSION PRODUCTS

1. Identification Of Corrosion Products

In order to specify the corrosion products, the surface of a coupled specimen with a thick corrosion layer were exposed in an X-ray diffractometer. But the film was

Table 6

Results of Corrosion Tests at 2 m/sec with 90-10 Cu-Ni in Synthetic Seawater

Run	Time of Exposure	Weight Loss			LPM			Remarks
		i_c	Mph	µmpy	$\bar{i}_c$	Mpy	µmpy	
1	24	-	-	-	7.7	6.4	163	galvanic Couple
2	24	-	-	-	6.3	5.2	132	galvanic Couple
6	24	7.3	5.6	143	9.2	7.6	193	2 specimens
14	44	9.0	7.4	189	-	-	-	
17	24	10.5	8.7	220	10.0	8.3	210	1 specimen

Table 7

Results of Corrosion Tests at 4 m/sec with 90-10 Cu-Ni in Synthetic Seawater

Run	Time of Exposure	Weight Loss			LPM			Remarks
		i_c	Mpy	µmpy	$\bar{i}_c$	Mph	µmpy	
7	48	10.3	8.5	216	6.5	5.4	136	2 specimens
3	24				7.5	6.2	157	galvanic couple
15	24	9.0	7.4	188	12.0	9.9	250	1 specimen

Table 8

Results of Corrosion Tests at 6 m/sec with 90-10 Cu-Ni in Synthetic Seawater

Run	Time of Exposure	Weight Loss			LPM			Remarks
		i_c	Mpy	µmpy	$\bar{i}_c$	Mpy	µmpy	
5	20	-	-	-	7.5	6.2	159	galvanic couple
8	45	10.5	8.7	221	-	-	-	2 specimens, LPM measurements stopped
16	24	13.1	10.8	275	13.0	10.7	272	1 specimen
18	24	10.5	8.9	221	14.0	11.5	292	1 specimen

either too thin or the size of the corrosion product particles was too small to give a coherent diffraction pattern. The only pattern detected was that of the base metal. Also, X-ray spectroscopy using the Scanning Electron Microscope in connection with a computerized X-ray analyzer, PGT 1000, did not give any additional information. Some other constituents other than those of the base metal could be detected, but the reliability of the determination was very poor because of lack of resolution.

Another way to determine the corrosion products is to make use of the light microscope to compare the actual colors of the products with those of the possible corrosion products given in the literature. Looking at the surface with the eyeball it seemed to be covered with a dark, dull looking layer, but the light microscope revealed also a green color ranging from light to dark. Imbedded in the green color were singular red spots and at some little areas the yellow-bronze color of the base metal shined through. The variation in green was probably due to varying thicknesses of the layer, the thicker it was, the darker the color became. This also could have caused the blackish appearance of the whole surface. At high magnification one could observe a blackish color along small lines of preferential corrosion.

Comparing these colors with those given by the Handbook for Chemistry and Physics [37] one could make the following selection of possible corrosion products:

copper: Oxides:

- natural cuprite Cu_2O (red)
- natural tenorite Cu O (black)
- peroxide $CuO_2 \cdot H_2O$ (brown or brownish black)

Chlorides:

- hydroxychloride $CuCl_2 \cdot 3Cu(OH)_3$ (green)
- copper chloride CuCl (brown)

Sulfides:

- CuS (black)

Nickel:

- nickel oxide NiO (green black)

Theoretically there exist more pssibilities, because one can notice the variety of constituents when looking at the table for synthetic seawater in Appendix A. But considering the possible results given the literature, only the oxides and chlorides are feasible corrosion products. A schematic of possible corrosion products is shown in Figure 25.

MacDonald and coworkers [10] mentioned in their newest report that the corrosion potentials ranging from about -0.05 to 0.15 V with respect to the Standard Hydrogen Electrode (SHE) in a solution with a pH-value of 8 lie in the stability region for the cuprous oxide Cu_2O, but also close to the equilibrium potentials for $Cu_2(OH)_3CL_2Cu_2O$. These results are taken from the diagram ph versus potential given by Bianchi and Longhi [11] (Fig. 39). They also

mention the existence of a thin green layer on the surface. Since those conditions were similar to the ones given in this study, one could assume similar corrosion products: Cu_2O is red and copperhydroxychloride is green, both are the dominant colors of the corrosion products of these specimens. However, this would not explain the black appearance of the surface.

Efird and Lee [38] wrote about a possible carbon reduction and precipitation in the presence of cuprous ions (Cu^{++}), sulfides and oxygen. The carbon could cause a black layer, but a simple test described by them showed that no carbon was reduced. In this test concentrated HCL was dropped on the black corrosion products. If it stayed black, the presence of carbon was proved, if it became green, carbon was not a constituent of the corrosion product.

Another possible reason for the dark color could be copper sulfide (CuS) which could have formed theoretically, because sulfur was contained in the solution although in a compound as Na_2SO_4. Calculations, however, of the potential necessary to form CuS from Na_2SO_4 revealed that it was with 1.3 V way above any potential applied or measured in these tests. Since there is no other way how the sulfur could have got into the solution, one has to eliminate this possibility. But to be sure, a test described by Feigl [39] was performed by putting a drop of sodium azideand potassium iodide solution together with a drop of the corrosion product. If at once a heavy reaction starts shown by rising bubbles

(sulfide acts as a catalyst for nitrogen evolution), sulfide is one of the corrosion products.

Since the corrosion layer was difficult to remove from the surface mechanically, the cleaning solution described earlier was used. Both the test solution and the corrosion product were poured together and a heavy reaction started. But further tests revealed that the HCL in the cleaning solution was the main reactant. Another test using mechanically removed solid corrosion products combined with a platinum wire (as described by Feigl) and the test solution did not show any reaction. Finally the electrolyte in the tank was tested in the same way, but no sign of any sulfide, although this method was supposed to detect sulfide in a very low concentration. The conclusion is that these tests showed no evidence of any sulfide contamination, as initially expected.

2. Morphology Of Corrosion Products

In galvanic couples of 90-10 copper nickel alloy and platinum (used to examine accelerated corrosion), after exposure of 24 hours a considerable layer of corrosion products established itself on the surface. Figure 26 shows an as exposed surface (not cleaned after exposure). Streaks with two basic directions are seen. The flow (left to right) had an obvious effect on the pattern of the corrosion layer (although the set of lines parallel to the flow were not caused by the flow, but are simply the grinding marks

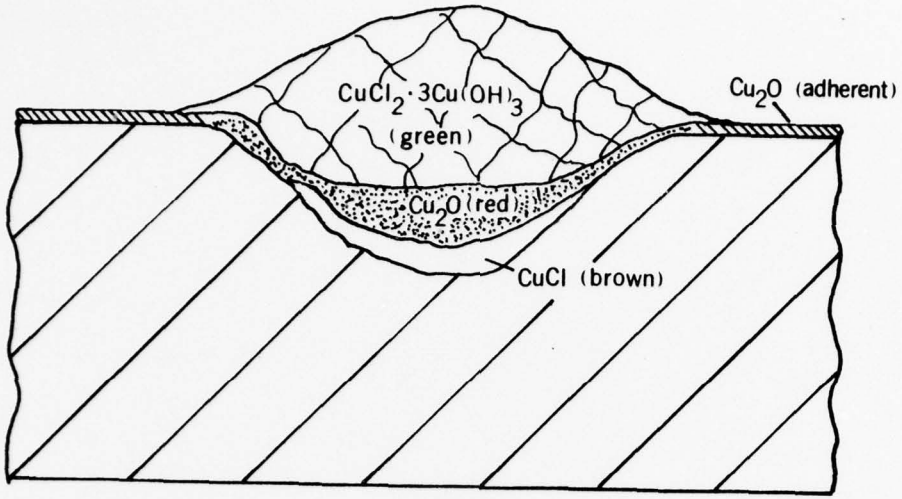

Figure 25. Schematic of possible corrosion products over a pit

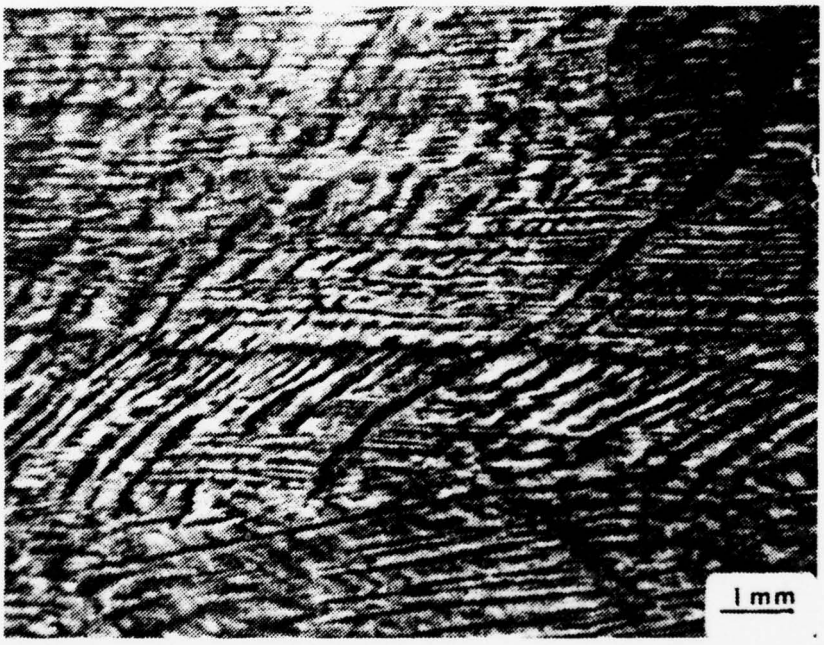

Figure 26. Cu-Ni surface, coupled with Pt, exposed at 6 m/sec for 24 hours, 10X

running parallel to the flow).

The sets of streaks at different angles to the flow direction may have originated in the flow pattern over the surface. They look similar to the small wave-like formations in sandy ocean bottoms. But whereas those are rather uniform, the surface of these specimens exhibit an irregular pattern which might have been caused by the irregular flow over the plate, such as due to side flow effects from the edges of the foil. Another cause for the irregular flow could be little crevices at the intersection of the specimen and the plate material, which could never be totally avoided. All specimens tested as couples showed a similar formation of corrosion products. One can see macroscopically that the corrosion layer appears flat black, and is irregular in thickness (in the streaked pattern). Figure 27 shows a closer view of those variations in thickness in photographs made with a standard light microscope.

In Figure 28 a SEM-photo shows a corroded surface at 6 m/sec. The white flecks on the surface are in reality dark as observed by the light microscope; they obviously have been charged by the SEM and appeared to be white. In Figure 28 one can see the grain boundaries of the base metal and sets of fine lines having different directions in different grains, which show local lines of dissolution. These fine lines probably correspond to those shown in Figure 29 on an etched surface; these are slip lines. Although still covered with corrosion products the surface in Figure 30

(a)

(b)

Figure 27. (a) Cu-Ni surface coupled with Pt, exposed at 4 m/sec for 24 hours, 100X.
(b) Cu-Ni surface, coupled with Pt, exposed at 4 m/sec for 24 hours, 400X

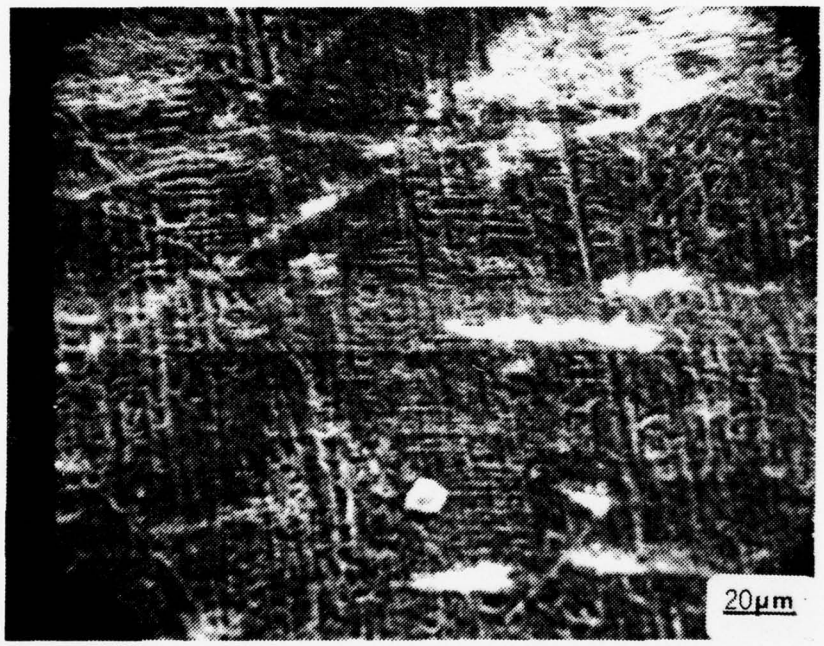

Figure 28. Cu-Ni surface, coupled with Pt, exposed at 6 m/sec for 24 hours, 500X (SEM)

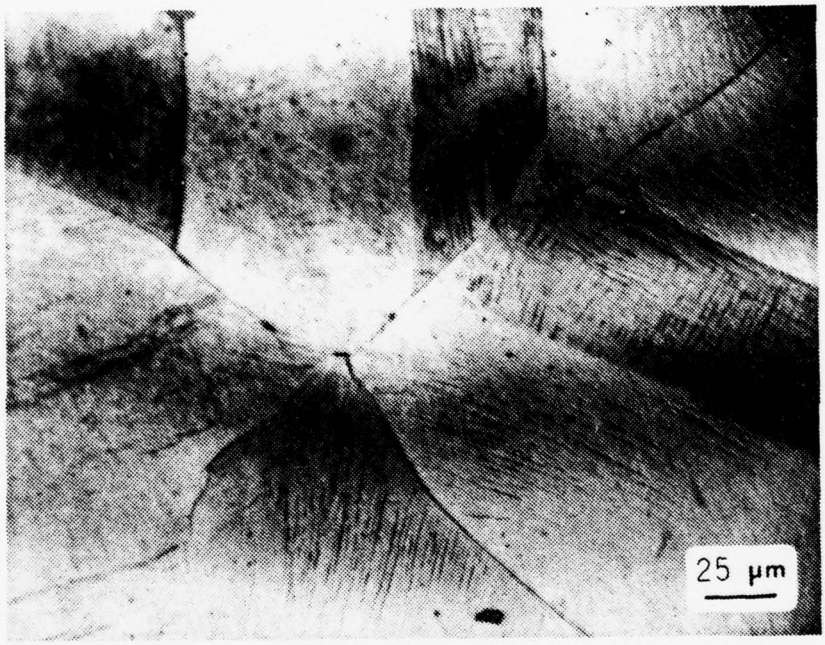

Figure 29. Cu-Ni surface,etched, 400X

Figure 30. Cu-Ni surface, coupled with Pt, exposed at 6 m/sec for 24 hours, 2000X (SEM)

exposes the regular fine-scale dissolution pitting structure. A cleaned surface like in Figure 31 offers a clearer view of these dissolution surfaces. Whereas on figure 31(a) one can still see some boundaries and observe the preferential attack along the grinding marks, Figure 31(b) allows the determination of the character and scale of the pitted surface. The individual pits are about 2-3 μm in diameter and very densely spread over the whole surface.

In the light microscope (Figure 32), the corroded, then cleaned surface of a coupled specimen shows a similar etched appearance as the metallographically prepared sample in Figure 29 described by Schack [14]. But the specimen corroded in seawater (Figure 32) shows many little curly lines of attack with a length of about 20 μm. It is not clear whether these lines have anything to do with the flow over the specimen. Because of the small size, these lines probably do not correspond to small eddies, as one might expect from their shape.

In simple metal exposures of up to 48 hours, the corrosive attack on a single specimen was much less than on a coupled one, as one could expect. Probably because of the lack of corrosion products, features of the wave pattern as seen on the coupled speciments were generally not detected; only the specimen exposed to the velocity of 6 m/sec showed the beginning of such a pattern. The surface was covered much more evenly by blackish dense corrosion layer. By

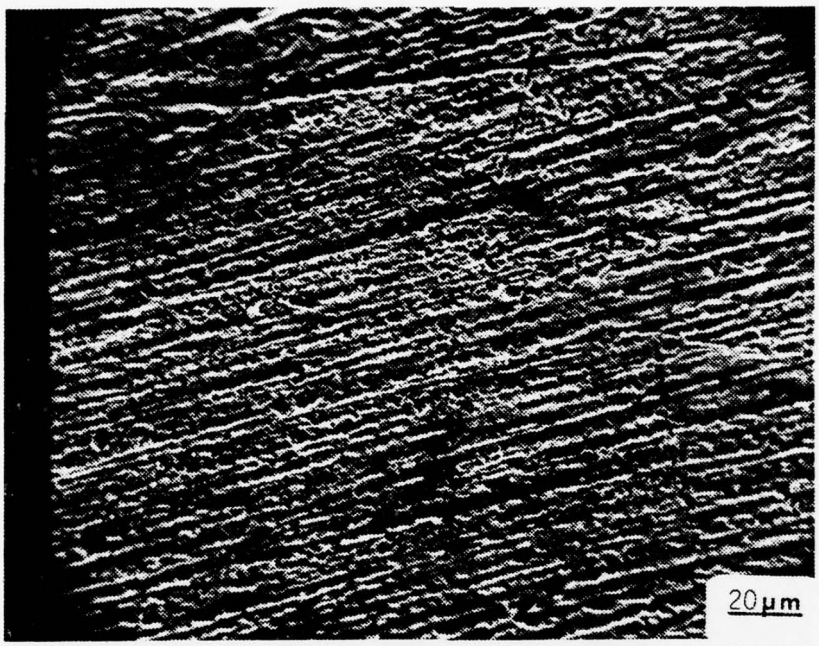

(a)

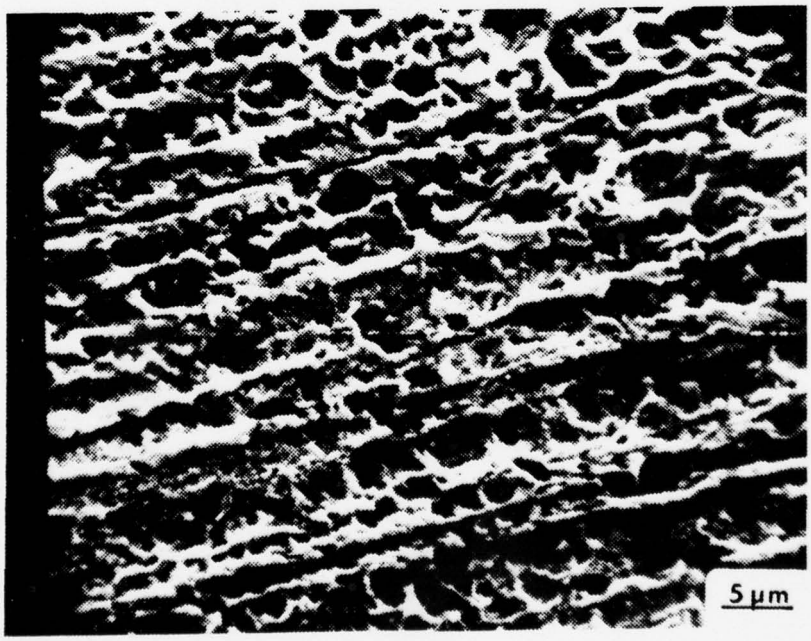

(b)

Figure 31. Cleaned Cu-Ni surface, coupled with Pt, exposed at 6 m/sec for 24 hours, (a) 500X (SEM), (b) 2000X (SEM)

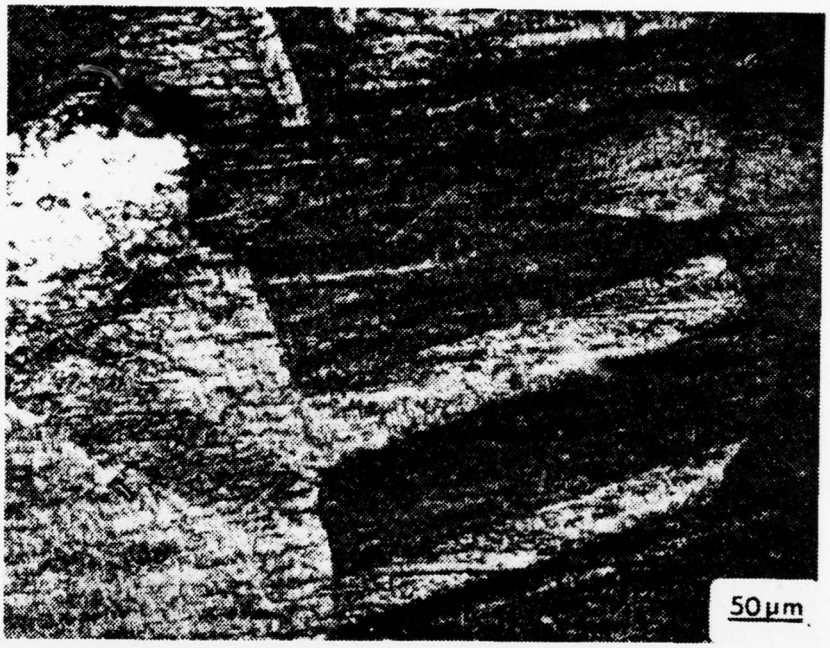

(a)

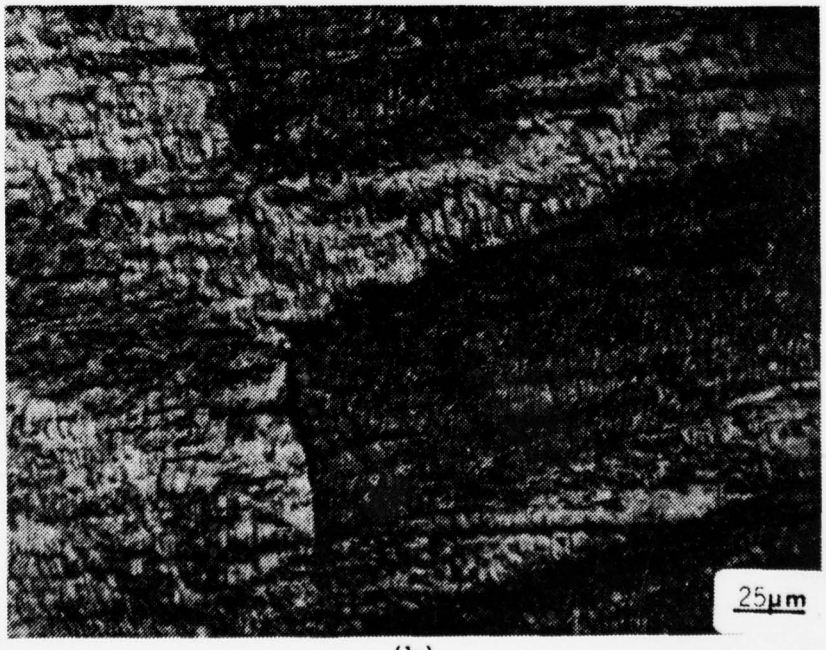

(b)

Figure 32. Cleaned Cu-Ni surface, coupled with Pt, exposed at 4 m/sec for 24 hours, (a) 200X, (b) 400X (light microscope)

looking carefully at the surface a purple shine could be detected on the corrosion layer.

Figure 33(b) exhibits no special features at a magnification of 100X, although it is an uncleaned corroded surface. The only difference from the initial surface (Fig. 33(a)) is that the grinding marks are not as distinguishable as they were before corrosion. The darker appearance of Figure 33(a) is caused by a shorter exposure time. Figure 34 reveals the preferential attack on the grinding marks, but no special feature which could be related to the effect of velocity.

Figures 35(a) and 35(b), however, are good examples of accelerated corrosion at higher velocities. At higher magnification both cleaned surfaces show again the preferential attack on the grinding marks and a few individual pits distributed over the surface; relative to the coupled specimen (Figs. 31(a) and 31(b)) the pit structure is much less uniform. But most remarkable is the visible difference in corrosive attack at 2 m/sec and at 6 m/sec (Figs. 35(a) and 35(b)). The specimen exposed to 6 m/sec has apparently corroded much more than the one exposed to 2 m/sec. Whereas the corrosion of the latter specimen took place for the most part at the grinding marks, the attack of the specimen exposed to the higher velocity seems to have occurred more evenly but not less intensively over the whole surface the entire upper layer of which appears to have been corroded away. The same conclusion is reached when looking

AD-A056 381 NAVAL POSTGRADUATE SCHOOL MONTEREY CALIF F/G 11/6
EFFECTS OF HYDRODYNAMIC VARIABLES ON CORROSION: STUDY OF 90/10 --ETC(U)
MAR 78 G H LEUMER

UNCLASSIFIED NL

2 OF 2
AD
A056381

END
DATE
FILMED
9-78
DDC

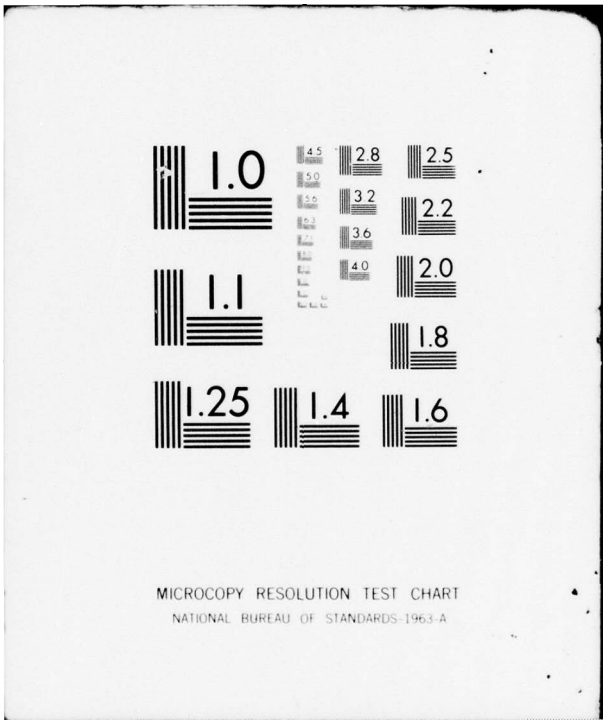
1.0
1.1
1.25
1.4
1.6
1.8
2.0
2.2
2.5
2.8
3.2
3.6
4.0
4.5
5.0
5.6
6.3
7.1
8.0
9.0
MICROCOPY RESOLUTION TEST CHART
NATIONAL BUREAU OF STANDARDS-1963-A

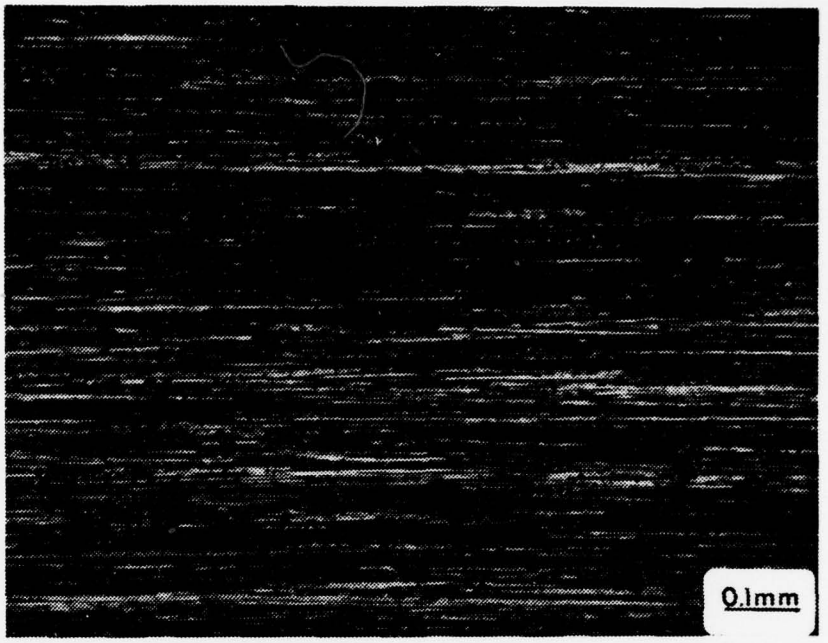

(a)

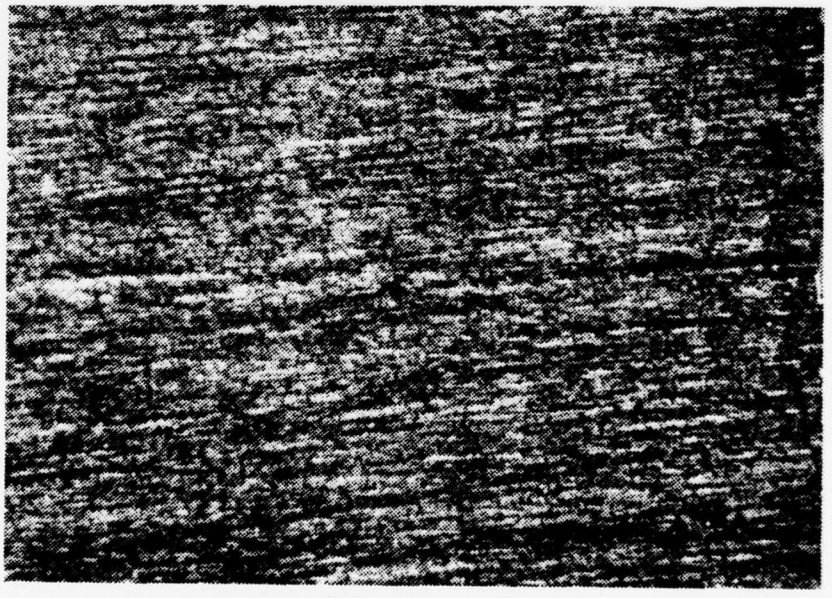

(b)

Figure 33. (a) Clean Cu-Ni surface after preparation for exposure, 100X
(b) Cleaned Cu-Ni surface, simple corrosion, exposed at 6 m/sec for 48 hours, 100X

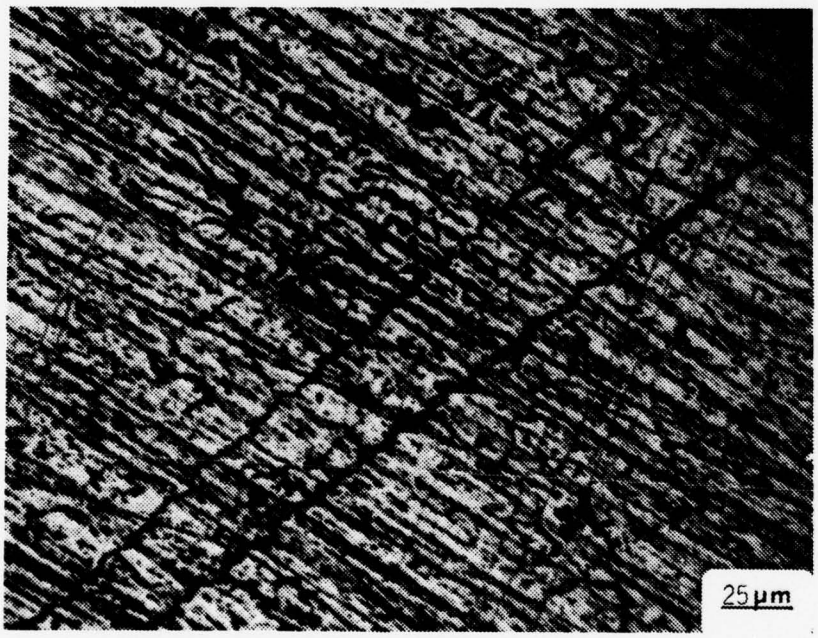

Figure 34. Cleaned Cu-Ni surface, single corrosion, exposed at 2 m/sec for 48 hours, 400X

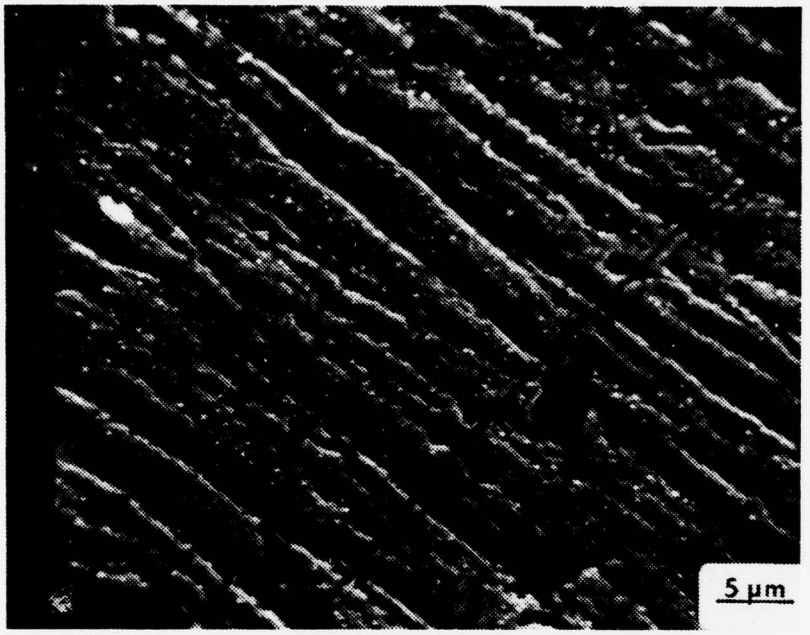

(a)

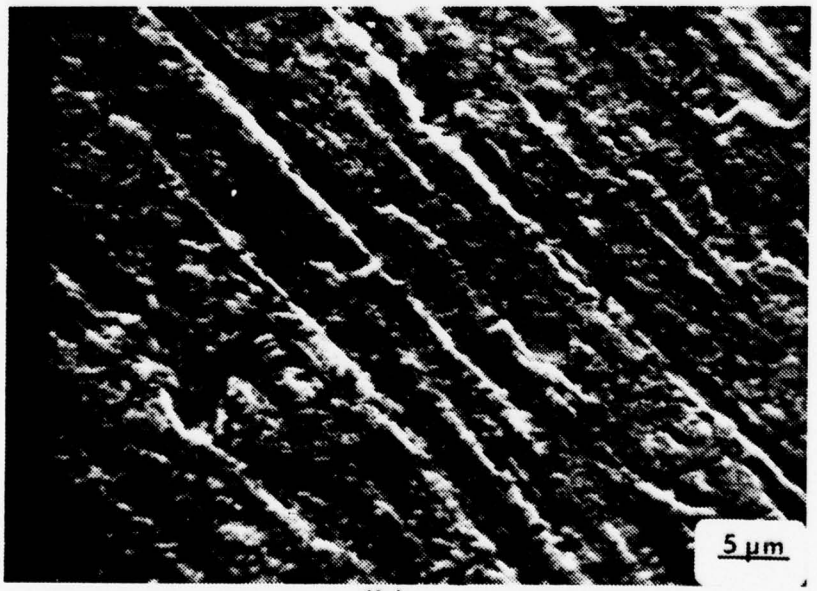

(b)

Figure 35. Cleaned Cu-Ni surface, single corrosion, exposed for 48 hours, 2000X, (a) at 2 m/sec, (b) at 6 m/sec

at Figures 36(a) and 36(b) with their lower magnifications; also, one may notice an increase in the number of dissolution sites (pits) corresponding to an increase in velocity.

Limited tests in static conditions were performed. After an exposure of three days with no extra aeration (that means that the oxygen content of the solution was much less than in a dynamic exposure) the specimens showed a different surface. The dominant colors were green and red, which were very shiny, but not nearly as dense as in the dynamic tests. At some spots a brownish layer could be detected, but no real black color like in the dynamic tests did appear on these specimens.

Figure 37 shows such a specimen, the black spots on the surface could not be identified, presumably it is a thin spotted layer of a different kind of corrosion products. In spite of a one day longer exposure the attack in general was much less severe than on those ones having experience a flowing electrolyte. The test specimen for the polarization plots accidentally let in the flask with synthetic seawater, however, showed after more than five days exposure a remarkable black color at some pronounced lines. In order to correlate the possible corrosion products to the result of the micrographs one should emphasize that the one feature of the surface of those specimens with an intensive attack proves the existence of copper hydroxychlorides as one important corrosion product: The fairly rough and non uniform attack as seen on the micrographs taken with the

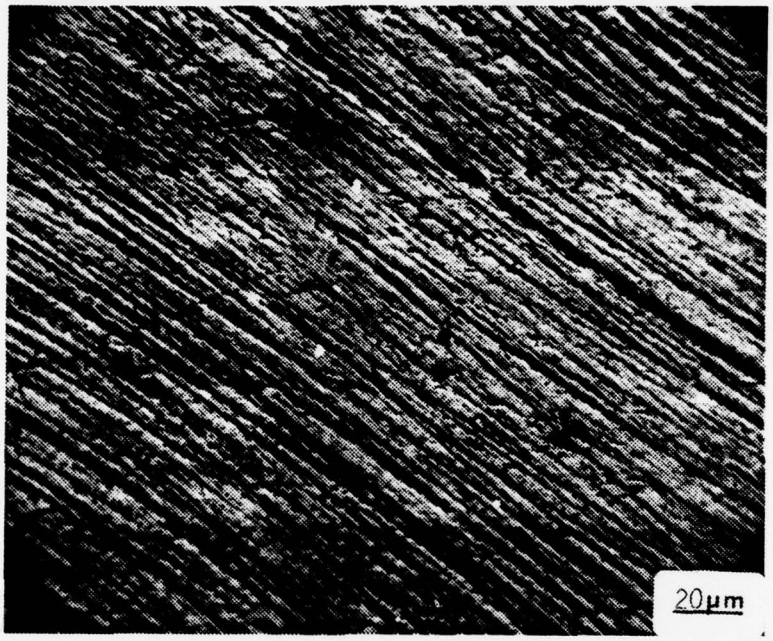

(a)

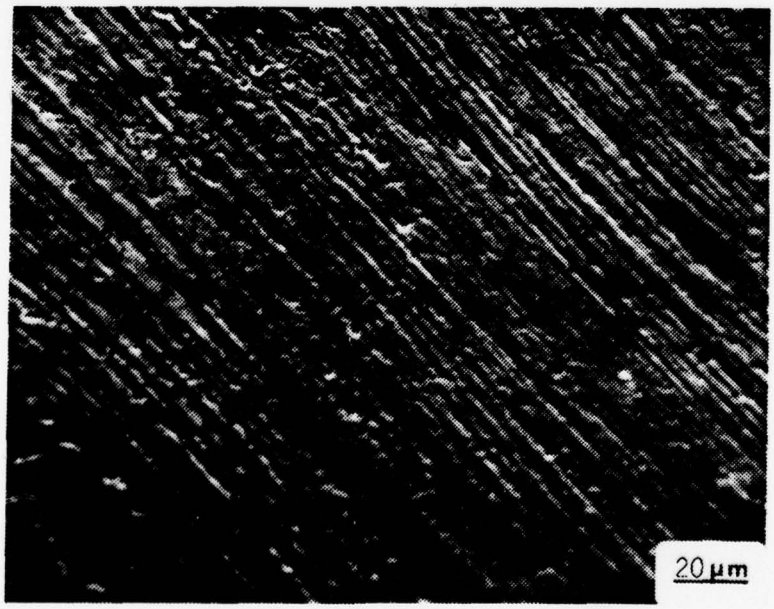

(b)

Figure 36. Cleaned Cu-Ni surface, single corrosion, exposed for 48 hours, 500X (SEM), (a) at 2 m/sec, (b) at 6 m/sec.

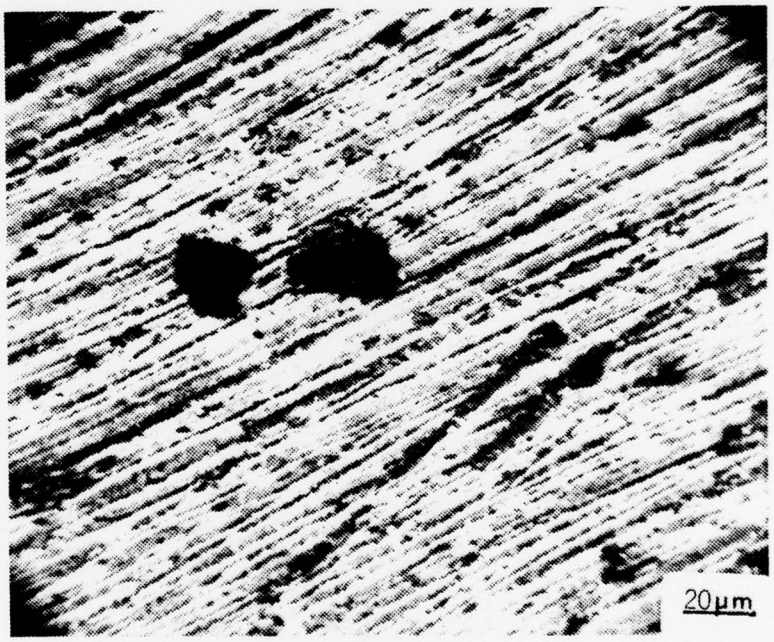

Figure 37. Uncleaned Cu-Ni surface, single corrosion, exposed statically for 3 days, 500X (SEM).

SEM is probably caused by precipitated copper hydroxychloride, because the oxides themselves are fairly uniform and small in thickness, independent of what kind of oxides are produced, as Blundy [39] pointed out. Both oxides Cu_2O and NiO have quite similar microstructure.

The pits which are to be seen on the cleaned surfaces result from localized accelerated corrosion. Marcel Pourbaix [41] wrote an article about corrosion of copper specifying different corrosion products by using his Pourbaix diagrams for different solutions. See Figures 38, 39 for a Pourbaix diagram of copper in a solution with high Cl content (3.5%). Pourbaix also mentioned the formation of pits in copper which supports the result of this study. Figure 25 presents a cross section fo a pit showing the two basic corrosion products of Cu-Ni: Cu_2O and $CuCl_2.3Cu(OH)_2$. That those pits are especially to be expected when using a couple with platinum is shown by Pourbaix who stated that any substance in the solution with a potential higher than +100mV with respect to the Standard Calomel electrode (SCE) as platinum hs promotes pitting of copper. Efird [38] also shows a similar development for pits including possible corrosion products which have been already mentioned. In general, low velocity supports the formation of pits as mentioned often in the literature [43]. In these tests, however, SEM photos revealed just the opposite: at a higher velocity more intensive pitting prevailed, independent whether the metal suffered from galvanic or single metal

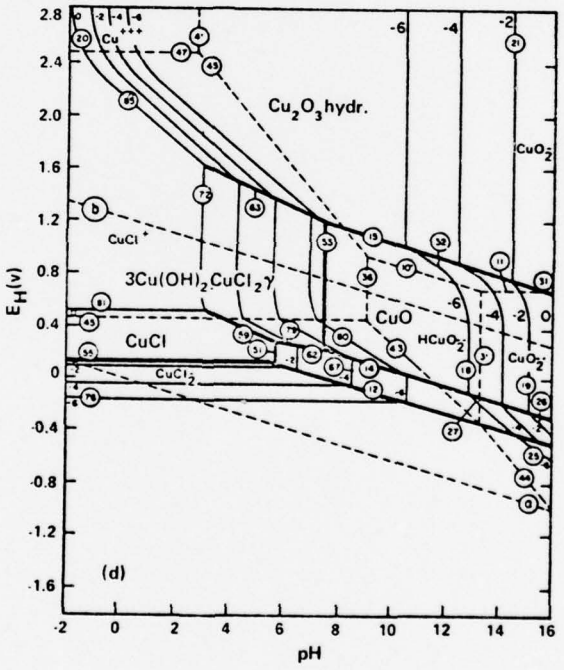

Figure 38. Pourbaix-diagram of Cu in an electrolyte containing a high percentage of Cl^- as given by Pourbaix [41] himself.

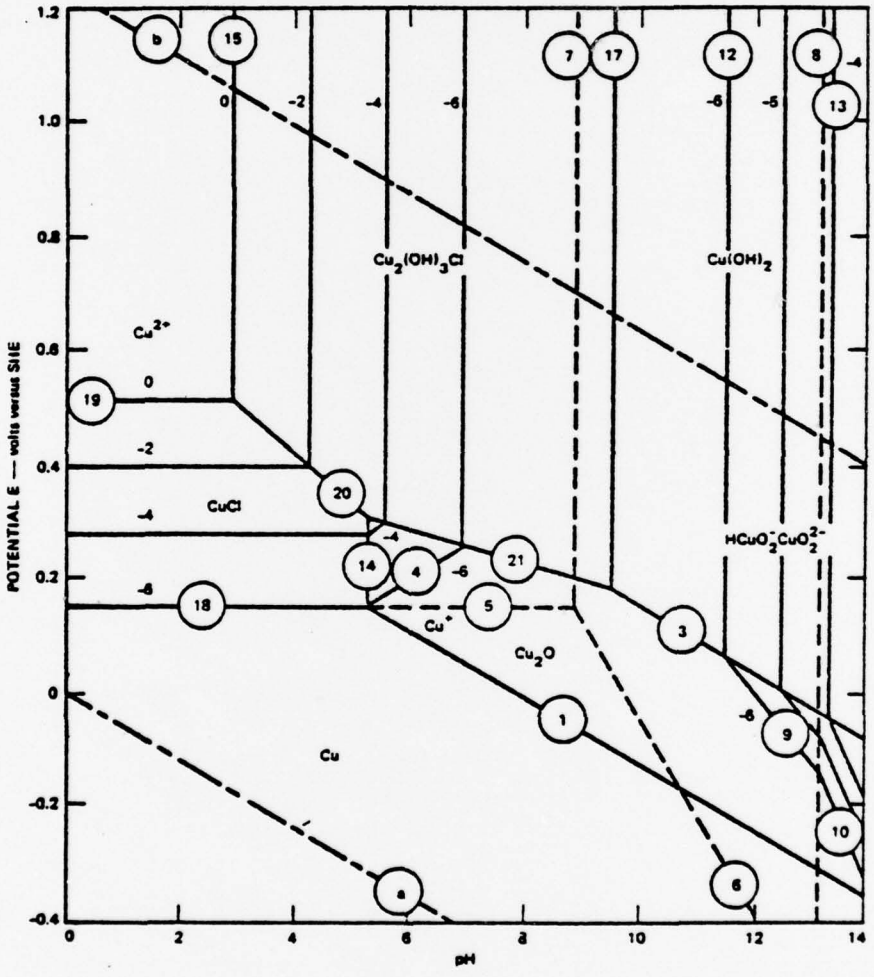

Figure 39. Pourbaix-diagram for Cu in seawater (source: Bianchi and Longhi [11])

corrosion. The possible reason for that contradiction might be that even the lowest velocity in these tests does not fall into the region of the "lower velocity". One other reason might be the morphology of the corrosion layer (see Chapter V.C.).

V. HYDRODYNAMIC CONSIDERATIONS IN CORROSION

A. BOUNDARY LAYERS IN TURBULENT FLOW

Basically there exist two flow regimes: laminar and turbulent flow. This study and that of Schack [14], performed concurrently at NPS, involved for the most part turbulent flow, so discussion of the boundary layer system in this chapter is restricted to turbulent flow only.

While this study used a foil as the specimen holder, Schack built a water channel. The flow system over the foil can be approximated by the flow over a flat plate, the hydrodynamic parameters of which are easier to determine theoretically and well known.

The boundary-layer thickness is generally defined as the distance from the "wall" to the point where the velocity becomes equal to 99% of the free stream velocity. Since this boundary layer is dependent only on hydrodynamics, it is called the hydrodynamic boundary layer (d_h). Most of the other boundary-layers are in one way or the other related to the hydrodynamic boundary-layer. Figure 40 shows the boundary-layers which were considered in this study. This configuration approximates the well-known Levich theory [18] except that Levich did not have a buffer zone in his model.

Above a critical velocity (in a system where all other variables are kept constant), the flow over a flat plate changes from laminar to turbulent in character. This does

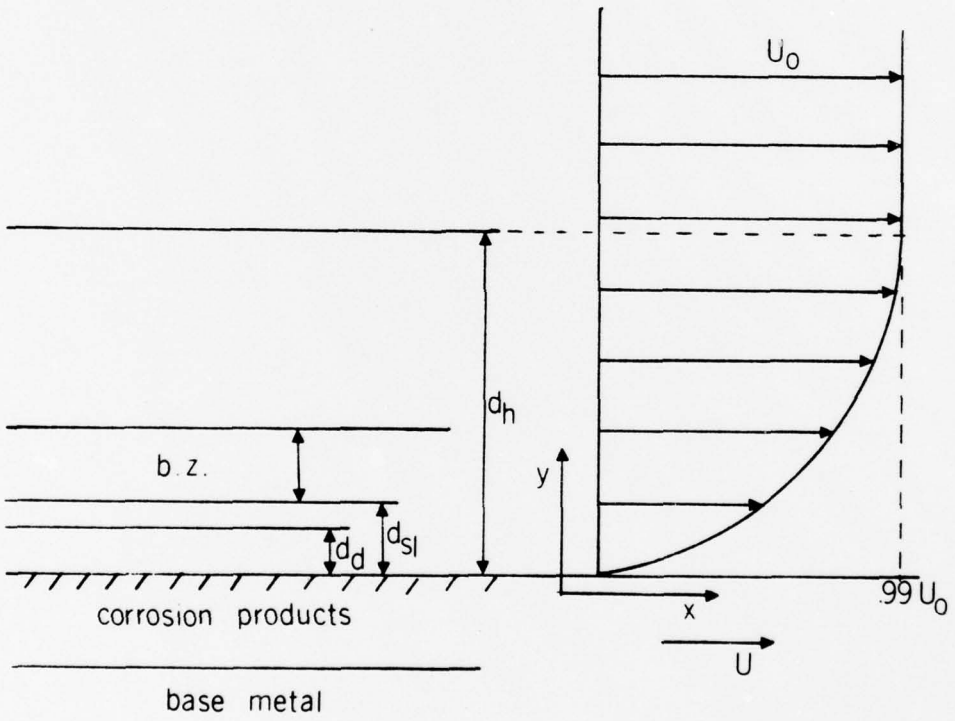

Figure 40. Schematic of boundary layers important for mass transfer (b.z. = buffer zone, d_h = hydrodynamic boundary layer, d_{sl} = viscous sublayer, d_d = diffusion boundary layer, U_o = free stream velocity)

not occur suddenly, but within a range called the transition range. The range in which transition from laminar to turbulent flow occurs can be determined by using a non-dimensional flow-parameter, the Reynolds number Re. The Reynolds number is defined as:

$$Re_x = U\, x/\nu$$

where

U = free stream velocity (m/sec)

x = characteristic length down the plate (m)

ν = kinematic viscosity (m^2/sec).

Transition may happen at a Reynolds number between 10^5 and 10^6 in case of a flat plate, depending on other factors such as free-stream turbulence intensity, surface roughness, pressure gradients (due to the shape of the body) and finally tripping (which was applied in the experiments of this study to ensure turbulent flow over the plate). The tripping, the high free stream turbulence intensity and the flow velocity are the reasons for the assumption of turbulent flow at the position of the specimens, whereas the characteristic length and the flow velocity are the important factors for turbulent flow in the flow-channel.

The turbulent boundary layer grows in thickness much more rapidly along the streamwise direction than does the laminar one. Due to the turbulent mixing, the shear stress in turbulent flow is greater than in laminar flow at the same boundary-layer thickness. Because of the random motion of the fluid particles in turbulent flow it is somewhat more difficult to determine the flow parameters theoretically by a model and it is also more difficult to measure them. In spite of these problems formulae for the hydrodynamic layer and viscous sub-layer are well established. Schlichting [22] mentions the following relations:

$$(1) \qquad d_h = 0.384 \times Re_x^{-.2}$$

$$(2) \qquad d_{sl} = 71.4 \times Re_x^{-.9}$$

The laminar sublayer, also called the viscous sublayer, is a region where the velocity has decreased to such an extent that the viscous forces dominate over the inertia forces; the flow is not considered to be perfectly laminar, so the term laminar sublayer is misleading. Between the laminar sublayer and the fully turbulent region there is a transition region called a buffer zone, where both the viscous and inertia forces are important, whereas in the outer, fully turbulent region only the inertia forces dominate.

The most important boundary layer for the purpose of this study is the diffusion boundary-layer, with thickness

d_d. The diffusion boundary-layer relates to the mass-transfer of species from the electrolyte to the corroding surface, or from the surface to the electrolyte; therefore this layer is also often called the mass-transfer boundary-layer. Unfortunately, there exist only a few literature sources which describe the actual thickness of this boundary-layer over a flat plate. In most publications about the diffusion boundary-layer the dimensionless Schmidt-number is used to set d_d in relation to the thickness of the hydrodynamic boundary-layer d_h by the formula:

$$(3) \qquad Sc^{1/3} = d_h/d_d$$

which is comparable with the relation

$$(4) \qquad Pr^{1/3} = d_h/d_T$$

in heat-transfer, where d_T is the thermal diffusion boundary layer and Pr the Prandtl number. The Schmidt number is fundamentally defined as:

$$(5) \qquad Sc = \nu/D$$

where

ν = kinematic viscosity (m^2/sec)

D = diffusion coefficient (m^2/sec).

The Prandtl-number in heat transfer is a similar dimensionless parameter as the Schmidt-number in mass-transfer:

$$(6) \qquad Pr = \nu/\alpha$$

where

α = thermal diffusivity (m^2/sec).

Wranglen and Nilson [12] calculated d_d for laminar and turbulent flow. They assumed that the velocity profile for laminar flow as given by Eckert [13] is equal to the concentration profile and by using the relevant boundary layer mass-transfer equations they determined d_d with an initial length; i.e. the corroding specimen is positioned a certain distance from the leading edge, a distance over which no diffusion is possible. Their result was:

$$(7) \qquad d_d = 4.53 \times Sc^{-1/3} \, Re_x^{-.5} (1-(x_o/x)^{.75})^{1/3}$$

where

x_o = initial length.

If one does not consider x_o and set it to zero, it is possible to show that the relation $Sc^{1/3} = d_h/d_d$ is valid for laminar flow. For laminar flow $d_h = 4.53 \times Re_x^{-.5}$ [13].

Using this relation for d_h in the ratio d_h/d_d one gets $Sc^{1/3} = d_h/d_d$.

However, the equation, Wranglen [17] found for the turbulent diffusion boundary layer does not show that the Schmidt-number is a valid criterion for the thickness of the turbulent diffusion boundary-layer. Assuming a linear concentration profile d_d can be determined as follows:

$$(8) \qquad d_d = 6.9 \text{ X } Sc^{-1/3} \; Re_x^{-.6} \cdot (1 - (x_o/x)^{.9})^{1/3}$$

Combining this equation with the one for d_h of turbulent flow, one could get

$$(9) \qquad d_d/d_h = (17.9 \; Re_x^{-.4}) \; Sc^{-1/3}$$

and it is obvious that the Schmidt number is not equal to the ratio of d_h and d_d, but only proportional to it with a proportionality factor of $17.9 \; Re_x^{-.4}$. This factor is smaller than unity from a Reynolds number of 1500 up, so that d_d determined by Wranglen is smaller than d_d determined by using the Schmidt-number to a degree which depends on the Reynolds number.

Figures 41, 42 show the different results for d_d relative to the determination method. $d_d(1)$ is the thickness

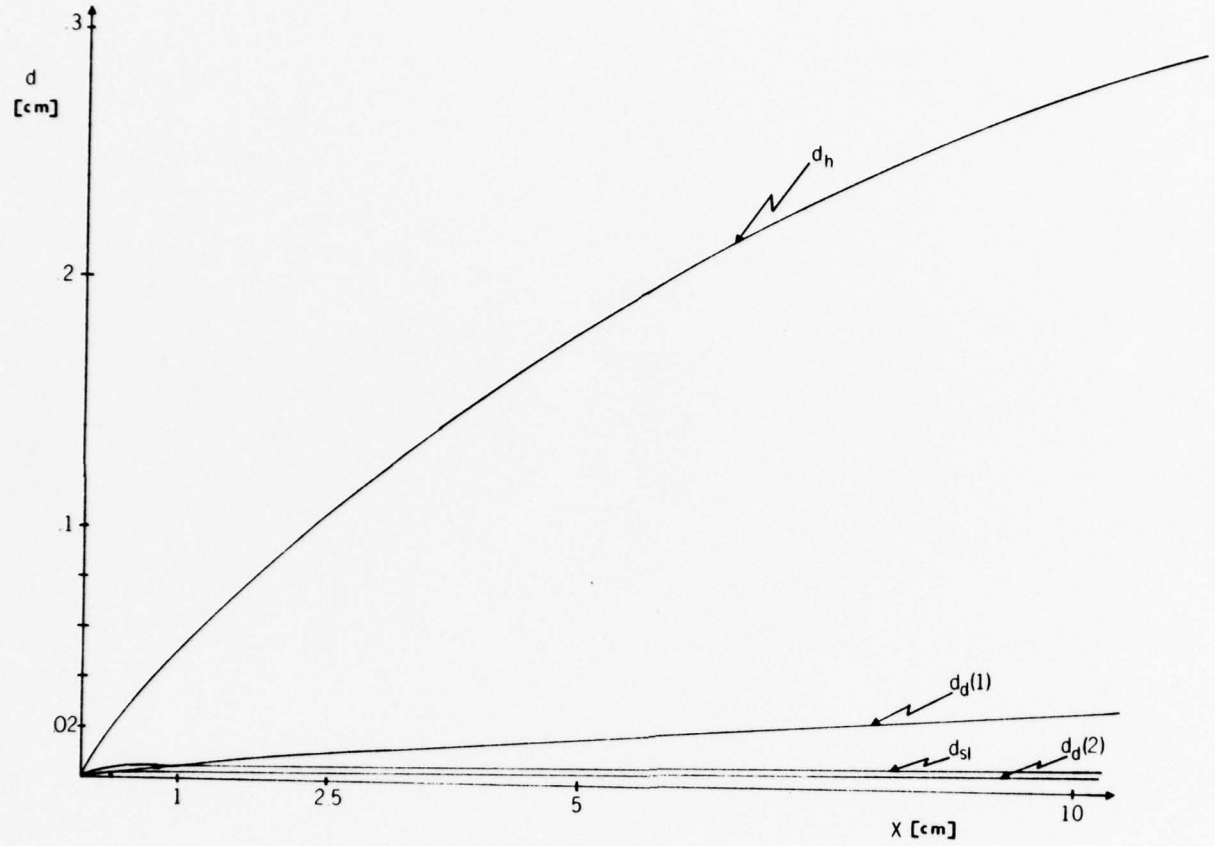

Figure 41. Boundary layers over a flat plate calculated by formulas given in the text using actual data

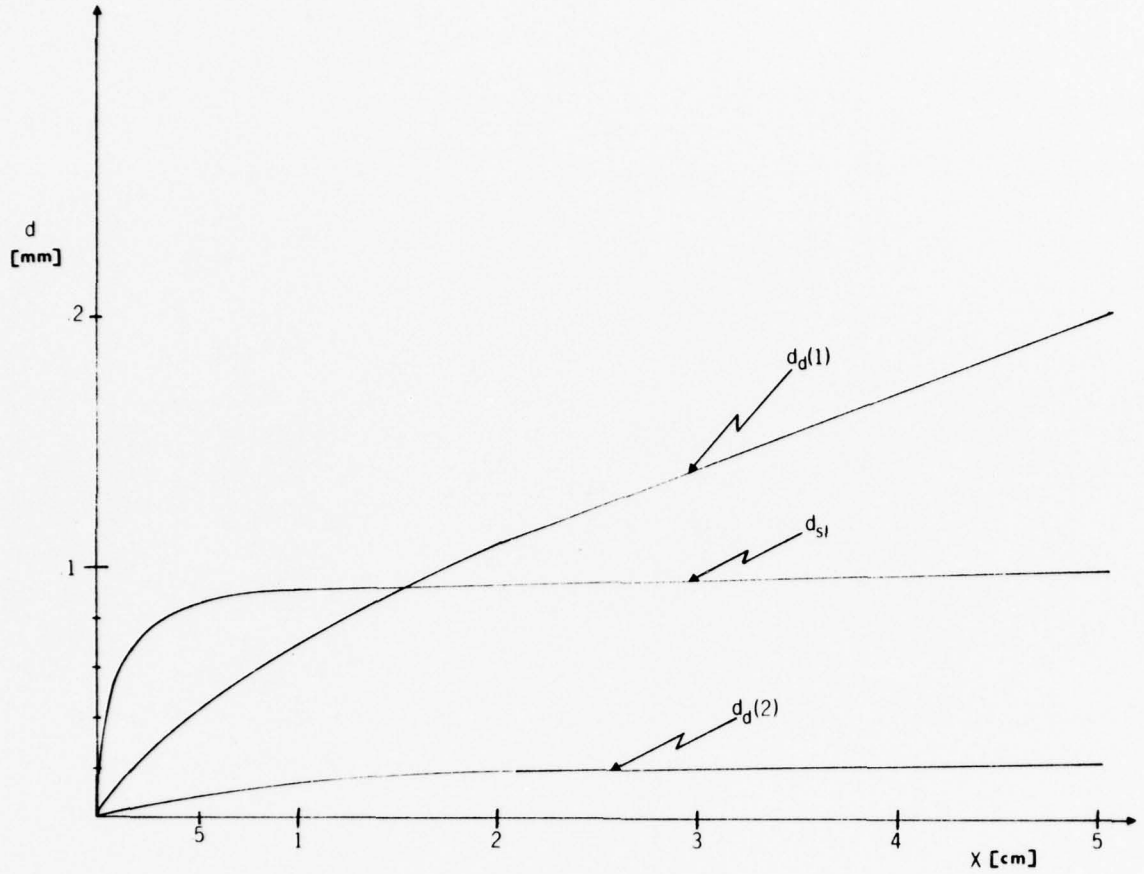

Figure 42. Boundary layers over a flat plate calculated by formulas given in the text using actual data (smaller scale than in Fig. 41).

calculated with Schmidt number, $d_d(2)$ the thickness using Wranglen's relation, whereas d_h and d_{sl} are the other velocity boundary-layers. As one can see, $d_d(1)$ soon becomes greater than the viscous sublayer. But the nature of the viscous sublayer demands that the diffusion boundary layer is normally smaller than the viscous layer. Also Levich [18] expresses that the turbulent diffusion boundary layer is less than the viscous sublayer and states that turbulent mixing ensures a constant concentration throughout the entire hydrodynamic layer and in part of the outer zone of the viscous sublayer. Also Ross [27] mentions that d_d in turbulent flow is less than d_d under the streamline conditions of laminar flow. This would however, not be the case if the relation $d_h/d_d = Sc^{1/3}$ is valid also for turbulent flow, because d_h (turbulent) is greater than d_h (laminar) as stated before. Ross also accepts the equations for d_d (turbulent) of Wranglen, although some years before that he stated the Schmidt-number to be a valid measure for d_d in general, without mentioning especially laminar and turbulent flow. The well established fact that the diffusion rate is higher in turbulent flow than in the streamline conditions of laminar flow at the same characteristic length gives a further reason for the assumption that the Schmidt-number is not a valid measure for d_d in turbulent flow. Higher diffusion rate demands a smaller diffusion boundary layer, but d_d in turbulent flow would be greater than d_d in

laminar flow using the Schmidt number, because d_h (turbulent) is greater than d_h (laminar). It has to be added that some literature does mention that the exponent of the Schmidt number when using the ratio d_d/d_h varies depending on the flow regime. However, it changes very little around 1/3, and there is no information in the literature on exactly how the exponent varies with velocity or Reynolds number, for example.

An additional feature of the Wranglen equation is the initial length which takes the distance where no diffusion is possible into account. This feature is very important, because at least in laminar flow the ratio of d_h and d_d is constant, only if both layers commence at the same point that means in this case at the leading edge.

As pointed out in the literature, if d_d starts at the leading edge, it grows fast in the beginning phase, and levels off at a larger distance x from the leading edge. Comparing both $d_d(1)$ and $d_d(2)$ on Figure 42 it is easily verified that only $d_d(2)$ has this feature. Further (according to equation (8) derived earlier), the higher the velocity, the greater the Reynolds number and the smaller is the diffusion boundary layer which encourages faster diffusive transport of oxygen to the metal surface, resulting in a higher corrosion rate.

B. MASS TRANSFER

Corrosion in electrolytes can be described by fundamental electrochemical reactions. The following mechanisms are important: (1) Transport of the attacking agent to the metal, (2) Reaction at the boundary metal/solution, and (3) Removal of the corrosion products. The mechanism by which ions arrive at and leave the corroding surface is generally diffusion, although one has to distinguish between different types of diffusion.

In a completely calm electrolyte, molecular diffusion due to a concentration difference is the dominant mechanism. As the diffusion coefficient in fluids is rather small, the reaction rate in such an electrolyte remains small, but as soon as particles are transported by a stream in addition to the latter mechanism, the amount of particles reaching the surface increases considerably. This transport is called "convective diffusion", consisting of convection in the solution and diffusion at the surface. Convection itself may be separated into free and forced convection. At any reasonable velocity the latter is dominant because only at static conditions or at very low velocity does free convection play any role.

Ross and Hitchen [27] added a term to this equation to account for the additional diffusion due to turbulence, the turbulence or eddy diffusion coefficient ε:

$$(9) \qquad j = (D + \varepsilon)\, c/d_d$$

This corresponds to the relation given by Holman [23] in heat transfer. Schack [14] gives a survey about turbulence intensity and its possible influence on corrosion.

The mass transfer equation reveals that an increase of the diffusion coefficient D results in an increase in the mass transfer rate. However, the increasing D causes a greater diffusion boundary layer thickness d_d (equation (8)). As seen in equation (1) and as mentioned often in the literature, a bigger d_d results in a lower mass transfer rate, because the concentration gradient is not as steep. This contradiction can be cleared by recognizing that d_d changes only as the 1/3 power of D, so that the direct effect of increasing D is only diminished slightly through its effect on d_d. Thus, the relative increase in D dominates the situation, giving a net increase in mass transfer. Furthermore, if a decrease in d_d is caused by a decrease in diffusion coefficient only, the general rule (as stated often in the literature) that a decrease in d_d accleerates the mass transfer fails in this case, because the decrease in D is heavier than the decrease in d_d resulting in a decrease in mass transfer (see equation (10)). The general rule is only applicable when the change of d_d is not caused for the most part by D, but also by other variables like the velocity and turbulence.

As E. Heitz [16] mentions in his report, when it was first tried to find a concept of the mass-transport, Nernst [17] believed in the existence of a stationary diffusion

boundary-layer on the surface with a certain thickness and above it the flowing liquid. There was a sharp distinction between diffusive and convective transport. But, because this assumption could never be proved, in the last twenty years the general model which has evolved considers the existence of a hydrodynamic boundary layer (a velocity layer) which in some way determines the diffusion boundary layer (in which the total change in concentration occurs).

The classical formula for mass transport is given by:

$$(10) \qquad j = D\,\Delta c/d_d$$

where

j = mass transported to the surface (mol/cm^2 sec)

D = Diffusion coefficient (m^2/sec)

Δc = Concentration difference between electrolyte and surface (mol/m^2)

d_d = effective diffusion boundary layer thickness (m)

As can be seen from this formula, a decrease in d_d results in an increase in the mass transport flux, j, and this corresponds to an increase in the corrosion rate.

Many experiments were performed to determine the effective diffusion boundary layer and the mass transport by using different equipment like rotating disks or cylinders

(Levich [18]) or tubes and channels (Cornet [19] and Lindolt [20]). Few publications deal with the case of the flat plate. One extensive mathematical determination of the mass transport on a flat plate was performed by Wranglen [12], who also calculated d_d as mentioned before.

A very useful non-dimensional parameter for the mass transfer is the Nusselt number, which is more often used in heat transfer problems than in mass transfer relations. The Nusselt number is defined by Wranglen as follows:

$$(11) \qquad Nu = j\, x/D(c_b - c_e)$$

where

j = diffusion rate density (mol/cm^2 sec)
x = characteristic length (m)
c = concentration (mol/m^3)
b = bulk electrolyte
e = electrolyte in contact with the electrode
D = diffusion coefficient (m^2/sec).

By using the appropriate concentration profile Wranglen determined the equation for the Nusselt number in turbulent flow:

$$(12) \qquad Nu = 0.17\, Sc^{1/3}\, Re_x^{3/5}$$

which is of the general form $Nu = C\ Re^m\ Sc^n$, where the constants c, m and n depend on the flow configuration.

The Nusselt number is a measure of the relation of the mass transfer rate and the diffusional capability of a system, represented in equation (12) by j and $\frac{D \cdot \Delta c}{x}$ respectively. It is also a number which takes into consideration the hydrodynamic parameters (i.e. the property of the flow) by being dependent on the Reynolds number and which accounts also for the properties of the fluid by being related to the Schmidt number which includes the viscosity and the diffusivity. An increase in D for example would not result in a higher Nusselt number, because it is not a direct measure of the mass transfer, but it would decrease revealing the increasing influence of molecular diffusion relative to the total mass transfer. The importance of one of the basic mechanism for mass transfer (convection and molecular diffusion) can be changed in equation (12) by varying the exponents m and n depending on the flow system and the fluid involved.

The correlation to heat transfer can be found by putting the Prandtl number instead of the Schmidt number into the equation which yields the relations given by Holman [23].

Instead of the Nusselt number, in mass transfer considerations very often the similar Sherwood number is preferably used. The definition of the Sherwood number is [24]:

$$(13) \qquad Sh = h_d\ x/D$$

where

h_d = mass transfer coefficient (m/sec)

which is comparable with h, the heat transfer coefficient. Because of the interchangeability of the Sherwood and the Nusselt number, the Sherwood number can also be expressed in terms of two other non-dimensional parameters, the Reynolds and Prandtl or Schmidt number:

$$Sh = f(Re,Pr) \quad or \quad = (Re,Sc)$$

Holman [23] states a formula for h_d over a flat plate:

$$(14) \qquad h_d = 0.0296\ Re_x^{-1/5}\ U_o\ Sc^{-2/3}$$

Here the Sherwood number becomes:

$$(15) \qquad Sh = 0.0296\ Re_x^{-1/5}\ U_o\ Sc^{-2/3}\ x/D$$

By mathematical operations and simplifications one can get:

$$(16) \qquad Sh = 0.0296\ Re_x^{4/5}\ Sc^{1/3}$$

which is significantly different from equation (12) of the Nusselt number given by Wranglen.

Another method to express the diffusional flow is described by Levich [18] and by Holman [23]. By using the local friction factor k_f, which varies along a flat plate with x as a fairly weak function, the total diffusional flux can be written as:

$$(17) \qquad I = b\, c_b\, U_o/(1.4.\ a\ Pr^{3/4}) \int_0^L k_f^{1/2}\, dx$$

where

b = width of the plate

c_b = concentration of solution

a = a constant to be determined by experiments, close to unity.

The factor k_f can be calculated by the relation:

$$(18) \qquad 1/k_f^{1/2} = 4.1\ \lg(k_f\ Re) + 1.7$$

or by the Blasius relation:

$$(19) \qquad k_f = 0.0396/Re^{1/4}$$

Substituting the total drag coefficient K_f into the equation for I:

$$(20) \qquad I = K_f^{1/2} \, c_b \, U_o \, \text{Area}/(1.4.\ a \, Pr^{3/4})$$

In a non-dimensional form this equation becomes:

$$(21) \qquad Nu = K_f^{1/2} \, Re \, Pr^{1/4}/(1.41\ a)$$

This is a relation for the mass transfer written in terms of the friction factor which determines the shear stress over a plate and of two other parameters, the Reynolds and Prandtl number.

Another important parameter in mass transfer is the limiting current density i_l . Newman [21] describes the limiting current as the highest possible rate of mass transfer to the surface. It is the amount of current which has to be supplied to each part of the protected surface. It is like the Nusselt number which also can be a measure of the corrosion rate. Davis [25] gives a general mathematical definition of the limiting current density:

$$(22) \qquad i_l = D \, n \, F \, c_b/d_d$$

where

n = number of electrons transferred

F = Faraday's constant

Davis used the relation $Sc^{1/3} = d_h/d_d$ to rewrite the equation:

$$(23) \qquad i_l = D^{.67}(n\ F\ c_b)v^{.12}\ U_o^{.2}/(.38\ L^{.08})$$

Since the author of this study regards the Schmidt number to be not valid for turbulent flow, the equation Wranglen [12] determined is taken into consideration:

$$(24) \qquad i_l = .143\ Z\ F\ D\ c_b/((1-n)x)\ Sc^{-1/3}Re_x^{.6}$$

where

Z = valence.

As can be seen from the formula (x is in the denominator), i_l decreases with x. The physical explanation for this is that the solution in the diffusion boundary layer has already been depleted by the reaction further upstream. On the other hand, i_l will increase as the velocity increases, because the Reynolds number increases also.

The limiting diffusion current (for example for oxygen) is in most cases the controlling cathodic process for corrosion in electrolytes with lower and medium velocities, but with increasing Reynolds number (typically greater than 10^6) the controlling process may shift to hydrogen evolution as Davis [25] and Gehring [26] pointed out. Above this

Reynolds number the change in velocity would not be expected to have any further electrochemical effect (at least on the basis of oxygen provision), but this high velocity may result in pronounced erosion-corrosion.

Ross and Hitchen came to the same result [27]. Newman [21] gives an excellent overview about different limiting current densities and Nusselt numbers for different flow situations like those occurring with rotating disk. rotating cylinder, and flow channels.

The Sherwood number is a good measure for the mass flux to the corroding surface:

$$Sh = \frac{x}{D \Delta c} j \quad \text{(see Eq. (8))}$$

where

j = mass flux,

if all the other variables in that equation stay constant. Since the mass flux is an important factor for the corrosion rate, it is possible to calculate the theoretical value of the mass transfer which is related to the limiting current density by the relation:

$$j = \frac{i_l}{z \cdot f}$$

where

z = valence

F = Faraday number

thus:

$$i_l = Sh \frac{(D \Delta c)}{x} \cdot z \cdot F$$

By using this equation it is possible to compare the maximum possible current density determined by the theory and the actual results gained in this study. Assuming: Δc_{O_2} = 10 ppm = 3.1×10^{-7} g mole/cm^3 , D_{O_2} = 1.08×10^{-5} cm^2/sec, $z = 1.1$, $F = 96500$ and using the equation from Wranglen [12] for the Sherwood number: $Sh = .17\ Sc^{1/3}\ Re_x^{3/5}$, one can achieve a relation between Sh and i_l : $i_l = 7 \times 10^{-8}$ Sh.

Getting the following values of Sh for the velocities 2, 4 and 6 m/sec: 1600, 2430, 3100 respectively, the values of i_l are determined to be:

i_l (2 m/sec) = 114 μA

i_l (4 m/sec) = 173 μA

i_l (6 m/sec) = 220 μA

This result seems to be rather high relative to the measured current density of 12 A/cm^2, but one has to take into consideration that i_l is the maximum possible current

density which does not describe the actual polarization behavior of the material. The comparison of the influence of velocity on both these values reveals that the theoretical increase of i_1 is greater than the actual increase: with ratios of the velocity of 1:2:3 the actual results have the ratios 1:1.17:1.33 , whereas i_1 has the ratios 1:1.5:1.9 which equals to the ratios of the Sherwood number. By using other relations for Sh than that one by Wranglen, this ratio of i_1 would reach closer to the ratios of the velocities, but move away from the actual results.

C. POSSIBLE PARAMETERS FOR CORROSION RATE CORRELATIONS

Since it has been stated in this study that the velocity alone is not a sufficient parameter for a correlation between the corrosion rate and both the hydrodynamic variables and the properties of the fluid itself, one has to find some parameters which includes these features. The Reynolds number describes the flow over different surfaces and includes even one property of the fluid (the viscosity); but it does not characterize both the fluid and the flow in a sufficient way, for example, it does not include the turbulent intensity. If, however, the Reynolds number is normalized by another specific Reynolds number, the so-called critical Reynolds number, more features of the flow would be included in this new parameter. The critical Reynolds number is a measure at what point of the flow over a specific

surface the transition from laminar to turbulent flow would be expected. The ratio of these two numbers would determine how far from the transition region the point of interest is away. By including the critical Reynolds number in the correlation, variables like velocity, free stream turbulence, surface roughness, pressure gradient and tube diameter would be eliminated from having an effect on the corrosion rate plotted versus Re/Re_c . Those variables are influencing the critical Reynolds number for a system. Even the turbulence intensity might be partially included, because the surface roughness and the free stream turbulence are the strongest influencing factors for it. One basic problem, however, is the exact determination of this number. There exists in the literature reports about methods to measure the transition region, but first it is difficult to achieve an exact number out of this transition range, and second are these methods very elaborate and demand sophisticated equipment and procedures.

The primary physical variables which might be expected to influence corrosion under flow conditions are the average velocity, the turbulence intensity and the oxygen content; these three, all varied with RPM in these tests. Two basic mechanisms, competing with each other, determine the corrosion rate of Cu-Ni: (1) the supply of more oxygen to the surface resulting in a higher rate and (2) the build-up of a corrosion layer increasing the resistance for the oxygen penetration to the metal.

Syrett [10] showed experimentally that an increase in oxygen content can cause a decrease in corrosion rate, because the oxide layer Cu_2O can grow faster and thicker. But at a certain oxygen level the polarization resistance drops resulting in an increase of the corrosion rate. That level of oxygen of about 7 ppm was below the oxygen content found in these tests (10 ppm). But even if the oxygen level were below the critical value, accelerated corrosion could be expected. The reason for this is the flow situation over the foil and the relative high turbulence, which provided the surface of the metal locally with such a high value of O_2 that the critical value could easily be reached. In addition to that, the "breakaway" velocity or the critical velocity might have been lowered, so that even the velocity of 2m/sec was apparently above this value for Cu-Ni which is generally assumed to be about 4m/sec. Below that velocity usually only a small increase of corrosion due to a higher velocity occurs. In this study the high turbulence caused locally a much higher shear stress which might have been strong enough to wear off some of the corrosion products, although the average shear stress at the specimen does not exceed 0.02 psi, which appeared to be too small to have a significant effect on the adhesive Cu_2O layer. The varying thickness of the layer as seen on the coupled specimen supports this assumption of having the local shear stress some influence on corrosion. This effect could be considered to be an onset of erosion-corrosion, through

which in this case not the base metal but the protecting corrosion layer is partially sheared away. The higher velocity alone is therefore not the only cause for an increase in corrosion, but only in combination with the turbulence the necessary shear stress may be provided. If it is assumed that the shear forces are not strong enough to wipe off the whole protective layer, one can think of a mechanism (caused by the turbulent shear forces) through that only small particles are ripped out off the surface and the layer becomes more porous. Higher porosity leads to higher sensitivity to pitting. Also, different layer thicknesses could be developed by the shear stress as seen on the micrographs (Figs. 26, 27) resulting in locally different resistances to corrosion and more importantly causing a rougher surface. Furthermore, a rougher surface results in a higher turbulence causing a higher shear stress again. One could think of this operation as a more and more devastating "Do-loop" which finally could wipe off the total surface layer, if the velocity is sufficently high.

However, since the shear stress necessary to remove any surface layers and the amplified local shear stress are not known, this reasoning can only be hypothetical. A more sophisticated apparatus may be able to measure those unknowns and approve these assumptions.

As already mentioned before, the Sherwood number includes both the flow and fluid considerations, so that

the most important factors for corrosion in a flowing system except the polarization behavior of a certain material are combined in one number. If also the turbulent intensity can be introduced into the Sherwood number, this parameter appears to be very efficient for a characterization of a flow and fluid system. This introduction could be performed by using the sum of the molecular diffusion as given by D and the eddy diffusion ε caused by turbulence in the expression for the Schmidt number:

$$S_c = \frac{\nu}{D + \varepsilon} \quad .$$

The same was done for the mass flux equation (see equation (10)). However, no exact mathematical definition of ε from which its value can be determined through hydrodynamic parameters was found in the literature.

Another parameter would be the theoretical mass flux j, but basically there would be no significant difference to the Sherwood number, because j is a function of D and d_d, which both combine the same parameters as the Sherwood number: Sc and Re.

Shear stress as a correlation does not reveal new considerations, because it is also directly dependent on the Reynolds number, surface roughness, etc. Those are variables which are expressed by the critical Reynolds number as mentioned before.

It is beyond the scope of this study to mention all possible parameters which may relate the corrosion rate or the mass transfer rate to the hydrodynamic parameters and variables. Therefore in the next paragraph some selected results in the literature are presented as a summary.

Tvarusko [30] tried in his paper to correlate special ratios of the Schmidt and the Sherwood number with different powers and also the turbulent intensity to the corrosion rate. Van Shaw [31] applied the Stanton number which can be expressed as Nu/(Re Pr) or as mass transfer coefficient/velocity, to find correlation in the entrance region of a pipe flow, and Cornet [32] researched the effect of Reynolds number on corrosion of copper in a pipe. Ross [27] described general effects of electrolyte velocity and Ellison [33] used a rotating disk to determine the equation for the Sherwood number.

Correlations between corrosion rate and parameters describing the whole system have not been completely successful, because it is difficult to determine the variables exactly by either the theory or by experiments. As already mentioned before, measurement of hydrodynamic variables demands a sophisticated equipment the application of which might lie beyond the scope of corrosion science. A corrosion scientist who wants to include both the hydrodynamic and material aspects in theory and practice in a flowing system has to have extensive knowledge and experience about both fields. The improvement of these both criteria was one of the achievements of this study.

VI. SUMMARY AND CONCLUSIONS

The following conclusions have been reached as a direct result from the experiments:

1. The corrosion rate increases with increasing velocity in a non-linear fashion. Doubling the velocity results in a 10-20% increase of the corrosion rate within the velocity range from 2 m/sec to 6 m/sec.
2. The variation of the corrosion as a function of time corresponds very well to the results in the literature. Starting at a high initial value the corrosion rate levels off after a period of time describing a parabolic curve.
3. Although pitting is assumed preferential only at lower velocities, these tests show more intensive dissolution through fine-scale pitting at higher velocities.
4. Higher turbulence intensity probably decreases the critical breakaway velocity, i.e. corrosion is enhanced beyond a lower velcoity than for lower turbulence.
5. It is difficult to find an apparatus to determine the necessary hydrodynamic parameters without having any effect on the measurement itself and without becoming too involved in complicated equipment and procedures.

The following conclusions have been reached from theoretical considerations:

1. The relation $d_h/d_d = Sc^{1/3}$ is not valid for turbulent flow.
2. The opinion often found in the literature that a decrease in the diffusion boundary layer thickness d_d generally results in an enhanced mass transfer rate is only valid when the change in d_d is not completely determined by a change in the diffusion coefficient D alone.
3. Taking the shape of the resulting curves into account, the equation for d_d from Wranglen seems to be more reasonable than others mentioned in the literature.
4. There exist basically two mass transfer mechanisms: convection and molecular diffusion. The ratio of both is given by the Sherwood or Nusselt number.
5. The Sherwood and the Nusselt number are reasonable non-dimensional parameters for a correlation with the corrosion rate, because both the hydrodynamic (flow properties) as given by the Reynolds number and the fluid and diffusion properties (ν,D) as given by the Schmidt number are combined in one number.
6. An even better correlation could be gained if it were possible to determine an extra diffusivity term ε (caused by turbulence) and to add this value to the molecular diffusion coefficient D in the equation

for the Schmidt number [$S_c = \frac{\nu}{D + \varepsilon}$] . By this method the turbulence intensity is included in the Sherwood number. The same could be achieved in the equation for the mass transfer [$j = \frac{(D + \varepsilon)\ \Delta c}{d_d}$] .

7. Re/Re_{cr} is another possible parameter for a correlation with the corrosion rate, which includes most of the hydrodynamic variables, but does not represent fluid properties other than the viscosity.

APPENDIX A

PREPARATION OF ARTIFICIAL SEAWATER

Synthetic standard seawater required during experimentation was prepared using the formula and procedure developed by Kester et al [46]. A concentrated stock solution was initially produced for ease in handling prior to use.

The following amounts of gravimetric and volumetric salts, combined with enough distilled water for a total weight of 1 kilogram, were used per kilogram of synthetic seawater solution.

A. Gravimetric Salts

salt	g/kg of solution
NaCl	23.926
Na_2SO_4	4.008
KCI	0.677
$NaHCO_3$	0.196
KBr	0.098
H_3BO_3	0.026
NaF	0.003

B. Volumetric Salts

salt	Conc M/L	ml/kg of solution
$MgCl_2 \cdot 6H_2O$	1.000	53.27
$CaCl_2 \cdot 2H_2O$	1.000	10.33
$SrCl_2 \cdot 6H_2O$	0.100	0.90

C. Distilled water to bring total weight to 1 kilogram

LIST OF REFERENCES

1. Storm, G., The Effect of Velocity on Corrosion of Galvanic Couples in Seawater, MSME-Mechanical Engineer Thesis, Naval Postgraduate School, Sept. 1977.

2. Pye, E., Ph.D., Report C-10, Practical Considerations in Performing Linear Polarization Measurements, supplied by Alpha Research.

3. Stern, M. and Geary, A.L., "Electrochemical Polarization Theoretical Analysis of the Shape of Polarization Curves," Journal of the Electrochemical Society, Vol. 104, No. 1, p. 56-63.

4. Princeton Applied Research, Manuals for Potentiostat/ Galvanostat Model 173 and for Programmer Model 175.

5. Hewlett Packard, Manual for x-y Recorder 4040 A.

6. Lyle, F., An Electrochemical Test to Determine Corrosion Rates in Automotive Engine Cooling Systems, Department of Material Science, Southwest Research Institute, San Antonio, Texas.

7. Lauer, G. and Mansfeld, F., "Technical Note: Measurement of Galvanic Corrosion at Zero External Impedance," Corrosion, Sept. 1970.

8. Fraunhofer, von, and Banks, C.H., Potentiostat and its Application, London, Butterworth, 1972.

9. Devay, J. et al, "Anwendung des Potentiostat zur Bestimmung des maximalen Korrosionsstroms von galvanischen Elementen", Acta Chemica Acad., Sci. Hungaricae, Tomus 62(2), p. 157-162, 1969.

10. Macdonald, D.D., Syrett, B.C. and Wing, S.S., Methods for Measuring Corrosion Rates of Copper Nickel Alloys in Flowing Seawater, presented at Corrosion 178, March 1978, Houston, Texas.

11. Bianchi, G. and Longhi, P., Corrosion Science, Vol. 13, p. 153, 1973.

12. Wranglen, G. and Nilson, O., "Mass Transfer under Forced Laminar and Turbulent Convection at Horizontal Plane Plate Electrodes, Electrochemica Acta, vol. 7, p. 121-137, 1962, Pergamon Press.

13. Eckert, E., Einführung in den Stoff-und Wärmeaustausch, p. 73, 1959, Springer Verlag.

14. Schack, R.P., "Effect of Hydrodynamic Variables on Corrosion: Study of 90-10 Cu-Ni in a Flow-Channel with Natural Seawater," MSME-Mechanical Engineer Thesis, Naval Postgraduate School, March 1978.

15. ASTM, Standard Recommended Practice for Preparing, Cleaning and Evaluating Corrosion Test Specimens, Designation G1-72, 1976.

16. Heitz, E., "Untersuchung von Transportvorgaengen bei der Korrosion," Wekstoff und Korrosion, Jahrgang 1964, Heft 1.

17. Nernst, W., Z. Phys. Chem. 47, p. 56, 1904.

18. Levitsch (Levich), V.G., Physiochemical Hydrodynamics, 1962, Prentice Hall.

19. Cornet, I., Journal Electrochem. Soc., p. 108, 1961.

20. Landolt, D., "High Rate Anodic Dissolution of Copper," J. Electrochem. Society, Oct. 1969.

21. Newman, J., Mass Transport and Potential Distribution in the Geometries of Localized Corrosion, National Ass. of Corrosion Engineers, 1974.

22. Schlichting,H., Boundary Layer Theory, 1968, McGraw Hill.

23. Holman, J. O., Heat Transfer, 4th Edition, p. 435, McGraw Hill.

24. Ross, T.K. and Jones, D.H., "Corrosion Inhibition in Moving Media," Journal Applied Chemistry, 12 July 1962.

25. Davis, J.A., Pitting Behavior of Aluminum Alloys in High Velocity Seawater, presented at Annual Conference of Electrochemical Society, Oct. 1976, p. 1-20.

26. Davis, J.A. and Gehring, G.A., Paper No. 78 represented at Corrosion /74, March 1974, Chicago, Illinois.

27. Ross, T.K. and Hitchen, B., "Some Effects of Electrolyte Motion During Corrosion," Corrosion Science, 19 Vol. I, 1961, Pergamon Press.

28. Devanathan, M. and Guruswany, V., "Investigation of Mass Transfer in Flowing Electrolytes," Department of Physical Chemistry, Ceylon, Electrochimiya, Vol. 7, p. 1818-1825, Dec. 1971.

29. Ross, T.K., "The Anodic Behavior of Iron-Carbon Alloys in Moving Acid Media," J. of Electrochemical Society, 1966.

30. Tvaruski, A., "Mass Transfer on Horizontal Wires in the Presence of Free and Combined Forced and Free Convection," J. Electrochem. Soc., Electrochemical Science and Technology, p. 490, April 1976.

31. Shaw, V., "Rates of Turb-lent Transfer in a Pipe Wall in the Mass Transfer Entry Region," A.I. Ch.E. Journal, May 1963.

32. Cornet, I. et. al, "Effects of Reynolds Number on Corrosion of Copper by Sulfuric Acid," Journal Electrochemical Society, p. 947-153, 1961.

33. Ellison, B.T., "Mass Transfer to a Rotating Disk," J. Electrochem. Society, p. 68-72, Jan. 1971.

34. Hinze, J.O., Turbulence, 2nd Edition, Mcgraw Hill.

35. TSI (Thermo System Incorporated), Manual TSI, Section III, Theory and Application, 1973.

36. Preece, C. and Macmillan, N., "Erosion," Am. Rev. Mater. Science, p. 95-121, 1977.

37. CRC Handbook for Applied Engineering Science, 2nd Edition, CRC Press.

38. Efird, K.D. and Lee, T.S., The Carbon Mechanism for Aqueous Sulfide Corrosion of Copper Base Alloys, presented at Corrosion /78, March 1978, Houston, Texas.

39. Feigl, F., Spot Tests in Unorganic Analysis, Elovier Publishing Company, p. 305, 1958.

40. Blundy, R.G. and Pryor, N.J., "The Potential Dependence of Reaction Product Composition of Copper-Nickel Alloys," Corrosion Science, p. 65-75, 1972.

41. Pourbaix, M., "Electrochemical Corrosion and Reduction," published in the YBS Special Publication 479, Corrosion and Artifacts, p. 15.

42. Pye, E.I., Report c-11, Corrosion Rate Measurements Using The Tafel Method, published by Alpha Research Company.

43. Popplewell, J.M., Marine Corrosion of Copper Alloys, An Overview, presented at Corrosion /78, March 1978, Houston, Texas.

44. Kester et al, "Preparation of Artificial Seawater," in Limnology and Oceanography, V. 12, p. 176-178, Dec. 1967.

45. Syrett, B.C., "Erosion-Corrosion of Copper-Nickel Alloys in Seawater and Other Aqueous Environment - A Literature Review," in Corrosion, V. 32, p. 242-250, June 1976.

INITIAL DISTRIBUTION LIST

		No. Copies
1.	Defense Documentation Center Cameron Station Alexandria, Virginia 22314	2
2.	Library, Code 0412 Naval Postgraduate School Monterey, California 93940	2
3.	Department Chairman, Code 69 Department of Mechanical Engineering Naval Postgraduate School Monterey, California 93940	2
4.	Professor A.J. Perkins, Code 69Ps Department of Mechanical Engineering Naval Postgraduate School Monterey, California 93940	6
5.	Professor T. Sarpkaya, Code 69Sl Department of Mechanical Engineering Naval Postgraduate School Monterey, California 93940	1
6.	Professor T.M. Houlihan, Code 69Hn Department of Mechanical Engineering Naval Postgraduate School Monterey, California 93940	1
7.	Marineamt - Al - 294 Wilhelmshaven Federal Republic of Germany	1
8.	Dokumentationszentrale der Bundeswehr (See) Friedrich - Ebert - Allee 34 53 Bonn Federal Republic of Germany	1
9.	Gerhard Leumer Wiesenkamp 122 2305 Heikendorf Federal Republic of Germany	3